A CHEMICAL REACTION
IN A
TURBULENT JET

Thesis by

John R. Shea, III

In Partial Fulfillment of the Requirements

for the Degree of

Doctor of Philosophy

California Institute of Technology

Pasadena, California

1976

(Submitted July 1, 1975)

ACKNOWLEDGMENTS

The author wishes to acknowledge the helpful guidance and encouragement of his advisor, Professor Hans W. Liepmann, during the course of this research. The consistent support of Dr. James E. Broadwell throughout the duration of the project is also deeply appreciated.

A number of others contributed significant ideas and suggestions which helped in the construction of the apparatus and the analysis of the data. Particularly notable among them were Professor Donald E. Coles, Dr. Robert E. Setchell, Dr. Garry L. Brown, Professor Anatol Roshko, Professor Frank E. Marble, Professor Frederick H. Shair, and Dr. Oliver R. Wulf. The author is also grateful to Mrs. Jacquelyn A. Beard and Mrs. Karen Cheetham, who helped with the preparation of the manuscript. The author also acknowledges a deep debt to his parents and friends, who made very significant contributions to the success of the entire project.

The author is indebted to the Fannie and John Hertz Foundation for their generous fellowship support during his course of studies and to the United States Air Force, who supported the research.

ABSTRACT

The turbulent mixing and subsequent chemical reaction of gases is an essential part of many technological processes ranging from gas furnaces to chemical lasers. Surprisingly, there is very little information, either theoretical or experimental, about the actual rate of the chemical reaction in such processes. Generally the chemical kinetics are well understood, but the process of turbulent mixing is not. Many measurements of mixing in turbulent jets have been made in the past, but they have generally failed to distinguish essentially unmixed gas in the turbulent mixing zone from gas which is mixed on a molecular scale. Knowledge of where turbulent fluid is mixed on a molecular scale is critical for predicting chemical reaction rates in the flow.

In this experiment the rate of a chemical reaction in an axisymmetric turbulent jet is studied, and the results are used to determine the rate of molecular mixing in the jet. A turbulent jet containing dilute ozone in an inert mixture of nitrogen and oxygen flows into a stagnant tank of nitric oxide and nitrogen. When the gases mix on a molecular scale, the ozone and nitric oxide rapidly react to produce oxygen and nitrogen dioxide. The rate at which the mixing and chemical reaction proceeds is determined by using an ultraviolet light absorption technique to measure the time averaged ozone concentration at points throughout the jets mixing zone.

The experiment establishes a criterion for determining when a reaction of known chemical kinetics is sufficiently rapid that

chemical nonequilibrium has a negligible effect on the mean reactant profile. When a reacting jet satisfies this criterion for equilibrium chemistry, the reactant profiles are found to be independent of jet Reynolds numbers from 4,000 to 32,000 based on the nozzle diameter.

In addition, a mixing fraction, η, is defined to measure the extent of local molecular scale mixing independently of a chemical reaction occurring in the jet. The fraction assumes values of unity in the unmixed primary jet, zero in unmixed ambient fluid, and intermediate fractions for mixtures of all proportions. Points on nonreacting jet profiles are related to time averages of η. A limiting highly reacting ozone profile, found when a large excess of nitric oxide is present in the ambient fluid, is related to the time average of an intermittency function, $J(\eta)$, defined equal to unity when η is within a specified neighborhood of one and zero elsewhere. Thus the experimental measurements of ozone profiles are directly related to the statistics of molecular scale mixing in the jet.

TABLE OF CONTENTS

TABLE OF CONTENTS (cont'd)

TABLE OF CONTENTS (cont'd)

LIST OF FIGURES

LIST OF FIGURES (cont'd)

LIST OF SYMBOLS

A = cross-sectional area of the jet

C_p = heat capacity of gas in the experiment (nitrogen), 6.97 cal/mole^{o}K

D = molecular diffusivity, cm^2/sec. This is directly proportional to the total tank pressure. At 1 atm and 295^{o}K, empirical values (Ref. 43) are

O_3 through N_2 = .145 cm^2/sec

NO through N_2 = .157 cm^2/sec

N_2 through N_2 = .145 cm^2/sec

For calculations a mean value was selected as $D = \nu$.

$\mathcal{D}$ = eddy diffusivity, an empirical analog to D for turbulent flows

d = nozzle diameter, .508 ±.002 cm

d^* = diameter, corrected for the presence of the nozzle layer

f = probability density function for mixing

f_1 = discrete probability of observing unmixed gas at $\eta = 1$.

H = brief notation for the logarithm of the profile intensity ratio, as defined by Equation 5-1

ΔH_f = heat of reaction for $O_3 + NO \rightarrow O_2 + NO_2$, exothermic at 47.7 kcal/mole (Ref. 24)

$I_o, I_o(x)$ = light intensity (volts) of ozone cell or across experimental tank with no ozone present

$I, I(x)$ = light intensity (volts) of ozone cell or across experimental tank with ozone present

LIST OF SYMBOLS (cont'd)

I_{bk} = background intensity to be subtracted from I, I_o and I(x), $I_o(x)$ (two separate measurements)

J = intermittency function defined equal to 1 in regions of unmixed gas from the primary jet and 0 elsewhere

k = homogeneous chemical reaction rate for $O_3 + NO \rightarrow O_2 + NO_2$; $k = 9.0 \cdot 10^{-13} e^{-1200/T}$ $= 1.6 \cdot 10^{-14}$ cm^3/molecule-sec (Ref. 24)

N, n = number density, or concentration of the subscripted species (molecules/cm^3). Because the temperature is constant these are directly proportional to mass density and partial pressure. Generally N is a uniform concentration of a species in unmixed gas, and n is a concentration measured in the flow

P = partial pressure of subscripted species, usually in unmixed gas

R = radius of jet cross-sectional area, generally determined from the ozone concentration profile of a nonreacting jet

r = distance from any point in the flow to the jet centerline ($r^2 = x^2 + y^2$ when x and y have origins on the jet centerline)

Re = Reynolds number of jet, $\rho u_o d/\mu$

Sc = Schmidt number

T = absolute temperature, ^oK

u = jet velocity in the downstream direction

u_o = nozzle velocity, mass-averaged across the nozzle exit

LIST OF SYMBOLS (cont'd)

x = position along axis of traversing motion

y = position along axis parallel to light beam path

z = position along jet centerline measured from nozzle exit

α = absorption coefficient for ozone at 2537A, $1.14 \cdot 10^{-17}$ cm^2/molecule (ref. 20)

δ = nozzle boundary layer thickness

δ^* = nozzle boundary layer displacement thickness

η = molar mixing fraction, defined relative to gas from the primary jet in Section 7.

μ = viscosity of the gas (N_2) at 275^oK = $184 \cdot 10^{-6}$ poise

ν = kinematic viscosity = μ/ρ = .15 cm^2/sec for 1 atm 295^oK nitrogen

ρ = mass density of the entire fluid or of the subscripted species

τ_c = characteristic time for breakdown of largest eddies in a turbulent mixing zone

τ_{chem} = characteristic time for chemical reaction between ozone and nitric oxide

τ_D = characteristic time for molecular diffusion across the smallest length scale in a turbulent mixing zone.

1. INTRODUCTION

The subject of chemical reactions in turbulent mixing zones is one of vast technological importance and arises in practical situations ranging from combustion devices to chemical lasers. The system of interest in this study is a second order chemical reaction limited by a turbulent mixing rate; is is similar in many respects to a turbulent diffusion flame. One of the two chemical reactants is contained in a primary stream of gas, and the other resides in a secondary gas. The two fluids meet in a turbulent mixing zone. The chemical reaction of two gases at the molecular level is well understood; however, at present, the rate of the molecular mixing in a turbulent mixing zone is not well understood and is, therefore, the principal interest of this study.

1.1 Background

In 1928 Burke and Schumann (Ref. 1) introduced the idea of a flame sheet for a laminar diffusion flame. They proposed that in the limit of an infinite reaction rate all chemical activity in a flame is confined to a very thin sheet fed by reactants drawn from either side by Fick's law of diffusion. Thus they recognized that the rate controlling mechanism for the flame is molecular diffusion and not chemical kinetics.

The concepts of unmixedness and large scale concentration nonuniformities in turbulent mixing zones arose in the 1940's with Hawthorne, Weddell and Hottel (Ref. 2), Damköhler (Ref. 3), and Shchelkin (Ref. 4). Hawthorne et al. measured the extent of molecular mixing at a point in a turbulent mixing zone using the mixing

fraction, a nondimensional concentration of gas originating from the primary jet. The mixing fraction, denoted by η throughout this work, varies from unity in samples of unmixed primary fluid to zero in samples of unmixed secondary fluid and assumes intermediate values for mixtures of all proportions. If chemical non-equilibrium is confined to thin sheets throughout the mixing zone, the local mixing fraction and the initial concentrations of reactants in the unmixed fluids determine the concentrations of both reactants and products. Hawthorne et al. realized that a time-averaged measurement of the fluid composition at a point in a turbulent jet gives very little information about the status of molecular mixing; one must consider a distribution of possible mixing fractions at the point in question. Most researchers prior to the mid 1960's assumed the probability density fraction for η to be Gaussian and, hence, determined by a single parameter, the variance.

Several techniques have been used to evaluate the variance of the Gaussian distribution. Thring and Newby (Ref. 5) estimated the concentration fluctuations by assuming a similarity to the root mean square velocity fluctuations, and Toor (Ref. 6,7) suggested using a point conductivity probe to sample mixing in aqueous solutions. Richardson et al. (Ref. 8) used a technique of extracting and analyzing cooled gas samples from a flame to test an alternative to the Gaussian probability distribution for mixing. By cooling gas samples taken from the flame, they quenched the chemical reaction and obtained time-averaged reactant concentrations of both fuel and oxidizer. Their alternative two parameter mixing

distribution function, however, did not differ significantly from the Gaussian.

In experimental research on turbulent mixing in jets and wakes Corrsin and Townsend discovered the existence of relatively sharp interfaces separating turbulent from nonturbulent fluid. The concept of "intermittency" was introduced by Townsend (Ref. 9), and the concept of "superlayer" by Corrsin and Kistler (Ref. 10) in their studies of these interfaces and their importance to turbulent mixing. In the meantime, a number of early turbulent flame studies also recognized patterns of large scale turbulent structures in flames. Karlovitz (Ref. 11, 12, 13) probed flame sheet structures with an ion probe, and Wohlenberg (Ref. 14) discussed islands of relatively unmixed fuel or oxidizer within a turbulent mixing zone. Kunugi and Jinno (Ref. 15) observed unmixed regions in an enclosed water jet with a flow visualization technique employing suspended aluminum spheres.

Though spark Schlieren pictures of turbulent flames, such as those presented by Wohl, Gazley and Kapp (Ref. 16) in 1949, clearly show large fluctuations of the edge of a turbulent flame zone, intermittency in turbulent mixing was generally not treated explicitly until the mid 1960's. The intermittent presence of nonturbulent and unmixed fluid from either the ambient secondary gas or the jet potential core adds a non-Gaussian aspect to the probability of observing gas mixtures at a fixed point in a mixing zone. In the works of Becker, Hottel and Williams (Ref. 17, 18), the developments in turbulence and flame research were fused in a

comprehensive study of a ducted jet as a model for turbulent burning. The importance of concentration intermittency was stressed, and concentration and concentration fluctuations were measured by a light scattering technique. Becker et al. measured concentration intermittency in the far field similarity region of a nonreacting axisymmetric jet, 30 to 70 diameters downstream of the nozzle. Their primary jet contained a heavy mist of oil droplets, which spread with the largest scales of the turbulence. Light scattering by the oil droplets in a sampling volume several millimeters in diameter was used to measure primary fluid concentration as a function of time at points through the jet. Becker et al. determined both the average position of the edge of the turbulent region of the jet and the probability distribution for the radial extent of the turbulent core, i.e., the intermittency. The information on intermittency was then used to convert the local, time averaged concentration and concentration fluctuation measurements to conditional averages within the turbulent fluid.

The recent fundamental work by Brown and Roshko (Ref. 19) on a heterogeneous turbulent mixing zone has essentially changed the conceptual basis of turbulent mixing. The two-dimensional mixing layer is particularly simple because it exhibits similarity even in the mixing of two different gases and hence conditions are in many ways simpler than in jet mixing. In the Brown-Roshko approach, the emphasis is placed on the interface dividing the two gases; this is a quite different approach from the "superlayer" of Corrsin and Kistler which divides turbulent and nonturbulent fluid.

The Brown-Roshko interface is a vortex sheet which is shown to roll up into a set of large scale coherent structures which entrain fluid by entanglement. The resultant instantaneous concentration distribution, at high Reynolds numbers, is very "spiky", alternating between regions containing nearly unmixed fluid from either side. Molecular mixing and hence chemical reactions take place only at these interfaces. Similar but more complex conditions must prevail in jet mixing as well, particularly in the initial phase which is of prime interest for the present work.

The probability density function in a turbulent jet or shear layer must admit a finite probability of observing unmixed gas at mixing fractions of $\eta = 1$ and $\eta = 0$. Therefore, the full probability distribution is expected to be at least bimodal. For fluid sampled within the turbulent core of a jet, however, a Gaussian probability density function appears to be an adequate approximation of the mixing fraction distribution. The mixing probability density function and the initial reactant concentrations prior to mixing provide all information necessary to predict reactant and product concentrations at points in a turbulent mixing zone.

1.2 The Present Research

The research reported here is an experimental investigation which employs a fast chemical reaction to study the mixing process in a turbulent axisymmetric jet flowing into a stagnant ambient atmosphere. Figure 1 shows the basic schematic of the experiment. The primary jet contains a small amount of ozone in an otherwise

inert mixture of nitrogen and oxygen as it emerges from a small contoured nozzle. The ambient atmosphere surrounding the jet consists of nitrogen and varying amounts of nitric oxide. Wherever the gases mix on a molecular scale, the ozone and nitric oxide react as follows:

$$O_3 + NO \rightarrow O_2 + NO_2$$

Since the reaction can occur only to the extent that local molecular scale mixing permits, the rate of molecular scale mixing can be determined from measured concentration profiles of the limiting reactant, ozone.

This reaction was selected for several reasons. Firstly, ozone is almost opaque to ultraviolet light (Ref. 20) and thus presents a method for detecting its presence in the mixing zone. Neither nitrogen nor nitric oxide nor nitrogen dioxide absorb light at the wavelength employed, 2537 Å (Ref. 21, 22, 23). Secondly, because we can detect very low concentrations of ozone with the optical technique employed, we can minimize the heat release from the reaction and can limit the maximum temperature rise in the mixing zone to a few degrees centigrade. We thus have very minimal beam distortion from index of refraction changes in the mixing zone and can assume constant density fluid dynamics. Thirdly, as the reaction is fast at room temperature (Ref. 24, 25, 26), we avoid ignition and extinction problems as well as the flame stabilization problems common to many combustion studies. Other chemical reactions between ozone, oxygen and oxides of nitrogen

are too slow to be of interest during the residence time of fluid in the mixing zone of the jets studied.

This approach to mixing presents an alternative to the use of a density probe from which the measurement of an instantaneous point quantity is always limited by probe interference with the flow and the space-time volume of the response. In this experiment time-averaged measurements are made of the concentration of ozone, which is a reactant existing locally as a function of the reactant concentrations in the unmixed gases and of the local proportions of molecular scale mixing. The unmixed reactant concentrations are always known, and in the limit of fast chemical kinetics we can relate the measured time average ozone concentrations directly to the statistical properties of the local, instantaneous mixing proportions of the turbulent jet. The spatial resolution of the measurement only needs to be sufficient to discern detail in the mean profiles. The only physical interaction between the jet and the measurement technique is through a very faint beam of ultraviolet light.

The geometry of the experiment is designed for maximum simplicity. The reacting jet is enclosed in a tank, which initially holds the stagnant NO, N_2 mixture. The nozzle for the ozone jet enters vertically from the top and extends an adjustable distance into the tank. The optical system is affixed to the side of the tank and sweeps across the jet in a horizontal plane during each run. The light source is the 2537 Å band of a low pressure mercury

lamp, and a photomultiplier tube measures light intensities while an automatic digital data acquisition system records the measurements. The measured absorption profiles can be readily converted to radial ozone concentration distributions.

The experimental program is directed towards answering four basic questions of the turbulent, chemically reacting jet.

1. How is the overall reaction rate related to the basic parameters of the jet?
2. What is the effect of jet Reynolds number on the mixing process?
3. When is the chemical reaction fast enough to produce a mixing limited jet profile?
4. What are the implications of the data for the problem of molecular mixing in the jet?

2. THE BASIC EXPERIMENTAL PROGRAM

The experimental program consists primarily of making measurements of profiles of ozone density as a function of radial distance from the jet centerline at four axial distances from the nozzle, 1, 2, 3 and 5 diameters downstream. We measure both nonreacting profiles for ozone spreading into a tank filled with pure nitrogen and reacting profiles of ozone spreading into a tank mixture containing various amounts of the reactant nitric oxide. The ozone profiles of the nonreacting jets determine time-averaged entrainment rates and the mean fraction of gas originating in the primary jet at points throughout the mixing zone. Measurements on reacting jets yield the mean molar density of gas originating in the primary jet which remains locally unmixed with the ambient fluid. Most of the experimental data consists of reacting and nonreacting ozone profile measurements for five different Reynolds numbers, based on nozzle diameter and ranging from 4,000 to 32,000, and for two tank pressures, 1.34 and 4.06 atmospheres.

The basic measurement in the experiment is quite simple in concept. A signal proportional to the intensity of a collimated beam of the filtered 2537 Å line from a mercury lamp can be measured with a photomultiplier tube. The ratio of two measurements, one with and the other without ozone present, determines the attenuation of the beam, and the logarithm of the intensity ratio is proportional to the number of molecules of ozone in the volume illuminated by the beam,

$$\ln I_o/I = \int_{\text{beam path}} \alpha \, n_{O_3} \, dy \qquad (2\text{-}1)$$

where I and I_o are the measured light intensities, in volts, with and without ozone present, α is the absorption coefficient for ozone at 2537 Å [$1.14 \cdot 10^{-17}$ cm^2/molecule, Ref. 20] and y is the ordinate along the optical path. In this work the variable N will refer to the initial concentration (molecules/cm^3) of the subscripted chemical species in unmixed fluid. The variable n will represent the concentration of the subscripted species in the mixing zone of the jet. As the temperature is always within a few degrees of 295°K in the experiment, N and n are proportional to both mass density and partial pressure.

Despite the simplicity of the basic measurement, the experiment entails certain practical difficulties. Ozone, oxygen and some oxides of nitrogen can explode if exposed to grease or combustible materials. Ozone decomposes on contact with container walls unless extreme care is taken in both design and maintenance. Most of the gases are not only poisonous but also corrosive to many common materials of construction and to most sensitive laboratory equipment. Even when the experiment is enclosed in a large tank, the expended gases quickly pollute the ambient gas, and their recirculation limits experimental run times to a maximum of seven seconds. As the gas in a jet must flush nitric oxide out of the internal nozzle cavity before the jet can reach a steady state operating condition, the entire measurement must take no longer

than 3 to 6 seconds. Because no ultraviolet lasers are currently available, the large size of the tank intensifies problems of obtaining light beam intensities from a mercury lamp large enough to measure easily. The beam used to probe the jet must be collimated with a lens through a very small aperture and must travel in excess of one meter through the experimental tank. We will discuss the resolution of experimental difficulties at greater length in Section 3.

The experimental parameters are

N_{O_3}, N_{NO}, N_{Tank}, u_o; k, d, D, ΔH_f, C_p where

N_{O_3} = Ozone concentration (molecules/cm^3) in unmixed primary jet.

N_{NO} = Nitric oxide concentration (molecules/cm^3) in unmixed ambient fluid.

N_{Tank} = Total molecular density in experimental tank (molecules/cm^3).

u_o = Nozzle velocity (cm/sec).

k = Chemical kinetic rate coefficient for ozone and nitric oxide = $1.12 \cdot 10^{10}$ cm^3/mole sec at 23°C.

d = Nozzle diameter, .508 cm.

D = Molecular diffusivity of jet gas (cm^2/sec), which is here equal to the kinematic viscosity μ/ρ, for nitrogen as the Schmidt number is approximately 1.0 for all chemical species.

ΔH_f = Heat of reaction for $O_3 + NO \rightarrow O_2 + NO_2$, which is exothermic at 47.7 kcal/mole, (Ref. 24).

C_p = Heat capacity of the gas (nitrogen), 6.97 cal/mole^{o}K.

T = Absolute temperature, 295^{o}K for all runs.

The first four parameters listed are varied in the experimental program. They can be organized into four nondimensional groups, each with a physical meaning:

Reynolds Number, $u_o d/D$

Dilution Number, $\dfrac{N_{O_3} \Delta H_f}{N_{Tank} C_p T}$

Reaction Speed, $k N_{NO} d/u$

Concentration Ratio, N_{NO}/N_{O_3}

2.1 The Reynolds Number

Of the four nondimensional numbers listed above, the Reynolds number appears to be the most likely parameter group upon which the molecular mixing rate may depend. But, the Reynolds number should affect the overall mixing rate only if diffusion across the smallest length scales in the turbulence limits the mixing process.

Turbulent motions occur over a variety of length scales. The overall dimensions of the mixing zone limit the size of the largest eddies. A wide range of smaller scale motions exists throughout the mixing zone, and the smallest scale, the Kolmogorov microscale, is limited by the action of molecular viscosity on the turbulent mixing process. The mixing process can be perceived

in terms of a cascade in which the breakdown of large eddies produces mixing on increasingly smaller scales until molecular diffusion becomes dominant at the Kolmogorov microscale. We can estimate the rates of both the large eddy breakdown and the molecular diffusion across the Kolmogorov microscale for each combination of experimental parameters considered in the experiments. The slower of the two will be the rate determining step for the entire mixing process.

The rate of the large scale eddy breakdown is determined by the scale of the mixing zone (the nozzle diameter, d) and the velocity difference from the center to the edge of the jet (the nozzle exit velocity, u_o). Thus the convective time scale τ_c for the inviscid, large scale eddy breakdown is

$$\tau_c = d/u_o \tag{2-2}$$

The value is also characteristic of the residence time of a fluid particle in the near field of the jet mixing zone.

The rate of the molecular diffusion across the smallest length scale of the turbulence is determined by the molecular diffusivity, D, and the Kolmogorov microscale length, λ,

$$\lambda = (\nu^3/\epsilon)^{\frac{1}{4}} \tag{2-3}$$

where ν is the kinematic viscosity and ϵ is the kinetic energy dissipation rate. For the purpose of defining a diffusion time scale we can take the dissipation rate as

$$\epsilon = u_o^3/d \tag{2-4}$$

The diffusion time scale then becomes

$$\tau_D = \lambda^2/D = d/u_o \left(\frac{u_o d}{\nu}\right)^{-\frac{1}{2}} \left(\frac{\nu}{D}\right) \qquad (2\text{-}5)$$

For the chemical species in this experiment $\nu = D$, and hence,

$$\tau_D = d/u_o \, (Re)^{-\frac{1}{2}} \qquad (2\text{-}6)$$

The values of τ_c and τ_D for this experiment are given in Table 1.

Cases		Convection Time, τ_c	Diffusion Time, τ_D
Re, $\frac{u_o d}{\nu}$	P_{tank} (atm)	(d/u_o), sec	$(d/u_o)(Re)^{-\frac{1}{2}}$, sec
12,500	1.34	$1.8 \cdot 10^{-4}$	$1.6 \cdot 10^{-6}$
5,000	1.34	$4.6 \cdot 10^{-4}$	$6.5 \cdot 10^{-6}$
15,000	4.06	$4.6 \cdot 10^{-4}$	$3.8 \cdot 10^{-6}$
4,000	4.06	$1.7 \cdot 10^{-3}$	$2.7 \cdot 10^{-5}$
32,000	4.06	$2.2 \cdot 10^{-4}$	$1.2 \cdot 10^{-6}$

TABLE 1

The table clearly indicates that the time scale for the breakdown of the large eddies exceeds the time scale for molecular diffusion across the smallest turbulent length scales by two orders of magnitude. Thus the rate controlling step for molecular scale mixing should be that of the inviscid breakdown, which is Reynolds number independent. Ozone profiles measured in this experiment do demonstrate Reynolds number independence, at least to within experimental error. Each Reynolds number case listed in Table 1

is identified in each appropriate figure presenting experimental data.

The Reynolds number independence of flame length in turbulent diffusion flames has been noted before [e.g., Hawthorne, Weddell and Hottel (Ref. 2), Wohl et al. (Ref. 16), Hottel (Ref. 27), and Yagi and Saji (Ref. 28)]. The explanations, however, differ from the argument of a rate-limiting step to the mixing process presented here. The general approach of the above authors is first to calculate a flame length for a laminar jet by using a known molecular diffusivity. They then modify their result for a turbulent jet by replacing the molecular diffusivity, D, for the laminar jet by an eddy diffusivity, $\mathscr{D}$, for a turbulent jet of the form

$$\mathscr{D} = .0025\, u_o d \qquad (2\text{-}7)$$

which is assumed constant across the jet. The result is a flame length dependent only on the concentration ratio, as is indeed observed, but we prefer the use of a rate controlling step to the use of an eddy diffusivity.

2.2 The Dilution Number

The addition of chemically reacting species to the jet and ambient fluid can have two effects on the jet properties. First, the addition changes the density of the carrier fluid. In this experiment the density changes are very small because we use only nitrogen, with less than 10% nitric oxide or oxygen. Ozone is heavier than the other species, but it is present at less than one part per thousand in the jet. Though additives may not affect the

jet density, dilute chemical species can have a marked effect in the flow through a second effect, the heat release from chemical reactions. In common examples of combustion this effect dominates the reaction zone. The heat of reaction released in the jet is

$$\text{Heat in} < N_{O_3} \Delta H_f \ (\text{cal/cm}^3) \tag{2-8}$$

Here the heat/unit volume is less than the expression in Equation 2-8 because the ozone containing primary jet must be mixed with some amount of nitric oxide containing ambient fluid before the energy is released. However, in cases where the concentration ratio, N_{NO}/N_{O_3}, is large, the primary gas needs to be diluted very little before all of the ozone is consumed. The heat capacity of the gas is

$$N_{Tank} C_p \ (\text{cal/cm}^3 \ ^\circ\text{C})$$

Thus, we can calculate the maximum temperature or density (ρ) change due to the heat of reaction as follows:

$$\frac{\Delta T}{T} = - \frac{\Delta \rho}{\rho} < \frac{N_{O_3} \Delta H_f}{N_{Tank} C_p T} = .02 \text{ to } .05 \quad . \tag{2-9}$$

For the experiments run this number was kept low, to a maximum of about 16°C temperature rise, by limiting the partial pressure of ozone in the primary jet to .003 atmospheres in most runs. At ozone partial pressures below .01 atm no heat release

effects have been noted.* In this experiment the dilution number is not an important parameter group.

2.3 The Reaction Speed Number

Chemical nonequilibrium in the mixing zone depends on a nondimensional reaction rate, the reaction speed number. References 24, 25, and 26 on the chemical kinetics of ozone and oxides of nitrogen indicate that mixed ozone and nitric oxide react as follows:

$$O_3 + NO \rightarrow O_2 + NO_2 \qquad (2\text{-}10)$$

to produce a decay of the ozone

$$\frac{d(O_3)}{dt} = - k(NO)(O_3) \quad . \qquad (2\text{-}11)$$

Then

$$\frac{(O_3)}{(O_3)_o} = e^{-k(NO)t} \qquad \text{where } (NO) \leq N_{NO}, \qquad (2\text{-}12)$$

the values in parenthesis being concentrations of the indicated chemical species. The nitric oxide concentration decreases from the unmixed value by dilution and by being consumed in the reaction, but for large concentration ratios it remains close to N_{NO}. The characteristic time for the chemical reaction is, then,

---

*An effect of heat addition was noted in preliminary experiments in which the ozone partial pressure exceeded .015 atm. Bright spots of five percent higher intensity than the blank measurement appeared at either edge of the profile for measurements at axial positions inside two diameters from the nozzle. The heated gas of the jet was acting as a lens and focussing light at the edge of the jet.

$$\tau_{chem} = \frac{1}{k\ N_{NO}} \quad . \tag{2-13}$$

In the experiments discussed the nitric oxide partial pressure corresponds to values of τ_{chem} between $1.6 \cdot 10^{-4}$ sec and $1.6 \cdot 10^{-5}$ sec.

The reaction speed number represents the ratio of two characteristic times of the turbulent reacting jet,

$$k\ N_{NO}\ d/u = \tau_c/\tau_{chem} \tag{2-14}$$

where τ_c is the characteristic time for the breakdown of the large scale eddies as discussed in Section 2.1 and tabulated for each investigated Reynolds number in Table 1. In Section 2.1 we found that τ_c limits the overall mixing rate because it is always much longer than the characteristic time for molecular diffusion across the small scales of the turbulence.

We can briefly consider two limits of the reaction speed number. When the number is small, the rate of the chemical reaction is the slowest step of the mixing and reaction process. The jet carries fully mixed chemical reactants which have not had time to react; this is the limit of frozen chemistry. When the reaction speed number is large, however, we approach the limit of equilibrium chemistry. The overall reaction rate is again controlled by the rate of the breakdown of the largest eddies because the reaction time is the shorter of the two processes. In this limit, the jet is mixing limited.

2.4 The Concentration Ratio

The concentration ratio is an important parameter in the turbulent reacting jet. When profiles are Reynolds number independent, mixing limited and not affected by the dilution number, the concentration ratio is the only parameter remaining to characterize the reaction zone. As mentioned in Section 2.1, the concentration ratio is directly related to turbulent flow length in References 2, 16, 27, and 28 in which the authors first compute a flame length for a laminar jet and then substitute a constant eddy diffusivity for the molecular diffusivity.

The extent of the reaction zone of a turbulent jet can be related to the concentration ratio by considering probabilities of observing mixtures above a critical mixing fraction at a given point in the flow. For a given reactant concentration ratio we can define a critical mixture, η_o, in which the chemical reactants combine in exact stoichiometric proportions. In the ozone-nitric oxide system of this experiment, we find ozone in mixtures with η in excess of η_o and nitric oxide in mixtures with η less than η_o. Since flame or chemical reaction will persist wherever some reactant from the primary jet remains, the edge of the reaction zone occurs where the probability of observing mixtures of η in excess of η_o drops to zero.

In flame studies the requirements for combustion demand that the concentration ratio be in the neighborhood of stoichiometric; the corresponding η_o is .5. Mixing in which no fluid contains a primary gas concentration η in excess of .5 is very thorough

mixing, and flame lengths are usually of the order of hundreds of diameters (Ref. 2, 5, 15, 16, 27, 29, 30).

In this experiment we use low ozone concentrations in the primary jet and high concentrations of nitric oxide in the ambient fluid; typical values of η_o are .90 to .98. In this limit ozone is consumed in almost all the gas actually within the turbulent mixing volume of the jet. Only inclusions of potential fluid from the core of the jet contain unreacted ozone, and these extend to a reaction length of only slightly over 5 diameters. Also, as the excess concentration of nitric oxide consumes ozone out to the edge of the turbulent-nonturbulent interface, the profiles become independent of concentration ratio as well as the other parameters.

2.5 The Effect of Reaction Speed and Concentration Ratio on a Typical Ozone Profile

We can consider the relative effects of the concentration ratio and reaction speeds upon a typical ozone profile in the three-dimensional representation in Figure 2. The ozone concentration averaged across the jet, normalized by the nonreacting average, is plotted on the vertical axis. The value can be easily measured at a particular axial station and can only decrease as the nitric oxide concentration in the tank increases. The speed of reaction number and the concentration ratio appear on the axes in the horizontal plane. Along the concentration ratio axis we have frozen chemistry. The profile parameter does not change because the reaction is not fast enough to change it from its nonreacting value.

Along the reaction speed axis the reaction may be inherently fast but the reactants are too dilute to affect the profile shape.

Two slices through Figure 2 are important. The first, the front face, is the profile change from increasingly fast chemistry at a fixed concentration ratio. Its asymptote will indicate a value of the reactant speed above which chemical nonequilibrium is not an important determinant of profile shape. The second slice, the side face of the diagram, shows the profile changing with concentration ratio at infinitely fast reaction speed. This will be very important because we will be able to assume that all significant chemical reactions have gone to completion locally when we make conclusions about the mixing from reaction measurements. The level plane that may appear at large reaction speeds and large reactant ratios will be called the highly reactive jet. It will be related to the probability observing fluid associated with the potential fluid at the core of the jet and not yet exposed to the process of molecular mixing.

3. THE EXPERIMENTAL APPARATUS

Designing and constructing an experimental apparatus occupied a large portion of the effort expended on the project. Elements of the apparatus fall into one of four categories. First is a contoured nozzle, which produces the axisymmetric jet. The nozzle is fed by a gas delivery system, which supplies ozone, nitrogen, and nitric oxide to the nozzle and experimental tank. The third equipment category includes the experimental tank which contains the turbulent jet. Finally, an optical system measures all ozone concentrations and is connected to a digital data acquisition system which automatically records the data. Each of the four categories will be described in turn.

3.1 The Nozzle

A diagram of the nozzle cross section appears in Figure 3. The ozone flow passes from a solenoid valve, through a metering valve, and down a length of heavy aluminum tubing into a cylindrical settling chamber 2.5 cm in diameter. In the settling chamber it passes through two layers of 218 mesh stainless steel screen before it reaches the nozzle contraction. The nozzle contour consists of a contraction section with a 1.0 cm radius of curvature followed by a .25 cm straight section. The exit diameter measures .508 cm $\pm$ .002 cm, producing a 25:1 area contraction from the settling chamber to the exit. This is sufficient to produce smooth and uniform flow across most of the nozzle exit.

A series of Pitot surveys were taken across the mouth of the nozzle to determine velocity profiles of the jet. The Pitot probe used was a total head tube ending with a piece of hypodermic tubing of .076 cm outside diameter. The dynamic pressure was measured with a Barocel pressure gauge, and the probe position was indicated by a linear potentiometer. Profiles were recorded graphically on a Hewlett Packard x-y recorder.

Aligning a traversing path through the center of a very small jet is not easy. A series of profiles had to be measured, each moved slightly to one side of the preceding traverse. As the paths were translated systematically, the path with the largest width and highest centerline pressure was assumed to have passed along a line through the jet center.

A typical traverse appears in Figure 4, where the dynamic pressure profile is plotted at 1.3 diameters from the nozzle. Two of the most important features of the profile are that it is symmetric and that the potential core is flat. The series of surveys includes the measurement of several profiles in the range of 1 to 5 diameters from the nozzle. A potential core extends to approximately 3.5 diameters from the nozzle, though the width of the probe (15% of the nozzle diameter) may have broadened the measurement somewhat. Centerline dynamic pressures remain constant downstream to the end of the core and then drop to 85% of the core value at 5 diameters from the nozzle.

A hot wire placed in the opening of the nozzle measured turbulence levels of less than .3%. Results of the turbulence level

measurement, the flatness of the potential core, and the symmetry of the velocity profile ease concern about the stagnation points in the nozzle at the beginning of the nozzle contraction. The stagnation region in the nozzle is a vestige of an earlier nozzle design which allowed radial inflow to the nozzle contraction. The earlier design was modified when the radial inflow produced problems with swirl and affected the symmetry of the jet. As an additional test of the nozzle design of Figure 3, ozone concentration profiles were measured at several orientations of the nozzle. In all cases the jet has proved symmetric.

Boundary layers in the nozzle are responsible for the short extent of the potential core. Other investigators (Ref. 31, 32, 33) report 4 to 6 diameters of potential core versus approximately 3 diameters observed here in the Pitot survey. Since the nozzle is quite small, boundary layers are virtually impossible to measure directly; however, we have two methods for estimating their thickness. In the first method we simply assume a flat plate boundary layer velocity profile with an effective origin inside the nozzle contraction. In the second approach we compute a displacement thickness from a known mass flow and a measured velocity in the potential core of the jet.

In the first estimate of the boundary layer we regard the nozzle wall as a flat plate. The nozzle contour is flat for the last .5 diameter before the exit and has only a small curvature in the final part of the actual contraction section. Thus the effective flat plate origin should be of the order of one diameter from the exit.

A typical Reynolds number is 12,000; therefore, in standard boundary layer notation at the nozzle exit

$$x = d$$

and

$$\frac{\delta^*}{x} = \frac{1.72}{\sqrt{Re}} = .016 \qquad (3\text{-}1)$$

where x is the distance from the flat plate origin and Re is the Reynolds number based on x. Two boundary layers across the diameter can produce some momentum deficit across almost 10% of the nozzle exit.

A second measurement of the boundary layer displacement thickness, δ^*, at the nozzle provides an independent verification of the above estimate. In Figure 4 the potential core of pure nitrogen at 1 atm has a dynamic pressure corresponding to a velocity, u_1, of 42.8 m/sec. An ozone storage cylinder, which normally supplies gas to the nozzle and is described below, provides a means for measuring mass flow through the nozzle. The average nozzle velocity, u_o, based on a uniform mass flow distributed across the entire nozzle diameter, d, for the conditions of Figure 4 is 39.9 ± 1 m/sec. Putting the entire mass flow through the diameter diminished by twice the displacement thickness,

$$d^* = d - 2\,\delta^* \qquad (3\text{-}2)$$

at the potential core velocity, u_1, we have

$$\rho u_1 (d^*)^2 = \rho u_o d^2 \qquad (3\text{-}3)$$

$$\frac{\delta^*}{d} = .022 \quad . \tag{3-4}$$

The latter number is accurate to only about 20% as it is obtained from the difference of two large numbers, but it provides an approximate confirmation of the first boundary layer estimate.

The presence of the boundary layer in the nozzle produces a 5% discrepancy between the mass averaged velocity, which is measured, and the actual velocity of the jet potential core. The boundary layer estimate above was calculated at a Reynolds number of 12,500; at other Reynolds numbers the relation between potential core velocity and mass averaged velocity should vary through the dependence of the nozzle boundary layer displacement thickness on Reynolds number. This velocity correction was not made for the data presented in this work, however, and the stated nozzle velocities are always the measured mass averaged velocities unless otherwise indicated.

The nozzle is supported through a pulley above the experimental tank and by the heavy tubing of its inlet line shown in Figure 3. The tubing passes through a carefully machined cylinder packed with teflon bushings at the top of the experimental tank to prevent any tilting of the nozzle. The nozzle can be raised and lowered over a range of 12 cm into the tank; thus the level of the delicate optical system can remain fixed to the experimental tank. By lowering the nozzle until it blocks approximately half of the optical beam, we can align the nozzle with the optical plane.

Measurements of small intensity changes in the partially blocked beam as the beam is traversed across the nozzle and observation of the illumination of small dust particles across the face of the nozzle indicate that the face of the nozzle is parallel to the optical plane to within .001 radians.

The distance z from the nozzle to the optical plane is measured with a micrometer attached to the experimental tank and contacting a plate bolted to a part of the nozzle inlet line. The zero level on the micrometer is measured by lowering the nozzle into the light beam. When the intensity of the blocked beam falls to half of its full intensity, the axial position of the nozzle is zero. Nozzle positions above that can be measured to an accuracy of .004 cm, or .01 diameter.

The nozzle position zero has been measured repeatedly throughout the experimental program, and it does not drift as long as the operating experimental tank pressure remains constant. When the tank operating pressure is changed, bulging of the tank top produces a zero shift of approximately .25 mm/atm.

3.2 Gas Delivery System

The gas delivery system encompasses equipment which supplies the four gases, nitrogen, nitric oxide, oxygen, and ozone to the experiment. Caltech and Linde high purity dry grade nitrogen comprise the bulk carrier gas of the experiment, and Matheson and Linde technical grade (98.5% pure) nitric oxide cylinders are used. An ozonizer converts bottled oxygen to ozone,

which is then stored briefly in a special ozone cylinder. The ozone is next diluted with nitrogen and pressurized to the desired delivery pressure in preparation for the experimental run. An exhaust system empties the experimental tank after each run and partially absorbs noxious gases used in the experiment.

Gas cylinder supply lines for nitric oxide and nitrogen are standard except for a special corrosion resistant gas regulator on the nitric oxide line. Corrosiveness of the nitric oxide dictates that valves, tubing, and tube fittings exposed to it be of stainless steel, and that an oxidant resistant material such as viton be used for all exposed O-rings. Although NO does not absorb light at 2537 Å, trace amounts of the impurities N_2O_3 and N_2O_5 attenuate the light beam passing through the tank. A partial pressure of .14 atm nitric oxide corresponds to a practical maximum of nitric oxide concentration. This pressure is associated with enough impurity to attenuate the optical beam to 60% of its pure nitrogen intensity and represents the minimum acceptable signal level for good measurement.

The ozone line is the most difficult part of the gas delivery system to design and maintain. Ozone concentration decays in a confined area at an exponential rate proportional to the surface-to-volume ratio of the enclosure and a constant characteristic of the surface material (Ref. 34, 35). Aluminum, glass and teflon are preferred for having extremely low constants; brass, most plastics, and hydrocarbon oils are unacceptable. Thus, everything in the ozone line and nozzle is aluminum, glass or teflon, except for a

few stainless steel fittings, valves, and screens in the nozzle line. In addition, to remove all traces of grease, everything exposed to ozone is thoroughly washed with xylene, acetone and methanol in order. Because of the precautions taken, the ozone decomposes at a rate of only a few percent per hour even in sections of small diameter tubing.

The ozonizer produces .75 liters of 2% ozone in pure oxygen in 10 minutes at a total pressure of 2 atm. Inside the ozonizer a 15,000 volt discharge across the oxygen produces the ozone. The percentage of ozone in the oxygen is dependent on the residence time of oxygen in the ozonizer and thus sensitive to the flow rate, which is controlled by a valve in the ozone cylinder. The oxygen and ozone mixture passes through a check valve and into the ozone storage cylinder.

A diagram of the ozone storage cylinder appears in Figure 5. It is a large cylinder carefully bored to a smooth inside diameter of $15.875 \pm .01$ cm. A piston rides through the center of the cylinder to separate the ozone-nitrogen mixture below from the reference nitrogen pressure set above. A thin rod attached to the piston passes through a seal in the top of the cylinder to the outside. The purpose of the rod is solely to indicate the piston position. A back-up ring behind the piston prevents its jamming in the cylinder, and pressure differences across the piston produce all motion. A spring loaded teflon ring produces a good seal between the piston and cylinder without lubrication and without causing a massive friction buildup.

Pressure in the cylinder is controlled by two valves above the piston, one leading to the nitrogen regulators and the other leading to the exhaust line. When ozone is filling the cylinder, the valve to the nitrogen line is closed, and the valve to the exhaust acts as a throttle to control the ozone flow rate. When the cylinder needs to be pressurized, the nitrogen line valve is completely open and the exhaust valve is either closed or slightly opened to bleed a small flow through the cylinder.

Three tubing lines enter the ozone portion of the cylinder. Ozone enters the cylinder through a check valve on one line. A safety relief valve prevents backflow and dangerous pressure build-up in the ozonizer itself. A second line leads to a stainless steel differential pressure gauge and pressure manifold. A side connection on the pressure gauge line leads to the nitrogen line and permits the introduction of nitrogen to the oxygen and ozone mixture. The third line is the nozzle inlet line. It leads through the ozone cell, where the ozone concentration is measured, through the nozzle solenoid and metering valves above the experimental tank, and on to the nozzle.

3.3 The Experimental Tank

The fluid dynamics of primary interest to this investigation take place in the experimental tank, a large vessel almost 2 m. high and .5 m. in diameter. It consists of two joining cylindrical sections, a stainless steel base of 43 cm inside diameter by 117 cm high, and a steel bell jar 39 cm inside diameter by 52 cm high on

top. Including window openings, instrumentation ports, and a transitional plate which connects the two vessels, the total volume is 238 liters. A pressure tap and a nitrogen-nitric oxide filling line lead to one instrumentation port on the shock tube section; a large diameter line to a mechanical roughing pump leads to another.

The steel bell jar was previously used by Tombach (Ref. 36) in his investigation of the spreading rate of axisymmetric jets. Two of four window mounts are used in the experiment, one with a quartz window through which optical measurements are taken, and the other with a shatter-proof plexiglass window for viewing of the nozzle. The nozzle inlet line enters the tank through the center of the top plate. Guided by a series of bushings along the inlet tubing, the nozzle can be adjusted over a 12 cm range above the optical beam plane of the experiment. The nozzle position measuring micrometer is attached to the top plate of the tank.

The experimental tank and associated tubing system is exposed to a number of corrosive gases. Nitric oxide is only mildly corrosive. When exposed to oxygen or ozone, however, it forms NO_2 and smaller amounts N_2O_3 and N_2O_5, which are more corrosive. In the presence of water these oxides of nitrogen produce nitric and nitrous acids, which are highly corrosive. Keeping even traces of atmospheric water vapor out of the tank proves helpful in maintaining equipment. Also, as some oxides of nitrogen, ozone, and oxygen are strong oxidizing agents, removing all traces of nonoxidation resistant grease and oil is important. O-rings resistant to the above gases are also necessary.

Aluminum, which forms a protective oxide coating, stainless steel, glass, teflon and viton are preferred materials, Brass tarnishes, and the steel bell jar tends to form a rust coating, but both are safe in large structural members which are not likely to corrode into each other. Quartz coated front surface mirrors survive very well in the toxic atmosphere.

Delicate pressure gauges present a more serious concern, with corrosive gases because they can corrode internally and produce systematic measurement errors without any outward sign of damage. A series of five mechanical pressure gauges are used in the experiment, a Wallace and Tiernan 0-25 mm Hg absolute gauge, a Burton Manufacturing Company 0-15 psia gauge, a USG 0-60 psig gauge, a 0-200 psig Heise gauge, and a 0-200 cmHg absolute Kollsman Instrument Corp. gauge. The gauges are protected from the corrosive experimental gases by a stainless steel differential pressure gauge placed between the pressure gauge manifold and the tank.

Recirculation of gas in the tank from the nozzle to the tank bottom and finally back into the jet itself limits the running time of experiments. Figure 6 shows the optical beam intensity measured at a fixed point in the jet and plotted against time for a jet Reynolds number of 32,000. When the nozzle solenoid is opened, the beam intensity immediately begins dropping from its unattenuated valve. After approximately 1.5 seconds it reaches a steady value indicative of a steady, established jet profile, and it holds the value for approximately 6 seconds. Slow reactions between oxygen, ozone,

and oxides of nitrogen begin to produce N_2O_3, which does absorb ultraviolet light, after several seconds. When the reacting gas cloud circulates up the sides of the tank to the level of the optical beam, it sharply attenuates the signal. Thus in this case, the time available for profile measurements begins 1.5 seconds after the nozzle opening and ends 7.5 seconds afterwards; the traversing carriage motor speed is adjusted accordingly. The first measurement taken for each different set of jet parameters considered is a determination of the steady state jet conditions; steady jet times vary from 3 to 7 seconds in the cases considered.

3.4 The Optical System

The optical system is designed to make the two primary ozone concentration measurements and represents the heart of the entire experimental apparatus. The optical system schematic, Figure 7, shows four arms of the system spreading out from a beam splitter. One arm contains a mercury lamp light source, and a second one holds a photomultiplier tube to monitor light intensity. One of the other two arms leads to the ozone cell, which monitors nozzle inlet line ozone concentration, and the other effects the measurement of the ozone concentration profile in the jet.

The light source for the experiment is a low pressure mercury lamp, Pen-Ray model 11 SC-1C, and the opening in the shield over the lamp is a pin hole .5 mm in diameter. The lamp gives high intensity light, drifts reasonably little, has a reasonably low noise level, and radiates most of its energy at 2537 Å, which is the ultraviolet wavelength used for all absorption measurements.

The lamp needs a high starting voltage (1000 V), but once running it has a low impedance and only requires a current of 10 to 15 milliamps. Two power sources are used in the experiment. The first is an AC power supply produced by the Pen-Ray company and recommended for the lamp. It enhances the stability of the lamp, reduces the lamp intensity drift to less than 5% per hour, and is used for time-averaged measurements of nozzle inlet ozone concentration. However, the AC source produces a 120 Hz flicker to the lamp intensity which significantly increases the noise level in the time and space resolved measurements of the jet ozone profile. A DC current source consisting of a regulated high voltage DC power supply and a 100 K load resistor produces a steady beam intensity for the profile measurement. Five minute pauses between power supply changes have proved sufficient to allow lamp intensity transients to settle.

All lenses, windows, and the beam splitter must be fabricated of u. v. quality quartz to transmit light at 2537Å. One surface of the beam splitter and both surfaces of the .75 mm focussing lens and the experimental tank optical window have anti-reflection coatings to reduce intensity losses from reflection at 2537Å. The reflecting surface of the beam splitter is coated to give 50% transmission at 2537Å. The band pass filter for the experiment can be adjusted for 20% transmission at 2537Å with a 134Å bandwidth.

The band pass filter was actually moved from the position shown in Figure 7 to in front of the light source for most of the

experimental runs discussed. A curtain covers the entire optical table to eliminate stray light from the room, and light shields and apertures block all light not in collimated beams. Light radiated from reacting ozone and nitric oxide (Ref. 37) presents a concern in moving the band pass filter, but the photomultiplier is sufficiently removed from the jet that the effect can not be detected. Moving the filter has made it easier to remove when aligning the system with a helium-neon laser, and the change has made the photomultiplier tube easier to shield from stray light.

The photomultiplier tube is an EMI model 9783B optimized for use with ultraviolet light. Ozone concentration profiles are measured with an overall voltage across the tube of 800 to 850 volts, which produces a quoted sensitivity of 200 a/lm. A two-stage operational amplifier preamp converts current from the tube to DC voltages of the order of 1 volt with a 30 ohm output impedance.

The ozone cell is located in the optical system arm opposite the mercury lamp. It contains a quartz viewing window and an internal quartz coated front surface mirror. A splitter plate 1.27 ($\pm$ .013) mm thick separates the window from the mirror, and spring loading the mirror against the window prevents any internal slippage. To prevent window breakage under high pressure conditions the window opening diameter is limited to .32 cm.

Estimating background radiation reflected from the cell window requires careful consideration. Light intensity coming from

the direction of the ozone cell is composed of the signal, which passes through the cell and reflects from the front surface mirror, and the background, which reflects directly off the quartz window without passing through the cell. To estimate the reflection coefficient for the cell front, the full beam intensity, I_o, from the ozone-free cell is first measured. Then an ozone-oxygen mixture is introduced to the cell with a fixed percentage ozone. As the total pressure of the mixture is increased by pressurizing the ozone storage cylinder, the intensity reflected from the cell, I, decreases from the known increase of ozone concentration. The absorption formula is

$$\ell n \frac{I_o - I_{bk}}{I - I_{bk}} = \alpha N_{O_3, \text{inlet}} w \qquad (3\text{-}5)$$

when I_{bk} is the unknown background intensity, α is the absorption coefficient for ozone, w is the absorption width (twice the splitter plate or .254 cm), and $N_{O_3, \text{inlet}}$ is the ozone concentration in the nozzle inlet line, which is a constant fraction of the total pressure. The proper choice of I_{bk} produces a linear dependence of $(I_o - I_{bk})/(I - I_{bk})$ on cell pressure when plotted on semilog paper. The reflection coefficient is thus evaluated as

$$I_{bk} = .103\ I_o \quad . \qquad (3\text{-}6)$$

The arm of the optical system which passes through the experimental tank is by far the most difficult design of the experiment. As indicated in Figure 7, the light path goes from the beam splitter to a 45^o front surface mirror on the traversing carriage,

through the limiting aperture attached to the tank side of the carriage, through the tank to an internally mounted front-surface mirror and back upon itself. Major problems come from the needs of temporal and spatial resolution. The beam must sweep the entire width of the jet in the 3 to 7 seconds of steady state operation of the jet. The beam has a cross section .25 mm wide and .50 mm high, and the half meter tank width requires that the beam remain collimated over a 1 meter path length while the carriage is in motion. The signal level produced by a lens and mercury lamp is very low, particularly in this arm of the optical system. A typical light intensity is of the order of 20,000 photons/millisec and is too low to affect the overall chemistry of the jet. No ultraviolet lasers were available for the experiment.

Several considerations contribute to the traversing carriage design. First, virtually all vibration and rotation of the carriage during traversing must be suppressed; otherwise maintaining alignment is impossible for so sensitive a system. Four linear bearings on two hardened shafts support the carriage. The traversing direction must be precisely aligned with the light beam from the beam splitter to hold the intensity maximum of the beam directly on the collimating aperture. The light returning to the photomultiplier tube is always that light contained in a path perpendicular to the back tank mirror and passing through the collimating aperture. Any alignment shift of the beam during traversing motion produces an intensity variation with beam position, which has an undesirable effect on signal-to-noise ratio.

A teflon anti-backlash nut connects the traversing carriage to a high helix screw, which is in turn connected to a reversible DC motor. A potentiometer geared to the high helix screw provides a voltage increasing linearly with carriage position. Backlash considerations dictate that measurements be taken while the carriage traverses in only one direction although the observed backlash is quite small.

The background intensity measurement for the tank arm is considerably easier than that for the ozone cell. All solid surfaces are sand blasted, covered with a nonreflecting finish and usually mounted at an oblique angle to the beam. The tank window is anti-reflection coated and mounted at an 85^{o} angle to the beam so that even small reflections from the coatings pass out of the optical plane. Thus, measuring the background intensity simply involves moving the mirror carriage over to block the beam with the window cover. The carriage is left in the beam blocked position after each measurement, and a shutter blocks the ozone cell beam after each ozone concentration measurement.

The two signals from the optical system are recorded on a digital recording system designed by Prof. Donald Coles in 1971. It is a mobile analog-to-digital converter interfaced to a synchronous digital tape recorder and controlled by GALCIT logical circuitry. When used in a 2 bytes/word mode, the a/d converter converts $\pm$ 10 volt signals to a 12 bit binary code with a resolution of approximately $\pm$ .005 mv. Data channels 0 and 1 are used in this experiment, and the tape recorder runs at a fixed rate of 30,000

bytes/second.

The mirror carriage potentiometer signal from the optical system connects directly to data channel 1. The carriage position appears in digital code on the analog-to-digital converter display when a sample button is pushed on the panel. The intensity signal leads through an oscilloscope and a digital volt meter before connecting to data channel 0 on the a/d converter. Time averaged intensity measurements from the ozone cell and the background intensity measurements are recorded directly from the digital volt meter. Profile measurements are written continuously for a preset number of data tape records over the traversing time of the motor.

4. THE EXPERIMENTAL RUN PROCEDURE

The compilation of approximately 150 ozone concentration profile measurements for jets exiting from the contoured nozzle under various combinations of experimental parameter values comprises the primary data source of this project. The procedure followed for each run developed through about 200 preliminary runs with various other nozzles and in varying stages of sophistication.

4.1 The Steps through an Experimental Run

Briefly the experimental procedure runs in five steps:

1. Preparing the experimental tank
2. Preparing the ozone mixture for the run
3. Measuring the jet ozone profile
4. Repeating the measurement of ozone concentration in the nozzle inlet line
5. Checking the jet Reynolds number and velocity.

The entire procedure, including the exhausting and pumping down of the experimental tank, requires approximately one hour for each run.

Preparing the tank involves several tasks. Before each run the tank is pumped down to 300μ Hg to remove contaminants from the previous run. Then the partial pressure of nitric oxide is set, usually in the range of 0 to .14 ($\pm$ .005) atm as measured on the differential pressure gauge. Then nitrogen is added to produce a mixture at the desired total pressure, usually 1.34 or 4.06 ($\pm$ .01) atm. Gas compression during the tank filling process heats the gas, and a five minute wait is necessary to reach thermal

equilibrium. The room temperature is also recorded; it varies from 20°C to 23°C for most of the experiments. Also at this step the nozzle is adjusted to within .01 diameter of the desired axial station for the run.

The second step involves the preparation of the ozone jet. The first task is to measure the intensity of light from the ozone cell in the nozzle inlet line with no ozone present; this gives an I_o. Next the ozonizer produces a supply of 2% ozone in oxygen as quickly as possible. Nitrogen is then added to dilute the ozone, and the ozone cylinder is adjusted to the desired delivery pressure. The resulting mixture is generally 80 to 90% nitrogen. After a bleeding of the inlet line to insure that the gas in the ozone cell is representative of the cylinder mixture, a second measurement of the light intensity from the ozone cell determines the absolute ozone partial pressure in the inlet line. A line pressure measurement determines the fraction of ozone in the gas; the relative concentration of ozone is preserved through the nozzle expansion and determines the ozone concentration at the nozzle. Although the ozone nozzle concentration can be measured to $\pm$ 3%, the process for preparing the mixture is sufficiently crude that the actual value can differ from the desired value by 20% to 30%. The ozone cell arm of the optical system is blocked after this measurement in preparation for the next step.

The best long-time stability of the mercury lamp light source is obtained using an AC power supply for the lamp. The 120 Hz

flashing of the lamp is acceptable for the long-time averaged intensity measurements in the ozone cell, but problems arise in trying to use it for the time and space resolved jet concentration profile measurements. To avoid aliasing problems, the lamp is changed briefly to a DC power supply during the run step. At least five minutes stabilization time must be allowed after the change to DC and again after the change back to AC after the run step.

Data for the profile measurement are written onto two files on digital magnetic tape. The first file contains $I_o(x)$, the intensity through what is to be the jet cross section before the jet is turned on. The second file contains I(x), the intensity measurements attenuated by ozone in the running jet.

The first $I_o(x)$ measurement begins by entering a file I. D. number on the magnetic tape for obvious identification purposes and recording the number in a lab notebook. Next the traversing motor and then the data system recording start. The data system automatically records the data at a fixed rate of 30,000 bytes/second on digital magnetic tape. Data are sampled alternately, the intensity on channel 0 and the position potentiometer voltage on channel 1. Using the analog-to-digital converter on the data system in a 2 bytes/word mode gives a resolution of .005 millivolts in signals of the order of 1 volt. The pairs of words are arranged at 8K bytes/record, and 15 to 25 records are written consecutively during the time that the motor traverses the jet.

After the I_o measurement, the I_o tape file is ended, and the motor is reset to its starting position. The starting position and

traversing speed are predetermined by the need for the beam to sweep the jet width during the few seconds of steady jet operation observed in each case.

An additional measurement of the background voltage on the intensity measurements not due to light passing through the jet cross section must be made at this point. The background, I_{bk}, arises from photomultiplier tube dark current, stray light in the optical system, and voltage offsets in the amplifiers. It averages around .025 volts of a 1 volt unattenuated signal.

The measurement of I(x), the ozone-attenuated beam intensity, is mechanically the same as the measurement of $I_o(x)$ except that the jet is running during the measurement. A new file I. D. number is written on the tape and recorded. The jet and motor are usually started simultaneously, and the data system follows immediately afterward. The jet and motor are turned off only after the data slicer stops recording to avoid including power line surges with the data. The only electronic difference between the I_o and the I measurement is that the nozzle solenoid valve on a separate electric line is powered continuously during the run. All mechanical motions are physically removed from the measuring apparatus, and the only coupling between optical system and jet is through the absorption of ozone in the jet, as desired. The I(x) magnetic tape file is ended; the experimental tank arm of the optical system is again blocked, and the lamp power supply reverts to AC. The measurement of both $I_o(x)$ and I(x) can be made within 30 to 40 seconds.

After a five minute lamp stabilization period a second measurement of ozone inlet line concentration is made as before. The I_o measurement for the ozone cell must wait until after the Reynolds number check, however.

The nozzle velocity and Reynolds number, once set by a needle valve adjustment and the selection of an ozone cylinder driving pressure, has always held steady to within 5%. Its measurement after each run requires little time, however, and permits a reassuring check on the experiment. If the tank pressure has measurably changed during the run, gas is exhausted to reset the starting pressure. The jet is run again into the tank during which time two measurements are made, the delivery pressure of the ozone cylinder and the piston velocity in the cylinder. Piston friction contributes to the few tenths of an atmosphere pressure difference between the running and static cylinder pressures. The piston velocity, u_p, is easily measured by timing the drop over a fixed distance of a rod attached to the piston and extending outside the cylinder.

Both the cylinder bore, d_c, and the nozzle diameter, d, are accurately known to be $15.88 \pm .02$ cm and $.508 \pm .005$ cm. Conserving mass in the system,

$$\rho_{inlet}\, u_p\, d_c^{\,2} = \rho_{tank}\, u_o\, d^2 \quad . \tag{4-1}$$

Thus, the nozzle velocity and Reynolds number are related to the measured parameters,

$$u_o = \left(\frac{\rho_{inlet}}{\rho_{tank}}\right)\left(\frac{d_c}{d}\right)^2 u_p \qquad (4\text{-}2)$$

$$Re = \frac{\rho_{tank}\, u_o d}{\mu} = \rho_{inlet}\, u_p \left(\frac{d_c^2}{\mu d}\right) \qquad (4\text{-}3)$$

where μ is the gas (nitrogen) viscosity at room temperature and ρ is the gas density at the subscribed location.

After the velocity measurement, the ozone cylinder is emptied and flushed with nitrogen and oxygen to remove all ozone. The blank ozone cell intensity is measured to complete the experiment. Gases in the experimental tank are exhausted through a solution of potassium permanganate and sodium hydroxide to absorb some of the noxious gases, and the tank is again pumped down to a vacuum to prepare for the next run.

The weakness of the experimental procedure is that it depends on the consistency of the mercury lamp intensity between measurements, both in the experimental tank and the ozone cell, of I_o and I. In the experimental tank, the intensity measurements outside the jet radius present a means of telling whether there has been an intensity drift between measurements. The intensity seldom drifts during the few seconds between measurements in the tank, and even when it does drift slightly, the intensity at the edge of the jet provides the information necessary to correct for the drift.

Intensity drifts during the 10 minutes between measurements in the ozone cell are more serious and produce most of the error of that measurement. However, the 10 minute delays cause little

difficulty because the average drift is only about 5% per hour. Also, measurements are made before and after the run in reversed order to further reduce the error. The inlet line ozone concentration measured before an experiment generally agrees with the measurement taken afterwards to within 2%; whenever the disagreement has exceeded 6% the entire run has been repeated.

Thus, an entire run consists of filling the tank and setting the nozzle, making ozone, measuring the jet profile, remeasuring the inlet ozone, and checking the jet Reynolds number. The entire record consists of several parameters recorded in a laboratory notebook and two digital data files on magnetic tape consisting of intensity and beam position measurements before and during the running of the jet.

4.2 The Preliminary Organization of the Data

A minimal amount of data reduction is necessary to transform the digital magentic tape records to useable data. Taking data at 15,000 data points per second for an average of four seconds needed to sweep across the jet width gives 60,000 intensity-beam position pairs of data on the magnetic tape record for each traverse. From this record we can make the transformation to a reasonable hard copy record of the experiment as described below.

The computer program which reads the original experimental data tape and transfers all information for the run to a master data tape also produces a preliminary hard copy record of the experiment. It divides the axis of the beam traverse across the width of

the jet into 100 divisions. Beam intensities are averaged into the mean value corresponding to their adjacent position measurements, x. The profiles of each run appear as two 100 element arrays of intensity measurements $I_o(x)$ and $I(x)$, in volts. The position of each measurement in the array corresponds to the position along the traverse at which the intensity was measured and averaged. The initial program also associates with the profile other parameters of the run, i.e., nitric oxide partial pressure, ozone partial pressure at the nozzle, tank pressure, Reynolds number and the distance from the nozzle exit to the traversing plane.

The meaningful form for the light absorption data is $\ell n (I_o/I)$ at each point along the axis of the traverse. The first step in the calculation is to subtract the profile background intensity from the points of I and I_o.

The I_o measurement contains a 3% nonrepetitive ripple and longer distance systematic variations caused by slight misalignments of the beam through the traversing path. Mathematical smoothing by a five-term Fourier series across the I_o data follows the reproducible variations and eliminates the nonrecurrent noise.

To form $\ell n(I_o/I)$ we need only take the natural logarithm of the ratio of the data points I to the series representation value of I_o at each point along the axis. Again, the location of a value in the array of 100 numbers corresponds to its position along the x axis. Data reduced to this extent for a typical run appear in Figure 8.

Measurements in the ozone cell line are combined to compute the nozzle exit ozone concentration, N_{O_3},

$$N_{O_3} = \left(\frac{N_{tank}}{N_{inlet}}\right) N_{O_3, inlet} \tag{4-4}$$

where the subscript "inlet" refers to the nozzle inlet conditions in the ozone cell line, and $N_{O_3, inlet}$ is the absolute ozone concentration in the line as calculated from Equations (3-5) and (3-6).

Reynolds numbers and nozzle velocities are calculated from ozone cylinder measurements as described earlier; the other parameters are the directly measured N_{tank}, N_{NO}, and z/d.

5. THE REDUCTION OF THE ABSORPTION PROFILES

Having measured a light absorption profile associated with a set of experimental parameters as described in Section 4, we next approach the problem of reducing the data to ozone concentration distributions in each case. The data, reduced to the form in Figure 8 as described above, already consist of the logarithm of the ratio of two experimental measurements, $I_o(x)$ and $I(x)$. The data are related to the jet ozone concentration by

$$H(x) = \frac{1}{2\alpha} \ln (I_o/I) = \int_{-\infty}^{\infty} n_{0_3}(r)\, dy \qquad (5\text{-}1)$$

optical axis

Solving the integral equation relates to the classical problem of Abel inversion.

Two to three percent errors in each intensity measurement can produce an uncertainty of nearly ten percent in the logarithmic intensity ratio. Thus, the sensitivity of the results of the mathematical procedures to experimental noise will be a primary concern.

Several features of the ozone concentration profile are evident from consideration of the integrated intensity measurements. In view of the sensitivity to experimental noise inherent in further breakdown of the data to profiles of ozone concentration against radial position, we will consider these results before discussing the results of the Abel inversion procedure.

5.1 The Ozone Concentration Radius

The first obvious feature of data in the form of Figure 8

is the jet ozone concentration radius. This radius is the distance from the jet centerline to the point $\ell n\,(I_o/I)$ falls to .05, a point just above the typical experimental random noise level. In processing data from profiles with very low ozone levels, care was taken to distinguish between the crossing of a mean intensity level and any premature crossing due to noise spikes in the data. In a nonreacting jet, the similarity between mass and momentum transport insures that the jet ozone radius is a measure of the cross-sectional area of the turbulent jet itself. In the reacting jet, the ozone radius falls inside the nonreacting ozone radius because of depletion of ozone by chemical reaction at the outer edge of the jet. In short, the ozone concentration radius is a measurement of the extent of the ozone bearing part of the jet.

Data for the jet ozone concentration radii appear on Figure 11a for the limit of a nonreacting jet. The angle formed by the data with the horizontal axis is the observed spreading angle, because both horizontal and vertical axes are drawn to the same scale. At the axial origin, $z = 0$, the jet radius is always $d/2$.

Several points cause the axisymmetric jet of this experiment to differ from ostensibly similar jets examined in other studies. First, the mixing zone spreads quite rapidly. The jet radius doubles to one diameter by axial distances of 2 to 2.5 diameters downstream. Other measurements of both Pitot surveys and concentration profiles indicate that the potential core of unmixed gas at the centerline of the jet ends at approximately the same

axial position. The shear layer in the initial mixing zone thus spreads symmetrically, inside and out, but the potential core length is shorter than the four diameters generally observed in other works (Ref. 31, 32, 33). Unavoidably thick boundary layers are largely responsible for the discrepancy.

The area of interest in finding unmixed gas from the primary jet extends from the nozzle exit out to five diameters down the jet centerline. Beyond that point observed levels of unreacted ozone are too low to measure well. This is an awkward region of the jet in which to work, particularly with the jet potential core ending at slightly over two diameters. Data are available in literature (Ref. 33) for a quasi-similarity region between the nozzle and the first few diameters downstream, where the shear layer thickness is small compared to the radius of curvature. In this experiment, the mixing layer thickness is less than the radius of curvature only at the station one diameter from the nozzle. At the one diameter station data scatter arises from laminar-turbulent transition causing small shifts in the virtual origin.

Jets do not reach a far field similarity regime until at least ten diameters from the nozzle. Therefore, most of the measurements of this experiment are in a transitional region in which the circumferential shear layer of the initial mixing zone transforms itself into a classical axisymmetric jet at axial distances greater than ten diameters. This geometrical transition, coupled with the thick boundary layers, produces such discrepancies

as the noticeably thinner jet radius at five diameters noted in the Reynolds number 32,000 case.

The ozone concentration radius of the highly reactive jet, Figure 11b, shows a nonspreading ozone profile. The data indicate that the ozone molecules at the outer edge of the highly reacting jet are mixed with and consumed by the nitric oxide in the ambient tank fluid. Within the first diameter, the ozone concentration edge spreads to a total width of 1.5 diameters (±.26) and holds approximately constant out to five diameters, at which point the overall ozone levels are so low that the profile becomes difficult to measure.

5.2 The Ozone Concentration Integral

The second jet characteristic available from the simple measurement of the light intensity ratio is the ozone concentration integral. We directly measure the intensities at points (x), along the beam traversing path, and relate the measurements to the ozone concentration through Equation 5-1. Integrating the measurements over the axis of the traverse we find that the ozone concentration integral is

$$\int_{-\infty}^{\infty} H(x)\,dx = \iint_{-\infty}^{\infty} n_{0_3}(r)\,dy\,dx$$

Jet cross-sectional area

$$= \iint n_{0_3}\,dA \qquad (5\text{-}2)$$

Jet cross-sectional area

In the nonreacting jet, the ozone concentration integral increases with increasing axial distance from the nozzle. Reasons for the increase are best seen from considering the far field region of the jet beyond ten diameters from the nozzle. There, the ozone concentration, like the velocity, scales inversely with z, the axial distance from the nozzle. The jet cross-sectional area for both momentum and mass diffusion increases as z^2 because the corresponding jet thicknesses increase as z. Thus the self-similar ozone concentration integral increases at a rate proportional to z. In the region under consideration, 0 to 5 diameters, the trend is not quite linear but it does increase for the same reasons. The numbers are quite sensitive to jet width, and Reynolds number variations observed in jet width in the nonreacting cases at five diameters produced marked scatter in this ozone concentration integral.

In a reacting jet the ozone concentration integral clearly decreases because the ozone is consumed by chemical reaction. Ultimately, by the end of the reaction zone, the ozone concentration goes to zero and so does the ozone concentration integral. In the reacting case, this integral, normalized to unity at the nozzle exit, approximates the ozone flux as will be described below.

5.3 The Ozone Flux Integral

The ozone flux represents the number of ozone molecules per second passing through the plane of the jet cross section. In a steady state nonreacting jet this number must be conserved. In

a reacting jet, destruction of ozone by chemical reaction causes the ozone flux to decrease.

We cannot evaluate the nonreacting ozone flux with data from this experiment other than to state its value at the nozzle exit, because we cannot measure the product ($n_{O_3} u$) directly. We can measure the time-averaged values of both n_{O_3} and u separately, but we do not know the correlation between them. Since both the ozone molecules and the jet momentum originate at the nozzle and spread at approximately the same rate through the flow, the correlation is likely to be significant.

We can approximate the ozone flux in the highly reacting jet after a careful consideration of the structure of turbulence in the mixing zone. Figure 9 shows two views of a turbulent jet. Figure 9b shows an instantaneous schematic photograph of a slice through the center of our axisymmetric turbulent jet. In the interior of the dotted mixing zone we have unmixed primary gas, gas 1, from the jet exit. Exterior to the mixing zone is the unmixed ambient fluid, gas 2. Along the interface between the two is a diffuse mixing zone, the dots, along which the two gases will mix on a molecular scale. All chemical activity occurs in the molecular mixing zone. The structure shown in the layer is that familiar in two-dimensional mixing layers; it has also been detected in mixing regions of turbulent axisymmetric jets. Lau and Fisher (Ref. 38) have measured this kind of structure at a mean spacing of 1.26 diameters and moving at a convection velocity of 0.6 times the exit velocity.

Vortex-like structures only appear, however, in a reference frame moving with the convection velocity, and care must be taken not to assume actual reverse flow in the laboratory coordinates. Figure 9a shows a typical streak line that an actual fluid particle may follow. Until the particle is overtaken by molecular mixing in a diffusion zone, its momentum can change only through the action of fluctuating pressure gradients in the jet. Some order to the fluctuations associated with large scale turbulent motion produces the patterns noted in Figure 9b. Basically, until the momentum deficit of the ambient fluid diffuses into the fluid particle, it moves downstream at approximately the exit velocity.

In the special case of the highly reacting jet the ozone concentration integral can be approximately related to the ozone flux. In that limit the jet profile becomes independent of the reactant concentration ratio because the observed ozone is present only in locally unmixed gas. The observed ozone density, $\overline{n_{O_3}}$, becomes the unmixed concentration weighted by the average of an intermittency factor,

$$n_{O_3\,\text{highly reacting}} = N_{O_3} J \qquad (5\text{-}3)$$

where J is a local, instantaneous intermittency factor equal to 1 where the fluid is unmixed and has originated from the primary jet and equal to 0 elsewhere. Justification for Equation 5-3 will be discussed at length in Section 6.

As the Schmidt number is close to unity in this experiment,

mass and momentum transfer at the same rate, and the only mechanism remaining to affect the velocity of the conditioned sample is the force of fluctuating pressure gradients in the jet. Fluctuating pressure gradients produce waves in the particle paths shown in Figure 9a, but may fail to produce a net change in the velocity of unmixed fluid. To this extent we can say

$$u_{\text{unmixed fluid}} = \overline{u_0 + u'} = u_0 \tag{5-4}$$

where u_0 is the nozzle velocity, and u' is a perturbation due to fluctuating pressure gradients. We can now relate the ozone flux to the ozone concentration integral. The term $\overline{n_{0_3} u}$ becomes

$$(\overline{n_{0_3} u})_{\text{reacting}} = N_{0_3} u_0 \overline{J} \tag{5-5}$$

The velocity then drops out of the nondimensional integral and we find

$$\frac{\iint \overline{n_{0_3} u}\, dA}{N_{0_3} u_0 A_{\text{nozzle}}} = \frac{\iint N_{0_3} \overline{J}\, dA}{N_{0_3} A_{\text{nozzle}}} = \frac{\iint \overline{n}_{0_3\,\text{reacting}}\, dA}{N_{0_3,\,\text{reacting}}}. \tag{5-6}$$

Data pertaining to this integral are plotted in Figure 12. At least one point is high, that of the 12,500 Reynolds number at one diameter which has a flux of 1.06 times that at the nozzle. The discrepancy can be understood as a combination of experimental noise and the presence of unmixed gas originating in the boundary layer of the nozzle. Unmixed fluid with a momentum deficit from the nozzle boundary layer would violate the assumption of Equation 5-4, but that fluid should also mix before it travels too far from the nozzle exit. If the fluctuating pressure gradients of the jet do

have a net effect of slowing the potential fluid, the data in Figure 12 will be systematically higher than the actual ozone flux.

5.4 The Ozone Concentration Averaged across Jet Cross Section

The cross-sectional average of ozone density is the physical quantity best associated with the ozone concentration integral. Having calculated the ozone concentration integral and knowing the jet cross-sectional area from its relation to the ozone concentration radius, R, in the nonreacting jet, we find the average of the ozone concentration over a cross section by taking the quotient of the two,

$$\overline{n_{0_3}}_{\text{ cross section}} = \frac{1}{\pi R^2}_{\text{nonreacting}} \left(\iint \overline{n_{0_3}} \, dA \right) \tag{5-7}$$

The ratio of reacting to nonreacting average ozone concentration is the best indicator of the effect of reaction on the profile. In that ratio, the jet cross-sectional area term drops out and

$$\frac{\left(\overline{n_{0_3}}_{\text{ cross section}}\right)_{\text{reacting}}}{\left(\overline{n_{0_3}}_{\text{ cross section}}\right)_{\text{nonreacting}}} = \frac{\left(\iint \overline{n_{0_3}}_{\text{reacting}} \, dA \right)}{\left(\iint \overline{n_{0_3}}_{\text{nonreacting}} \, dA \right)} = \frac{\left(\int H(x) \, dx \right)_{\text{reacting}}}{\left(\int H(x) \, dx \right)_{\text{nonreacting}}} . \tag{5-8}$$

Mean values of the averaged ozone concentration in the nonreacting and highly reacting cases appear in Figures 13a and 13b, and the ratio indicated in Equation 5-8 appears in Figure 13c.

Although the averaged ozone concentration is an important indicator of changes in the profile, the average conceals the detailed

physics of the mixing process. By taking an average across the entire jet cross section, we obscure all spatial variations in the time-averaged mixing ratios. Thus, the information needed to construct even the most naive eddy diffusivity model for the mixing process is lost. Further, the average itself in no way distinguishes molecular unmixedness associated with intermittency in turbulent regions of the jet from unmixed regions in the potential core near the nozzle exit.

5.5 The Effect of Chemical Reaction on the Ozone Profile

Having selected the reacting to nonreacting ratio of the ozone concentration integral (to be referred to as "reacting ratio" for brevity) as an appropriate measure of chemical reaction's effect on the entire profile, we can consider the variations of the profile indicated schematically on Figure 2. The vertical axis represents the reacting ratio, the value derived from basic data by Equation 5-8.

The first project is to derive a condition on the chemical reaction speed number beyond which we can assume infinitely fast chemistry. With infinitely fast chemistry we can make the important assumption that ozone and nitric oxide cannot coexist at the same location at any instant of time; this will greatly simplify understanding the problem of mixing and chemical reaction. An axial position of three diameters was selected for primary consideration for several reasons. First, profiles show the effects of reaction strongly at this point, the reacting ratio being .20 to .40

in most experiments run. Secondly, other measurements show that the potential core has disappeared by three diameters, leaving the full time-averaged jet cross section turbulent and characterized by intermittency and mixing interfaces. Finally, enough ozone remains in all cases to produce an adequate signal-to-noise ratio.

Figure 10a shows a projection of data taken at an axial position of three diameters projected on the plane of the concentration ratio axis of Figure 2. As expected from such a projection there is a great deal of scatter; each symbol represents a different Reynolds number case, and each point represents a single experimental run. Figure 10b shows a cross plot of all the points above a concentration ratio of 12.5 ($\pm$ 2.5) against the reaction speed number.

A consideration of figures 10a and 10b shows that reaction speed numbers in excess of 8.0 produce profiles which are independent of further changes in reaction speed number and which are only functions of concentration ratio. Figure 10c shows a plot of the same values as the projection of Figure 10a but under the constraint

$$k N_{NO} \, d/u \geq 8 \quad . \tag{5-9}$$

Under this constraint, the data indicate one further important result, that the profiles are independent of Reynolds number to within experimental error. In the plot of Figure 10c, values for the Reynolds number 5000 case appear to be slightly above the others, but this is simply an artifact of experimental scatter.

Points of Reynolds number 4000 case appear on the opposite extreme of the data spread.

In further examination of Figure 10c, one notices a definite leveling off of the reacting ratio at values of the concentration ratio greater than ten. This regime,

$$k N_{NO} \, d/u > 8 \qquad (5\text{-}10a)$$

$$N_{NO}/N_{O_3} > 10 \qquad (5\text{-}10b)$$

is the precise definition of the highly reacting jet mentioned in Section 2.5. Consideration of data at one, two and five diameters, indicates that these same criteria are appropriate there as well.

More precise experiments may expect a threshold of infinitely fast chemistry to vary somewhat as a function of position. For instance, distances closer to the origin than three diameters allow less time for cumulative effects of chemical reaction to affect the profile. A constraint of the form

$$k N_{NO} \, z/u > 24 \qquad (5\text{-}11)$$

was considered to relate to different axial positions, but the alternative condition was not adopted. To a certain extent, experimental noise in the experiment makes the definition arbitrary. It would eliminate some data at one and two diameters presently included, but the basic trend of the curves shown would change very little. Equations 5-10a and b still appear to be the best definition of a highly reacting jet for this work.

The condition on the concentration ratio has an important

relationship to the presence of unmixed regions in the flow when we have a mixing limited jet. If all regions in the mixing zone of a jet were mixed to some significant extent with ambient fluid, then increasing the concentration ratio of a fast chemical reaction should ultimately consume all ozone in the mixing zone. The presence of a non zero asymptote is indicative of fluid within the jet which is completely unmixed on a molecular level.

Figures 11 through 16 show averages of all experiments run under the appropriate concentration ratio/reaction speed restraints in each Reynolds number case studied for the nonreacting jet, the highly reacting jet, or the ratio of the two. Results are plotted against axial position.

The averages of the ozone across the jet cross section (Figs. 13b and 13c) define the length of the reaction zone in the highly reacting jet limit to be slightly over five diameters. As discussed in Section 2.4, this is much shorter than corresponding flame lengths of turbulent flame studies (Ref. 11, 12, 13) because of the concentration ratios employed. Turbulent flames usually consist of relatively concentrated fuel from the primary jet mixing with a dilute oxidizer, air; the corresponding concentration ratio as defined in this work is less than 1. For the highly reacting jet we consider concentration ratios in excess of 10. From these results we can state that all unmixed primary jet gas is contained in an approximately uniform cylinder 1.5 diameters wide and 5 diameters long.

5.6 Calculation of Radial Ozone Concentration Profile

We next return to the basic data record of the experiment and consider the inversion of Equation 5-1 to compute the radial ozone concentration distribution $n_{0_3}(r, z)$ for each run. Two approaches were originally used to apply the Abel inversion to the data of this experiment. The first is a direct application of an exact solution to the integral equation. Mathematically, the procedure works well, but the results are highly sensitive to experimental noise. A second approach assumes an appropriate family of density profile shapes and uses the integral equation (Eqn. 5-1) to evaluate various parameters of the profiles by comparison to the observed data. The second was the approach used for the full data analysis.

The exact solution to the Abel integral equation is well known. For H(x) defined in Equation 5-1 the radial ozone concentration is given by

$$n_{0_3}(r) = -\frac{1}{\pi}\int_r^\infty \frac{H'(x)}{\sqrt{x^2 - r^2}}\, dx \qquad (5\text{-}12)$$

which can be derived from a solution of Equation 5-1 by Fourier transform techniques. A data reduction procedure based on Equation 5-12 produced good results at the outer edge of the jet, but the solution at the jet centerline showed an unacceptable sensitivity to experimental noise. The centerline concentration computed by Equation 5-12 is very sensitive to the curvature of the function used to smooth the data for H(x) at the center of the profile.

The second approach to applying the Abel inversion

abandons the attempt to calculate the concentration at each point from the data alone. Instead, the following family of allowable ozone profile shapes is assumed:

$$\begin{aligned} n_{0_3} &= n_1 \qquad\qquad , \quad r \le c \\ n_{0_3} &= n_1 \, e^{-(r-c)^2/a^2} \, , \quad r > c \end{aligned} \tag{5-13}$$

where we have three parameters n_1, a, and c. Instead of calculating an entire profile from the data, we look for only three parameters, which determine an approximate size of the profile. In the process we are guaranteed a physically realistic concentration profile, and errors are distributed over the entire profile instead of concentrated at the centerline.

The profile parameters each have physical significance. The centerline density, n_1, is always an important profile parameter. In addition, we know a potential core of unmixed fluid exists near the centerline for the first several diameters axially downstream of the nozzle. Being unmixed, the concentration would be constant out to the core radius, c. The parameter a is the characteristic width of the mixing zone of the profile.

If we transform the assumed ozone concentration profile by the integral equation for the observed data (Eqn. 5-1), we derive a three parameter family of intensity profiles,

$$\begin{aligned} H(x-x_0) &= \int_{-\infty}^{\infty} n_{0_3}(r) \, dy \\ &= 2n_1 a \ \text{Smog fn} \left(\frac{c}{a}, \frac{x}{a} \right) \end{aligned} \tag{5-14}$$

The expression is quite easily handled as a few parameters times a tabulated special function of two variables,

$$\text{Smog fn } \left(\frac{c}{a}, \frac{x}{a}\right) = \sqrt{\frac{c^2}{a^2} - \frac{x^2}{a^2}} + \int_{\sqrt{\frac{c^2}{a^2} - \frac{x^2}{a^2}}}^{\infty} e^{-(r-c)^2/a^2} d\left(\frac{y}{a}\right) ; \; x<c \tag{5-15}$$

$$= \int_0^{\infty} e^{-(r-c)^2/a^2} \, d\left(\frac{y}{a}\right) \quad ; \; x \geq c$$

A standard nonlinear curve fit procudure selects these three parameters, n_1, a, and c and a fourth, x_0, the centerline position of the jet, to minimize the mean square variation of the computed profile from the data. The centerline position calculation is almost completely uncoupled from the other calculations, and will be ignored for the rest of the discussion.

Several problems still remain. The impact of a and c on the computed intensity profile is quite similar. Therefore, a and c appear highly coupled in the full curve fitting procedure, and the two can be mutually in error very easily. Also, in regions near the nozzle, the computed centerline concentrations in potential core regions tend to be 5 to 10% higher or lower than the known nozzle exit ozone concentration. This is certainly due to noise in the profile measurement and presents an unnecessary error in the determination of the concentration profile.

To reduce the coupling of the parameters and to introduce the known nozzle ozone concentration to the calculation, two steps

must be taken. The first is to apply a constraint to the computed concentration profile. The integral of the density over the cross-sectional area of the jet must agree with the ozone concentration integral, which is computed from the integrated intensity measurements as described earlier. The integral of the assumed profile is

$$\iint_{\text{Jet cross section}} n_{0_3}\, dA = \pi n_1 (a^2 + c^2 + \sqrt{\pi}\, ac) \qquad (5\text{-}16)$$

and Equation 5-2 evaluates the integral from the integrated intensity data. This eliminates one of the three degrees of freedom.

The second step is to restrict the concentration profile family to two cases depending on axial distance from the nozzle. Upstream of the end of the core, we demand

$$n_1 = N_{0_3} \quad , \text{ case A} \qquad (5\text{-}17a)$$

the nozzle ozone concentration being known from independent measurement. This leaves a and c free to vary under the constraint of Equation 5-16. Downstream of the end of the core, we let

$$c = 0 \quad , \quad \text{case B} \quad . \qquad (5\text{-}17b)$$

This leaves a and n_1 free to vary. Thus in each case, we have a one degree of freedom fit to the data consisting of two unassigned parameters and one independent constraint.

The end of the potential core is found, by trial and error, to be at about 2.5 diameters downstream of the nozzle. If case

b is assumed upstream of that point, computed values of the centerline density exceed N_{0_3}. If case A is assumed downstream of that point, the computed intensity profiles do not fit the data well.

The actual inversion of intensity to concentration is exact. The assumptions made only introduce additional information to the calculation. As long as the computed intensity curve lies within the error spread of the data, the resulting concentration profile is at least as valid as results of the first approach. Insofar as the constraints and assumptions eliminate physically objectionable features of the profiles and introduce new information to the calculation, the parametric approach to the Abel inversion is far better than the exact solution.

The parametric approach to the Abel inversion does require that the computer be told which of the 100 $\ell n (I_o/I)$ points to weight as part of the absorption profile. If too many points beyond the jet edge are included as data, the computer sometimes sees the random noise in that region as evidence of non-zero ozone concentration. The resulting profile is then incorrectly broadened to include the outer spurious ozone and produces an obviously poor fit to the intensity data. Simply trimming the weighting of regions beyond the jet edge has always produced excellent agreement of computed intensity profile and the data under the one degree of freedom fit.

Figures 14, 15, and 16 display the computed profile parameters by Reynolds number case in the form of averages over

the highly reacting or nonreacting jets plotted against axial position. A number of trends are immediately apparent. First, we have the same Reynolds number independence as noted in the earlier profile averaged data. The jet e - folding radius, a + c, or the radius at which the concentration falls to 1/e of its centerline value behaves qualitatively like the ozone concentration radius. Beyond the end of the potential core, the centerline concentration decreases in the nonreacting case; it decreases much faster in the highly reacting case.

All of these trends appear in Figures 17a, b, c and d which consist of radial ozone profiles drawn for highly reacting and nonreacting jets at each axial station. The profiles are plotted by assuming the profile shape of Equation 5-13. Individual values for each parameter are found by averaging the data of Figures 14, 15 and 16 over all Reynolds numbers at the appropriate axial position and reaction state. Error bars shown represent one standard deviation on each parameter.

5.7 Conclusions from the Reduced Data

At this point we can make several important conclusions about the nature of turbulence in a chemically reacting turbulent jet. First, we find a well defined set of conditions under which a chemically reacting jet reactant profile becomes not only mixing limited (independent of chemical kinetics) but also independent of the concentrations of other reactants in the system. The reactants are

a. $k N_{NO} d/u > 8$

b. $N_{NO}/N_{O_3} > 10$

The former relation identifies a regime where chemical kinetics no longer has a large impact on the profile, and the latter a regime where changes in the excess reactant concentration no longer have an impact. The latter is indicative of gas completely unmixed on a molecular scale within the turbulent mixing zone. The two form a limit called the highly reacting jet.

Second, this region of the mixing zone still containing unmixed gas from the primary jet has limits depending only on the jet geometry. The limiting reaction length and width form a uniform cylinder approximately 1.5 diameters wide and 5 diameters long.

Third, we can answer the question of when a chemical reaction is fast enough to justify critical assumptions on whether the jet is mixing limited. By considering actual measurements of a reactant profile taken as a function of a nondimensional chemical kinetic rate coefficient at a fixed concentration ratio, we arrive at an operational criterion, $k N_{NO} d/u > 8$, for a mixing limited jet. This is a considerably weaker condition than most of those mentioned in other studies (Ref. 39, 40), which have generally compared reaction rates to Kolmogorov scales in the turbulence.

Knowledge of the actual concentration profile shapes at each point in the jet (Fig. 17) provides detailed information missing in the averaged measurements. In particular, the profile shapes

allow us to distinguish between unmixed gas in the potential core of a jet, where its presence has never been doubted, and unmixed gas in the mixing region of the jet. In the next section the nonreacting jet profiles of Figure 17 will be related to the time-averaged mixing fraction of gas from the primary jet. The highly reacting jet profiles of Figure 17 will be related to the probability of finding unmixed gas from the primary jet throughout the mixing zone.

The final conclusion is that Reynolds numbers, based on nozzle diameter and varied from 4000 to 32,000, impart no systematic variations in excess of 10% of the reactant concentrations. Tank pressure changes from 1.34 to 4.0 atm. and corresponding changes in dilution number also have no effect on the profiles. All variations must be inside the experimental error limits, approximately a 10% band across the average profile ozone concentration. The implications of the Reynolds number independence are that the presence of unmixed gas is a property of only the largest scales of turbulence, and that geometry alone controls its distribution.

6. INTERPRETATION OF THE CONCENTRATION MEASUREMENTS

In the previous section, the time averaged ozone concentrations throughout the flow field of the axisymmetric jet, in cases with and without chemical reaction, have been calculated. The point measurements are time averaged over a period, τ, long compared to turbulent fluctuations,

$$\bar{n}_{0_3}(r, z, N_{NO}/N_{0_3}) = \frac{1}{\tau} \int_0^{\tau} n_{0_3}(r, z, N_{NO}/N_{0_3}, t)\, dt \qquad (6\text{-}1)$$

The measurements have been shown to be independent of Reynolds number when the jet is mixing limited. They are presented in graphical form on Figure 17abc and d in two limits, the nonreacting and the highly reacting jet. Figure 17 displays the time averaged ozone concentrations, $\bar{n}_{0_3}/N_{0_3}$ as a function of radial distance from the jet centerline for axial stations of $z = 1, 2, 3,$ and 5 diameters from the nozzle. We will now relate this concentration measurement to the statistics of mixing in the flow.

6.1 The Definition of Mixing in the Jet

Before we can have any meaningful discussion of mixing in any kind of flow situation, we need a clear definition of mixing itself. To mix is defined in general usage as to unite or blend into one mass. For technical discussion we need a fundamental number defined throughout a flow field which will tell us to what extent this mixing process has occurred.

In principle we can identify every molecule in a nonreacting jet by its place of origin; all gas in the mixing zone was originally a part of either the primary jet or the ambient fluid. In the classical sense of a point density measurement we can define two number densities at every point in a flow as follows:

n_1 = the number of molecules/cm^3 originating from the primary jet; and

n_2 = the number of molecules/cm^3 originating in the ambient fluid.

In the general case of a reacting mixing zone, we must consider a third group of molecules, the products of chemical reaction, which may not obviously fall into either gas 1 or gas 2. Nevertheless, we will extend the definitions of gas 1 and gas 2 to include all species in a chemically reacting mixing zone. The resulting reacting number densities will be equivalent to the corresponding number densities in a nonreacting mixing zone under similar conditions.

Formally we can assign product species, NO_2 and O_2, according to their parent reactants, O_3 and NO, which are directly associated with gas 1 or gas 2. To clarify the arguments, we will imagine that every nitrogen atom in the tank, in both the N_2 and NO molecules, is the isotope N^{14}; the only isotope of nitrogen allowed in the primary jet will be N^{15}. We then denote molecules in the mixing zone as follows:

gas 1: any molecule not containing the isotop N^{14}

($N_2{}^{15}$, O_3, O_2)

gas 2: any molecule containing the isotope N^{14}

($N_2{}^{14}$, NO, NO_2)

Under these terms the chemical reaction consists of the transfer of one oxygen atom from ozone of gas 1 to nitric oxide of gas 2; no molecules change status.

On the basis of the above definitions of gas 1 and gas 2 we define the molar mixing fraction, η, as

$$\eta = \frac{n_1}{n_1 + n_2} = \frac{n_1}{N_1} \qquad (6\text{-}2)$$

where $N_1 = N_2$ is the total number density in the gas of the jet. The value of η represents the fractional concentration of gas from the primary jet, defined to be independent of chemical reaction and normalized to vary from zero in unmixed ambient gas to unity in unmixed primary gas.

The intention of the remainder of this chapter is to relate the statistical properties of η to the ozone concentrations measured.

6.2 Relationship of Local Ozone Concentration to η and N_{NO}/N_{O_3}

Given the molar mixing fraction, $\eta(r,z,t)$ and given the reactant concentrations in the unmixed fluid, we can predict the concentration of unreacted ozone at that point. Our intent will be to use the concentration of ozone as a measure of η in the jet.

Several assumptions are necessary. The most important assumption is that reactant profiles are always in chemical equilibrium. This restricts the discussion to a set of data in which the reaction speed number exceeds 8, as discussed in section 5.5.

If we cannot assume that the chemical reaction goes immediately to completion, the ozone concentration at a point is a complicated function of the previous mixing history of the fluid in question. We furthermore must assume that the diffusion coefficients are the same for each species.* If we have equal binary diffusion coefficients, all the chemical species in the primary fluid (N_2, O_2, O_3) diffuse in the same proportions. Reactants and products will then be distributed simply by the mixing fraction, η, and considerations of the stoichiometry.

For example, in the nonreacting jet a one-to-one correspondence exists between the ozone concentration and η. The concentration of ozone in unmixed gas is N_{0_3}. In a sample of mixing fraction η, we have (ηN_{0_3}) molecules/cm^3 contributed from the primary jet. No ozone is contained in the (1-η) fraction of gas from the ambient fluid, and no chemical reaction reduces the ozone concentration of the original primary jet fraction. Thus

$$\frac{n_{0_3}}{N_{0_3}\ \text{nonreacting}} = \eta \quad . \tag{6-3}$$

We now consider that the chemically reacting jet proceeds in two steps, the mixing of the reactants and the chemical reaction to completion. By the same arguments used to derive Equation 6-3, we can calculate initial reactant concentrations. Then we consider the stoichiometry,

*At one atmosphere the diffusion coefficients for O_3, NO, O_2 and N_2 through nitrogen are all within 5% of .15 cm^2/sec.

$$O_3 + NO \rightarrow O_2 + NO_2$$

which indicates that one molecule of NO consumes one molecule of O_3 until only the species locally in excess remains. Thus

Initial O_3 concentration $= \eta\ N_{0_3}$ molecules/cm^3

Initial NO concentration $= (1-\eta)\ N_{NO}$ molecules/cm^3

Excess O_3 concentration $= \eta N_{0_3} - (1-\eta) N_{NO}$ molecules/cm^3

If $(\eta N_{0_3} - (1-\eta) N_{NO})$ is negative, then nitric oxide is the excess species. Thus we find ozone when

$$\eta > \eta_o = \frac{N_{NO}/N_{0_3}}{1+N_{NO}/N_{0_3}} \quad . \tag{6-4}$$

Consequently, the relative ozone concentration is given by

$$\frac{n_{0_3}}{N_{0_3}} = p\ (\eta,\ N_{NO}/N_{0_3}) \tag{6-5}$$

where

$$p = \eta - (1-\eta)\ \frac{N_{NO}}{N_{0_3}} \qquad \text{for } \eta > \eta_o$$

$$= 0 \qquad \text{for } \eta \leq \eta_o \quad . \tag{6-6}$$

The proposition that the concentration of all of gas 1 can be tracked by observing the presence of ozone is crucial for the preceding derivation of Equation 6-5. A more formal proof of the proposition and an alternative derivation of Equation 6-5 from the fundamental species conservation equations can be found in Appendix A.

The function p is linear and ranges from 0 below the critical value of η_o to 1 at $\eta = 1$. Figure 18 shows p plotted with sample values of N_{NO}/N_{0_3} as parameters.

An important limit of p occurs when N_{NO}/N_{O_3} goes to infinity. As

$$N_{NO}/N_{O_3} \rightarrow \infty \ , \quad p(\eta) \rightarrow J(\eta) \tag{6-7}$$

where

$$J(\eta) = 1 \quad \text{for } \eta = 1 \tag{6-8}$$
$$= 0 \quad \text{for } \eta < 1$$

In this limit, p behaves like an intermittency function in the jet. Physically, when we put a large enough excess of NO into the jet, the ozone is consumed anywhere mixing occurs.

6.3 The Definition of "Unmixed" in the Jet

A definition of "unmixed" in literal terms is not appropriate. Gas in the turbulent jets of this study contains approximately 6×10^{19} molecules/cm^3; to define unmixed primary jet as a mixture containing no molecules whatsoever from the ambient tank is neither useful nor reasonable for this study. The kinetic theory of gases indicates that diffusion of trace amounts of gas occurs almost immediately throughout the entire region of the jet. However, mixing levels in the parts per billion range are simply too low to affect any reactant concentration in this experiment, and very low mixing levels cannot be distinguished from ideally unmixed gas.

The distinction between mixed and unmixed gas may be primarily a semantic problem, but the issue becomes important for this study when a substantial amount of the data presented consists of what we would like to describe as conditional samples of unmixed gas. We must have a clear understanding of such expressions as

"$\eta = 1$" in the definition of $J(\eta)$ (Eqn. 6-7) in the context of the experimental measurements under discussion. The limits of experimental resolution must determine what we call mixed and what we call unmixed.

Equation 6-5, relating the observed ozone concentration to the mixing fraction and the concentration ratio, provides a method for determining a reasonable criterion for unmixedness in terms of the effect of mixing on chemical reactant concentrations. To discuss mixing meaningfully in the context of a chemical reaction, we can classify local mixtures of gas into one of three categories by considering the equilibrium ozone concentration.

The three classifications of mixtures are defined in Table 2.

Category	Condition	Included Mixing Fraction
1	$n_{O_3}/N_{O_3} = 0.$	$0. \leq \eta \leq \eta_o$
2	$0. < n_{O_3}/N_{O_3} \leq .9$	$\eta_o < \eta \leq \eta_1$
3	$.9 < n_{O_3}/N_{O_3} \leq 1.$	$\eta_1 < \eta \leq 1.$

TABLE 2

Equation 6-4 defines the first dividing mixing fraction, η_o, as a function of the concentration ratio. If we substitute the condition for the threshold of ozone concentration between category 2 and category 3 into Equation 6-5, we find

$$\eta_1 = \frac{.9 + N_{NO}/N_{O_3}}{1 + N_{NO}/N_{O_3}} \qquad (6\text{-}9)$$

Each category represents a characteristic ozone concentration, and the included mixing fraction in each case is dependent upon the concentration ratio. Category 1 represents mixed gas containing no ozone at all. Category 2 represents mixed gas containing ozone at levels substantially lower than N_{0_3}. Small changes in the concentration ratio produce proportionally large changes in the observed ozone concentration for mixtures in this category. Category 3 represents gas which may have mixed and reacted to some extent, but is not easily distinguishable from ideally unmixed and unreacted gas.

Category 3 defines unmixed gas for this study. It is unmixed in the sense that neither dilution nor chemical reaction has substantially reduced the ozone concentration below its initial value at the jet exit. In this experiment concentration ratios did not exceed 50. At that level

$$\eta_1 = .998 \quad . \tag{6-10}$$

Thus, to the highest resolution of these experimental mixing measurements, any mixing fraction $\eta > .998$ appears unmixed.

It is worth pointing out again that Equation 6-5 always determines excess ozone and that both mixing fraction and concentration ratio must always be stated to form a well posed question of the excess reactant concentrations. Equation 6-10 represents a limit of the highest concentration ratio and, therefore, the highest mixing resolution employed. The fact that lowering the concentration ratio by a factor of 5 does not significantly change any of the

observed ozone concentration profiles indicates a low probability of observing mixing fractions in Category 2 for the corresponding concentration ratios.

6.4 Relationship of the Measured Ozone Concentration to the Mixing Fractions and Concentration Ratios.

Substituting Equation 6-5 into 6-1, the time averaged point ozone concentration is

$$\frac{\overline{n}_{O_3}}{N_{O_3}} = \frac{1}{\tau} \int_0^\tau p\,(\eta(t))\,dt \quad . \tag{6-11}$$

Several limits are of direct interest.

In the nonreacting case, $N_{NO} = 0$. Then at each point in the jet

$$\frac{n_{O_3}}{N_{O_3}} = \eta$$

and the time average becomes

$$\frac{\overline{n}_{O_3}}{N_{O_3}}_{\text{nonreacting}} = \frac{1}{\tau} \int_0^\tau \eta\ (t)\ dt = \overline{\eta} \tag{6-12}$$

The nonreacting ozone concentration profile is identical to the unconditioned average of the molar mixing ratio across the reacting jet.

In the highly reacting limit we have a highly conditioned sample. Substituting Equation 6-7 into Equation 6-1,

$$\frac{\overline{n}_{O_3}}{N_{O_3}}_{\text{highly reacting}} = \frac{1}{\tau} \int_0^\tau J\,(\eta(t))\,dt = \overline{J} \tag{6-13}$$

is the average of the intermittency function J. The highly reacting concentration profile is then the profile of the average concentration of unmixed gas from the primary jet.

At intermediate values of the concentration ratio we find average ozone concentrations falling between the above limits. As we increase the ratio from zero, more and more ozone is eliminated from the mixing zones of the jet and is thus not included in the averages. Figure 19 shows a schematic plot of $n_{0_3}(t)$ flowing past a point in the jet where ozone concentration is measured. Repetitions of the same sample for three concentration ratios are shown, $N_{NO}/N_{0_3} = 0,\ 1,\ 50$. In the first sample we have $n_{0_3}/N_{0_3} = \eta$. In the second we have partial reaction by Equation 6-5, and in the third we have an intermittency sampling (Eqn. 6-7).

6.5 Relationship of the Measured Ozone Concentration to the Mixing Distribution Function in the Jet.

As a long-time average becomes equal to an ensemble average over all possible values of η at a given point in the jet, we can formulate the values of the ozone concentration measurements with the probability density function for the jet mixing.

Formally, we can define a function $f(\eta)$ where

$f(\eta)d\eta$ = Probability {the molecular fraction, η, of gas from the primary jet in a given sample is between η and $\eta + d\eta$}.

This distribution function completely describes the mixing at every point. In general it varies with position in the jet as the character

of the mixing changes. As the concentrations of chemical species in the flow are related to the mixing fraction η, appropriate moments of the mixing probability distribution function completely determine the mean reactant concentrations for given initial concentrations. In the case of the observed ozone concentration, we weight the instantaneous ozone concentrations by the probability of observing the corresponding mixing fractions, or averaging

Equation 6-5

$$\bar{n}_{O_3} / N_{O_3} = \int_0^1 p(\eta)\ f(\eta)\ d\eta \qquad (6\text{-}14)$$

Substituting 6-6 into 6-14,

$$\bar{n}_{O_3} / N_{O_3} = \int_{\eta_0}^1 \left[\eta - (1-\eta)\ \frac{N_{NO}}{N_{O_3}} \right] f(\eta)\ d\eta \qquad (6\text{-}15)$$

represents the observed point ozone concentration explicitly as a function of the concentration ratio and the mixing probability distribution.

The usual method of experimentally determining the mixing probability density function is to observe the discrete probabilities that η is within a small division $\Delta\eta$ of the full range of values from 0 to 1 that η may assume. Typically a point concentration probe at position $\vec{x}$ produces a signal $\eta(t)$, similar to that shown in Figure 19, which can be divided into a large number of points η_i. Discrete probabilities are calculated by counting the number of points of the set η_i which fall into each of the divisions $\Delta\eta_j$.

As the number of arbitrary divisions ($\Delta\eta_j$) is increased, well-behaved data will converge to a constant probability per unit $\Delta\eta$, the probability density. Near $\eta = 1$ and $\eta = 0$ the data for computing the probability density are frequently not well behaved because unmixed gas is observed with a finite probability which is independent of the width of the divisions $\Delta\eta$ containing $\eta = 1$ and $\eta = 0$. A mathematical description of this singularity in the distribution density concentrates the finite probabilities of observing unmixed gas by making them proportional to delta functions, $\delta(\eta)$ or $\delta(1-\eta)$.

In principle this experiment presents an alternative method for computing the same probability density distribution described above from the experimental determination of the time averaged point ozone concentration measurement, $\bar{n}_{O_3}/N_{O_3}(r,z, N_{NO}/N_{O_3})$. The relationship is the solution to the integral equation, Equation 6-15. Unfortunately the data of this experiment does not permit the full solution of Equation 6-15, but a solution can be obtained in the neighborhood of $\eta = 1$. Thus, although the data do not permit the determination of all scales of mixing in the jet, they do permit the calculation of the finite probability of observing unmixed gas and confine the spectrum of "unmixed" mixtures to the unmixed region discussed in section 6.3.

The measurement of $\bar{n}_{O_3}/N_{O_3}(r,z, N_{NO}/N_{O_3})$ could not be obtained explicitly in a form suitable for the solution of Equation 6-15 for two reasons. First, the experimental noise scatter is too large to differentiate the point concentration data meaningfully. We must at least determine the increment in a point ozone

concentration due to a small change in the concentration ratio. The results of Figure 17 represent point ozone concentrations, but they include only two concentration ratios, 0 and a limiting average above 10 for which profiles remain invariant.

The second problem arises from the need to assume chemical equilibrium for this analysis. The maximum heat release requirements on the jet limit the maximum ozone concentration, and thus when the desired concentration ratio is below 10, the nitric oxide concentration must be low. We then have trouble satisfying the requirement of Equation 5-9 for chemical equilibrium. The lack of data makes the curve ill-defined.

A level asymptote from concentrations of 10 to 50 indicates much about the distribution function. The weighting function $p(\eta)$ (Fig. 18) is simply a linear function going from 0 at $\eta = \eta_o$ to 1 at $\eta = 1$. As we increase the concentration ratio continuously from 10 to 50, η_o goes from .91 to .98 with no visible change in the observed ozone density. The only simple distribution with those properties is one with most of the probability concentrated at $\eta = 1$. Then, we assume a distribution of the form

$$f(\eta) = f_0 + f_1 \, \delta(1-\eta) \qquad (6\text{-}16)$$

which is to be valid for mixing fractions near $\eta = 1$ for constants f_0 and f_1. Here we use standard delta function notation to indicate a finite probability of finding unmixed gas and to combine all the continuous mixture probability density into a constant average value. A solution for the two constants f_0 and f_1 is then readily obtained

from Equation 6-15 as

$$\frac{\overline{n}_{0_3}}{N_{0_3}} = f_1 + \frac{f_0}{2\left(1 + \frac{N_{NO}}{N_{0_3}}\right)} \qquad (6\text{-}17)$$

These values are then simply related to the experimental curve. Any slope reasonably measured as a coefficient to a functional trend of

$$\frac{1}{1 + N_{NO}/N_{0_3}} \cong (N_{NO}/N_{0_3})^{-1}$$

is then half of the average probability density for mixtures in the range near $\eta = 1$. The important result, however, is that the asymptotic value at the limiting values of large N_{NO}/N_{0_3} is the probability of finding unmixed gas from the primary jet, or the coefficient of the delta function at the end of the mixing probability density function.

6.6 Summary of the Experimental Interpretations

We have three conclusions relating the radial ozone concentration profiles shown on Figure 17 to molecular scale mixing in the jet. The nonreacting ozone profiles can be interpreted as

$$\left(\frac{\overline{n}_{0_3}}{N_{0_3}}(r,z)\right)_{\text{nonreacting}} = \overline{\eta}\ (r,z) \qquad (6\text{-}18)$$

where η is the average of the molar mixing fraction over all values it assumes at any point (r,z) in the jet. The highly reacting profile is the average of the intermittency function J or the conditioned

time average of the concentration of unmixed gas originating in the primary jet.

$$\left(\frac{\overline{n}_{0_3}}{N_{0_3}}\ (r,z)\right)_{\text{highly reacting}} = \overline{J(\eta(r,z))} \qquad (6\text{-}19)$$

An alternative interpretation of points on the highly reacting jet profiles is that they represent the probability f_1 of observing unmixed gas from the primary jet at each (r,z) in the mixing zone,

$$\left(\frac{\overline{n}_{0_3}}{N_{0_3}}\ (r,z)\right)_{\text{highly reacting}} = f_1 \qquad (6\text{-}20)$$

and hence, it is the discrete probability of observing unmixed gas at the $\eta = 1$ edge of the mixing probability density function.

7. CONCLUSIONS

An optical technique has been developed to study chemical reactions in turbulent flow. This technique has been applied to the ozone-nitric oxide reaction in turbulent mixing in which a turbulent jet containing ozone discharges into a dilute nitric oxide atmosphere. The measured ozone concentration is related to the degree of mixing in the molecular scale (the "mixedness") at all points in the jet.

Experimental findings from a large body of data are presented with particular attention to the determination of the condition for chemical equilibrium in the mixing zone and the effect of Reynolds number on the ozone profiles. In the limit of the highly reacting jet, the measured ozone concentrations are related to the presence of unmixed gas from the jet.

The experimental technique is based on the large absorption coefficient of ozone for ultraviolet radiation. A small cross-sectional beam of Hg light at 2537Å crosses the turbulent mixing zone of the axisymmetric jet, which carries the ozone as it discharges into a tank containing a dilute mixture of nitric oxide and nitrogen. During each run, the beam traverses the mixing zone, and both position and beam intensities are recorded. The assumption of axial symmetry permits the calculation of the time-averaged ozone concentration, $\overline{n}_{0_3}(r, z)$, from the recorded data.

An analysis of the measurement shows that the ozone concentration is directly related to the local fraction of fluid from

the primary jet. The relative ozone concentration of a nonreacting jet measures the time average of the mixing fraction,

$$\left(\frac{\overline{n}_{0_3}(r, z)}{N_{0_3}}\right)_{\text{nonreacting}} = \overline{\eta}(r, z) \qquad (7\text{-}1)$$

When we can justify the assumption that the chemical reaction rate is infinitely fast, we can relate the ozone concentration in reacting jets to moments of the mixing probability distribution. In the limit of the highly reacting jet, we can interpret the time-averaged relative ozone concentration in two ways,

$$\left(\frac{\overline{n}_{0_3}(r, z)}{N_{0_3}}\right)_{\text{highly reacting}} = \overline{J(\eta(r, z))} = f_1(r, z) \qquad (7\text{-}2)$$

where J is an intermittency function defined equal to unity in unmixed primary fluid and zero elsewhere. The value f_1 is the probability of observing unmixed gas from the primary jet. The results obtained with the optical technique described in this work are similar to data which could, in principle, be taken by various types of concentration probes, but the results presented here are derived from very different considerations.

Independent variations of the nondimensional chemical reaction rate and the reactant concentration ratio indicate that an ozone profile becomes independent of the reaction rate when

$$k N_{NO} d/u \geq 8 \quad . \qquad (7\text{-}3)$$

This criterion for chemical equilibrium in the mixing zone is less stringent than previously proposed criteria in which characteristic chemical reaction times are compared to the Kolmogorov time

scales in the turbulence. If the reaction rate satisfies Equation 7-3, we can assume that ozone and nitric oxide coexist only in thin reaction sheets occupying an insignificant fraction of the mixing zone.

The data of the experiment confirm the Reynolds number independence of the molecular mixing process as noted in a number of turbulent flame studies. Test Reynolds numbers, based on nozzle diameter, varied from 4000 to 32,000, and the Reynolds number independence has been verified by independent variations of both density and nozzle velocity.

Increases in the reactant concentration ratio, N_{NO}/N_{0_3}, always drive reaction sheets farther into fluid otherwise occupied by unreacted ozone, but the reaction zones can never be driven beyond the region of molecular mixing. When the reaction ratio becomes large, approximately

$$N_{NO}/N_{0_3} > 10 \qquad (7\text{-}4)$$

ozone profiles become independent of further increases in the concentration ratio, at least to within experimental accuracy. The conditions 7-3 and 7-4 define the highly reactive jet, and ozone concentrations measured in this limit represent ozone contained in unmixed fluid from the jet. In all cases considered, the ozone in the highly reactive jet is confined to a cylindrical volume 1.5 nozzle diameters in diameter and extending 5 diameters downstream of the nozzle exit.

APPENDIX A

The argument leading to Equation 7-5, the basic relation between observed ozone and the local molecular mixing level in the jet, uses the assumption that reactants are distributed proportionally to the molecular mixing fraction. Here we formally derive the same relation through the Schvab-Zeldovich formulation (Ref. 41, 42) for the general species conservation equations to demonstrate that the standard flame sheet model for the mixing of reacting fluids is consistent with the assumption.

We can write the basic conservation equation for the number density n_1 of gas 1 from the primary jet as follows:

$$\frac{\partial n_1}{\partial t} + \nabla \cdot (n_1 \vec{v}) = \nabla \cdot (D \nabla n_1) \qquad (A\text{-}1)$$

In writing the species conservation equation in that form we make several assumptions. We ignore any body forces tending to separate species within the gas (N_2, O_3, and O_2) as well as additional diffusion due to thermal gradients and pressure gradients. In writing the equation for molar concentrations, the velocity $\vec{v}$ should be a mole averaged velocity rather than the usual mass averaged velocity, but the difference is negligible because the jet is almost entirely nitrogen. Also, when we include several chemical species in each gas, we must assume binary diffusion coefficients for the species through nitrogen which are identical and equal to D. Empirical estimates of the binary diffusion coefficients (Ref. 43) for this experiment indicate that the latter is a good assumption.

We can divide Equation A-1 by N_1, the total number density of the jet, to put the equation in the form of the molar mixing fraction

$$\frac{\partial}{\partial t}\eta + \nabla \cdot (\eta \vec{v}) = \nabla \cdot (D \nabla \eta) \qquad (A-2)$$

with boundary conditions

$\eta = 1$ in unmixed primary jet and

$\eta = 0$ in unmixed ambient fluid.

For reacting species within gases 1 and 2, we can write equations similar to Equation A-1 with the same approximations,

$$\frac{\partial n_{O_3}}{\partial t} + \nabla \cdot (n_{O_3} \vec{v}) = - k n_{O_3} n_{NO} + \nabla \cdot (D \nabla n_{O_3})$$

$$\frac{\partial n_{NO}}{\partial t} + \nabla \cdot (n_{NO} \vec{v}) = - k n_{O_3} n_{NO} + \nabla \cdot (D \nabla n_{NO})$$

By subtracting, we eliminate the chemical reaction term,

$$\frac{\partial}{\partial t}(n_{O_3} - n_{NO}) + \nabla \cdot ((n_{O_3} - n_{NO}) \vec{v}) = \nabla \cdot (D \nabla (n_{O_3} - n_{NO})) \quad . \qquad (A-3)$$

If we nondimensionalize the difference of the reactants concentrations we have a reactant concentration

$$\varphi = \frac{n_{O_3} - n_{NO} + N_{NO}}{N_{NO} + N_{O_3}} \qquad (A-4)$$

which reduces the equation to the same form as the equation for η:

$$\frac{\partial}{\partial t}\varphi + \nabla \cdot (\varphi \vec{v}) = \nabla (D \nabla \varphi) \qquad (A-5)$$

with boundary conditions

$\varphi = 1$ in unmixed primary jet and

$\varphi = 0$ in unmixed ambient fluid.

Having both identical boundary conditions and identical equations for η and φ, we conclude that

$$\eta = \varphi \tag{A-6}$$

everywhere in the jet.

We next assume equilibrium chemistry. Then, where ozone exists,

$$n_{NO} = 0 \quad \text{for} \quad n_{O_3} \geq 0 \quad . \tag{A-7}$$

Thus, in regions of the flow where ozone remains,

$$\eta = \frac{n_{O_3} + N_{NO}}{N_{NO} + N_{O_3}} \quad . \tag{A-8}$$

Solving for n_{O_3},

$$\frac{n_{O_3}}{N_{O_3}} = \eta - (1-\eta)\frac{N_{NO}}{N_{O_3}} \tag{A-9}$$

which is true only where n_{O_3} is positive. The later condition implies

$$\eta > \eta_o = \frac{N_{NO}/N_{O_3}}{1 + N_{NO}/N_{O_3}} \quad . \tag{A-10}$$

Thus we have a rigorous expression identical to the result of the simplistic mixing approach (Eqn. 6-5)

$$\frac{n_{O_3}}{N_{O_3}} = p(\eta \, , \; N_{NO}/N_{O_3}) \tag{A-11}$$

where

$$\begin{aligned} p &= \eta - (1-\eta)\frac{N_{NO}}{N_{O_3}} && \text{for } \eta > \eta_o \\ &= 0 && \text{for } \eta \leq \eta_o \end{aligned} \tag{A-12}$$

The function p is plotted for sample values of the concentration ratio in Figure 18.

REFERENCES

1. Burke, S. P. and T. E.W. Schumann, Ind. Eng. Chem., 20, p. 998 (1928).

2. Hawthorne, W. R., D. S. Weddell, and H. C. Hottel, "Mixing and Combustion in Turbulent Gas Jets," Third International Symposium on Combustion, p. 266 (1949).

3. Damköhler, G., Z. Electrochem, p. 601 (1940).

4. Shchelkin, K. I., J. Tech. Phys. (USSR), (1943).

5. Thring, M. W. and M. P. Newby, "Combustion Length of Enclosed Turbulent Jet Flames," Fourth International Symposium on Combustion, p. 789 (1952).

6. Toor, H. L., "Mass Transfer in Dilute Turbulent and Non-Turbulent Systems with Rapid Irreversible Reactions and Equal Diffusivities," A. I. Ch. E. Journal, 8, p. 70 (1962).

7. Vassilotos, G., and H. L. Toor, "Second Order Chemical Reactions in a Nonhomogeneous Turbulent Fluid," A. I. Ch. E. Journal, 11, p. 666 (1965).

8. Richardson, J. M., H. C. Howard, and R. W. Smith, "The Relation between Sampling-Tube Measurements and Concentration Fluctuations in a Turbulent Gas Jet," Fourth International Symposium on Combustion, p. 814 (1952).

9. Townsend, A. A., The Structure of the Turbulent Shear Flow, Cambridge University Press, London, (1956).

10. Corrsin, S., and A. L. Kistler, "The Free-Stream Boundaries of Turbulent Flows," National Advisory Committee for Aeronautics, Technical Note NACA TN 3133, (1954).

REFERENCES (cont'd)

11. Karlovitz, B., "Open Turbulent Flames," Fourth International Symposium on Combustion, p. 60 (1952).

12. Karlovitz, B., D. W. Denniston, D. H. Knapschaffer, and F. E. Wells, "Studies on Turbulent Flames," Fourth International Symposium on Combustion, p. 613 (1952).

13. Karlovitz, B., "The Growth and Burn Out of Flame Surface in a Turbulent Stream," Seventh International Symposium on Combustion, p. 604 (1958).

14. Wohlenberg, W. J., "Minimum Depth of the Flame Front for Stable Combustion and Maximum Time Mean Energy Release Rates over an Interval of Combustion Progress for Second Order Reactions in a Gaseous System at Constant Pressure," Fourth International Symposium on Combustion, p. 796 (1952).

15. Kunugi, M. and H. Jinno, "Turbulent Diffusion Flames," Sixth International Symposium on Combustion, p. 311 (1956).

16. Wohl, K, C. Gazley and N. Kapp, "Diffusion Flames," Third International Symposium on Combustion, p. 288 (1949).

17. Becker, H. A., H. C. Hottel and G. C. Williams, "Concentration Intermittency in Jets," Tenth International Symposium on Combustion, p. 1253 (1964).

18. Becker, H. A., H. C. Hottel, and G. C. Williams, "The Nozzle Fluid Concentration Field of the Round, Turbulent, Free Jet," J. Fluid Mech., 30, p. 285 (1967).

REFERENCES (cont'd)

19. Brown, G. L., and A. Roshko, "On Density Effects and Large Structure in Turbulent Mixing Layers," J. Fluid Mech., 64, p. 775 (1974).

20. Griggs, M., "Absorption Coefficients of Ozone in the Ultraviolet and Visible Regions," J. Chem. Phys., 49, p. 857 (1968).

21. Hudson, R. D., "Critical Review of Ultraviolet Photoabsorption Cross Sections for Molecules of Astrophysical and Aeronomic Interest," Nat. Stand. Ref. Data Ser.--Nat. Bur. Stand., 38, p. 306 (1971).

22. Melvin, E. H., and O. R. Wulf, "Ultraviolet Absorption of Mixtures of NO, NO_2 and H_2O," J. Chem. Phys., 3, p. 755 (1935).

23. Jones, E. J., and O. R. Wulf, "The Absorptive Coefficient of Nitrogen Pentoxide in the Ultraviolet and the Visible Absorption Spectrum of NO_3," J. Chem. Phys., 5, p. 873 (1937).

24. Herron, J. T., and R. E. Hine, "The Reaction between NO and O_3," J. Phys. Chem. Ref. Data, 2, p. 292 (1973).

25. Johnston, H. S., and H. J. Crosby, "Rapid Gas Phase Reaction between NO and O_3," J. Chem. Phys., 19, p. 799 (1951).

26. Johnston, H. S., and H. J. Crosby, "Kinetics of Fast Gas Phase Reaction between O_3 and NO," J. Chem. Phys., 22, p. 689 (1954).

27. Hottel, H. C., "Burning in Laminar and Turbulent Fuel Jets," Fourth International Symposium on Combustion, p. 97 (1952).

REFERENCES (cont'd)

28. Yagi, S. and K. Saji, "Problems of Turbulent Diffusion and Flame Jets," Fourth International Symposium on Combustion, p. 771 (1952).

29. Weddell, D., "Turbulent Mixing in Gas Flames," Ph. D. Thesis, Massachusetts Institute of Technology, (1941).

30. Kent, J. H., and R. W. Bilger, "Turbulent Diffusion Flames," Fourteenth International Symposium on Combustion, p. 615, 1972.

31. Bradshaw, P., D. H. Ferriss, and R. F. Johnson, "Turbulence in the Noise-Producing Regions of a Circular Jet," JFM, 19, p. 591 (1964).

32. Davies, P. O. A. L., M. J. Fisher, and M. J. Barratt, "The Characteristics of the Turbulence in the Mixing Region of a Round Jet," JFM, 15, p. 337 (1963).

33. Kuethe, A., "Investigations of the Turbulent Mixing Regions Formed by Jets," ASME Transactions, 2, p. A-87 (1935).

34. Sabersky, R. H., D. A. Sinema, and F. H. Shair, "Concentrations, Decay Rates, and Removal of Ozone and Their Relation to Establishing Clean Indoor Air," Environmental Science and Technology, 7, p. 347 (1973).

35. Axworthy, A. E., and S. W. Benson, "Mechanism of Gas Phase Decomposition of Ozone," Advan. Chem. Ser., 21, p. 388 (1959).

REFERENCES (cont'd)

36. Tombach, I. H., "Velocity Measurements with a New Probe in Inhomogeneous Turbulent Jets," Ph. D. Thesis, California Institute of Technology (1969).

37. Clough, P. N., and B. A. Thrush, "Mechanism of Chemiluminescent Reaction between Nitric Oxide and Ozone," Trans. Faraday Soc., 63, p. 915 (1967).

38. Lau, J. C., and M. J. Fisher, "The Vortex-Street Structure of Turbulent Jets, Part 1," J. Fluid Mech., 67, p. 299 (1975).

39. Gibson, C. H., and P. A. Libby, "On Turbulent Flows with Fast Chemical Reactions. Part II. The Distribution of Reactants and Products Near a Reacting Surface," Combustion Science and Technology, 6, p. 29 (1972).

40. Alber, I. E., and R. G. Batt, "An Analysis of Diffusion Limited First and Second Order Chemical Reactions in a Turbulent Shear Layer," AIAA Paper 74-593, AIAA 7th Fluid and Plasma Dynamics Conference, Palo Alto, Calif. (1974).

41. Williams, F. A., Combustion Theory, Addison-Wesley, pp. 9, 414 (1965).

42. Hirschfelder, J. D., C. F. Curtiss, R. B. Bird, and E. L. Spotz, "The Transport Properties of Gases and Gaseous Mixtures," Thermodynamics and Physics of Matter, Vol. 1, High Speed Aerodynamics and Jet Propulsion, Princeton University Press, p. 339 (1955).

43. Rohsenow, W. M., and N. Y. Choi, Heat, Mass and Momentum Transfer, Prentice-Hall, p. 383 (1961).

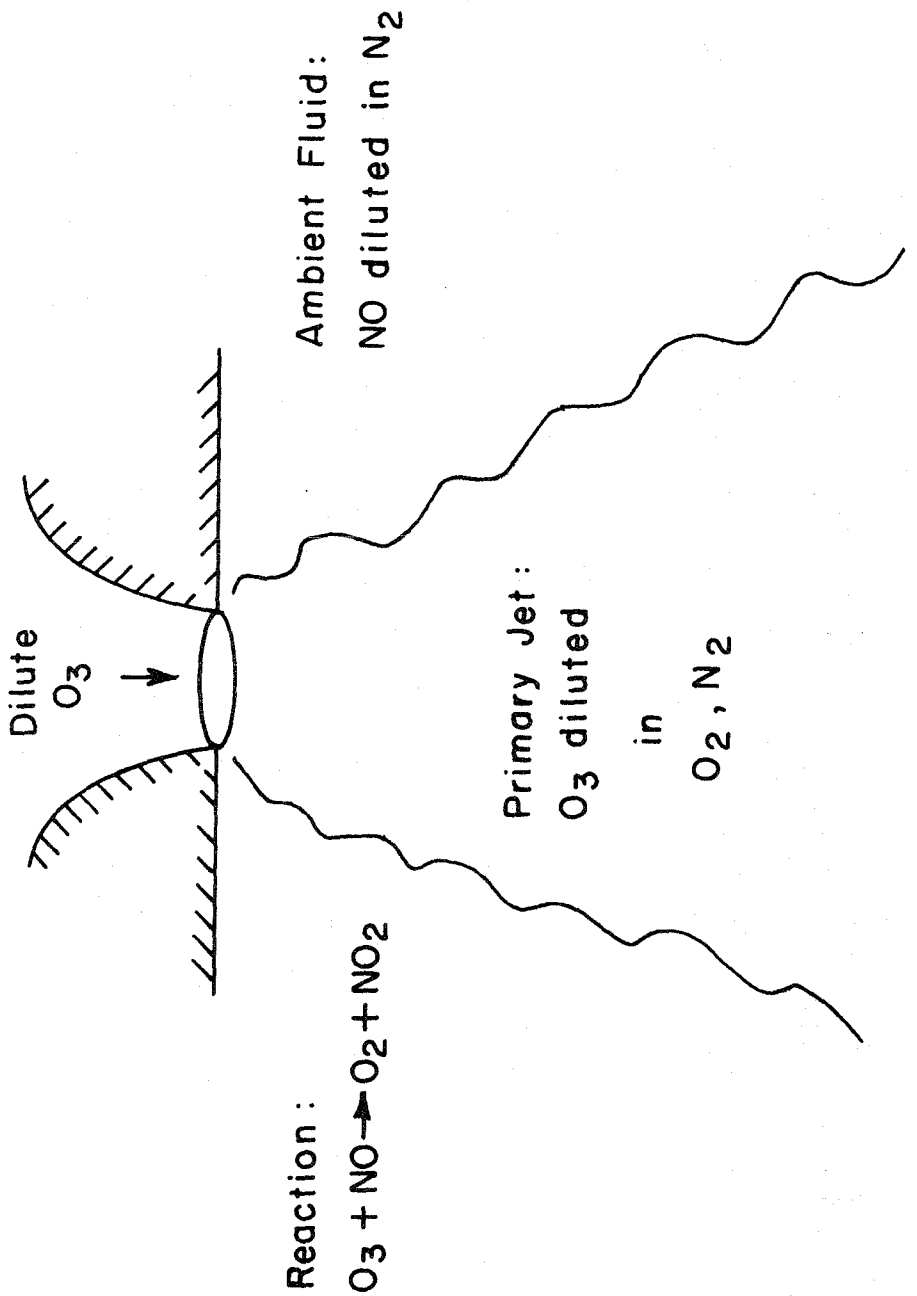

CHEMICALLY REACTING JET EXPERIMENT

Figure 1.

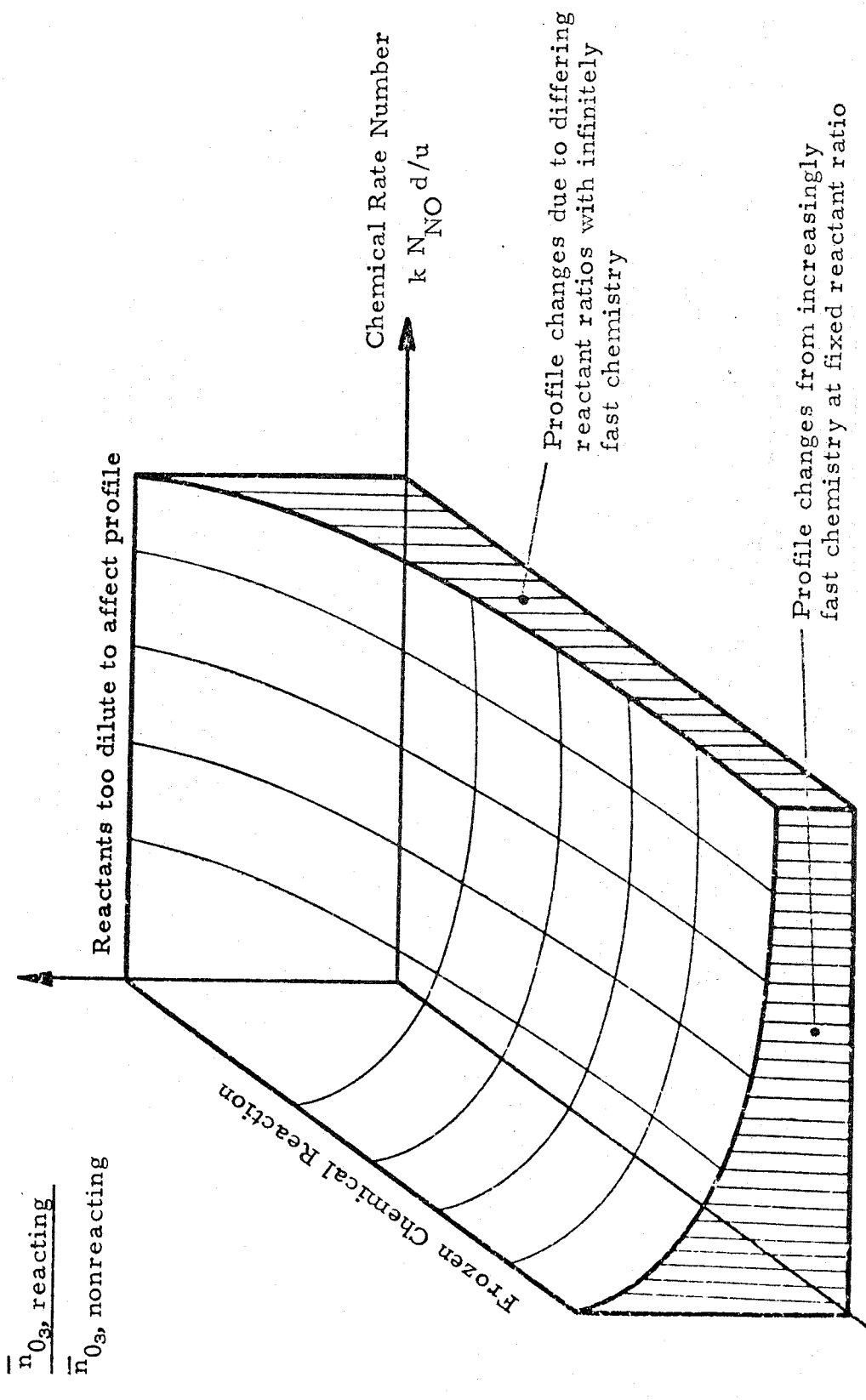

Figure 2. The Effect of Chemical Reaction on a Profile

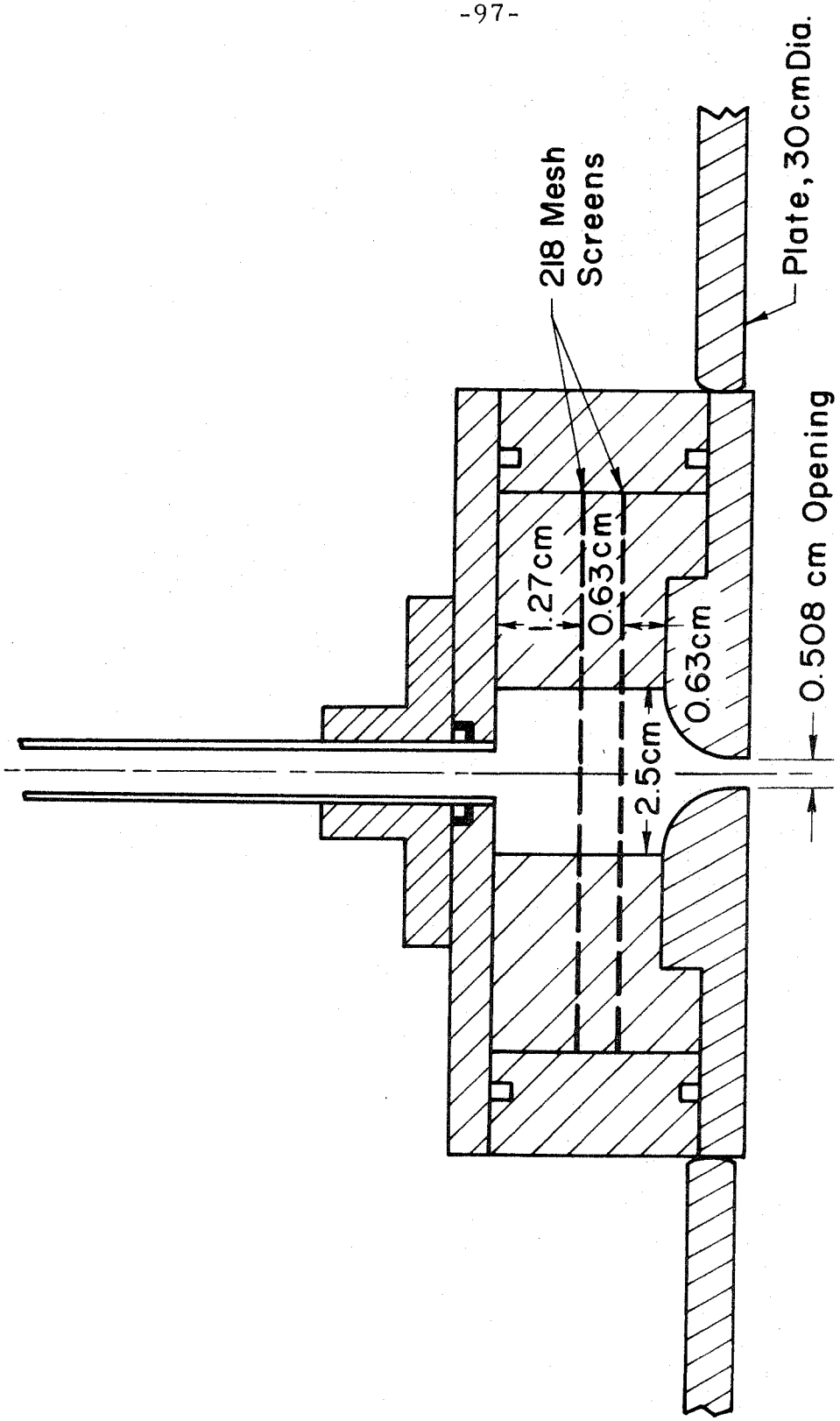

AXISYMMETRIC NOZZLE

Figure 3.

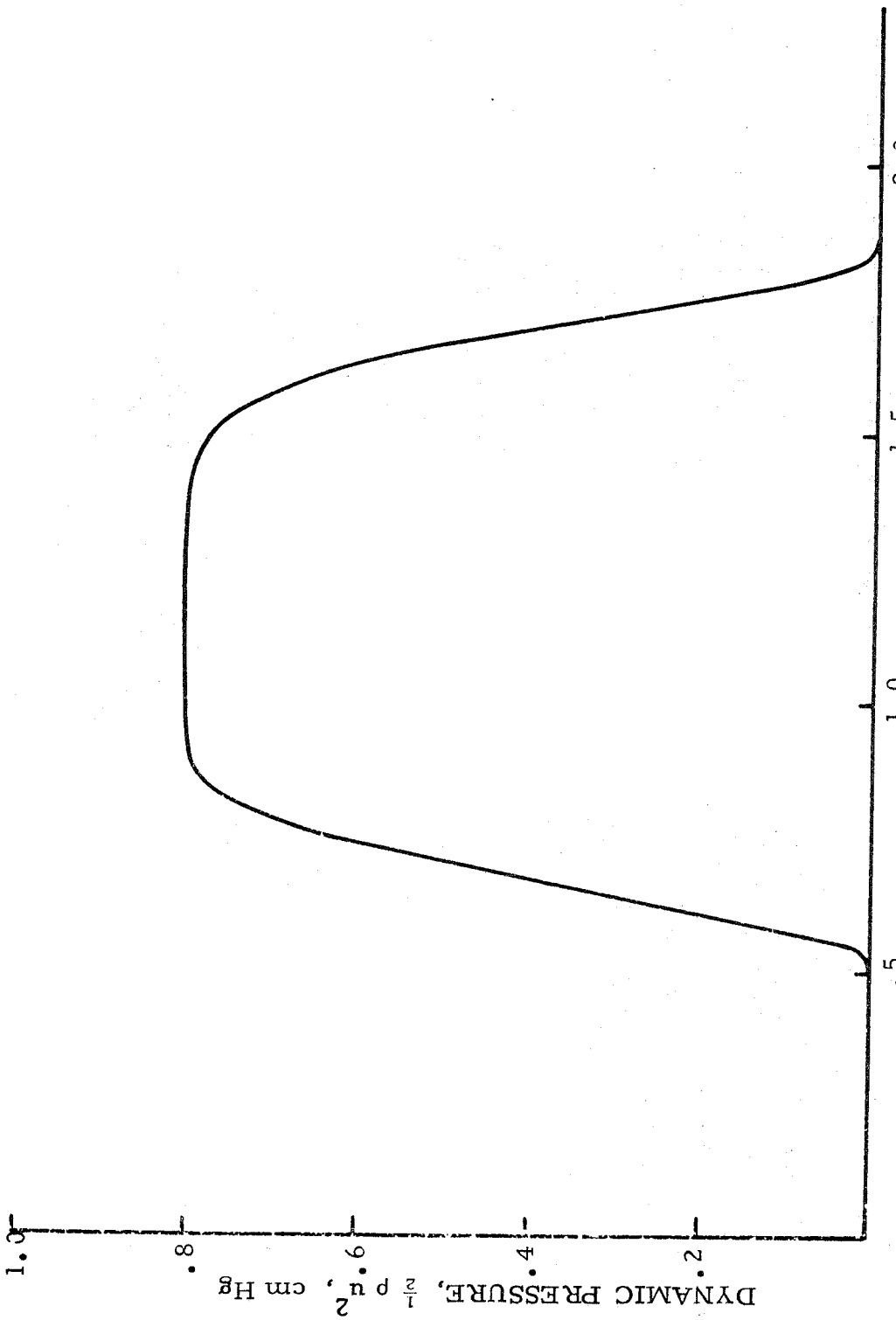

Figure 4. Typical Pitot survey of Jet; Re = 12, 000, u_1 = 42.8 m/sec, z/d = 1.3

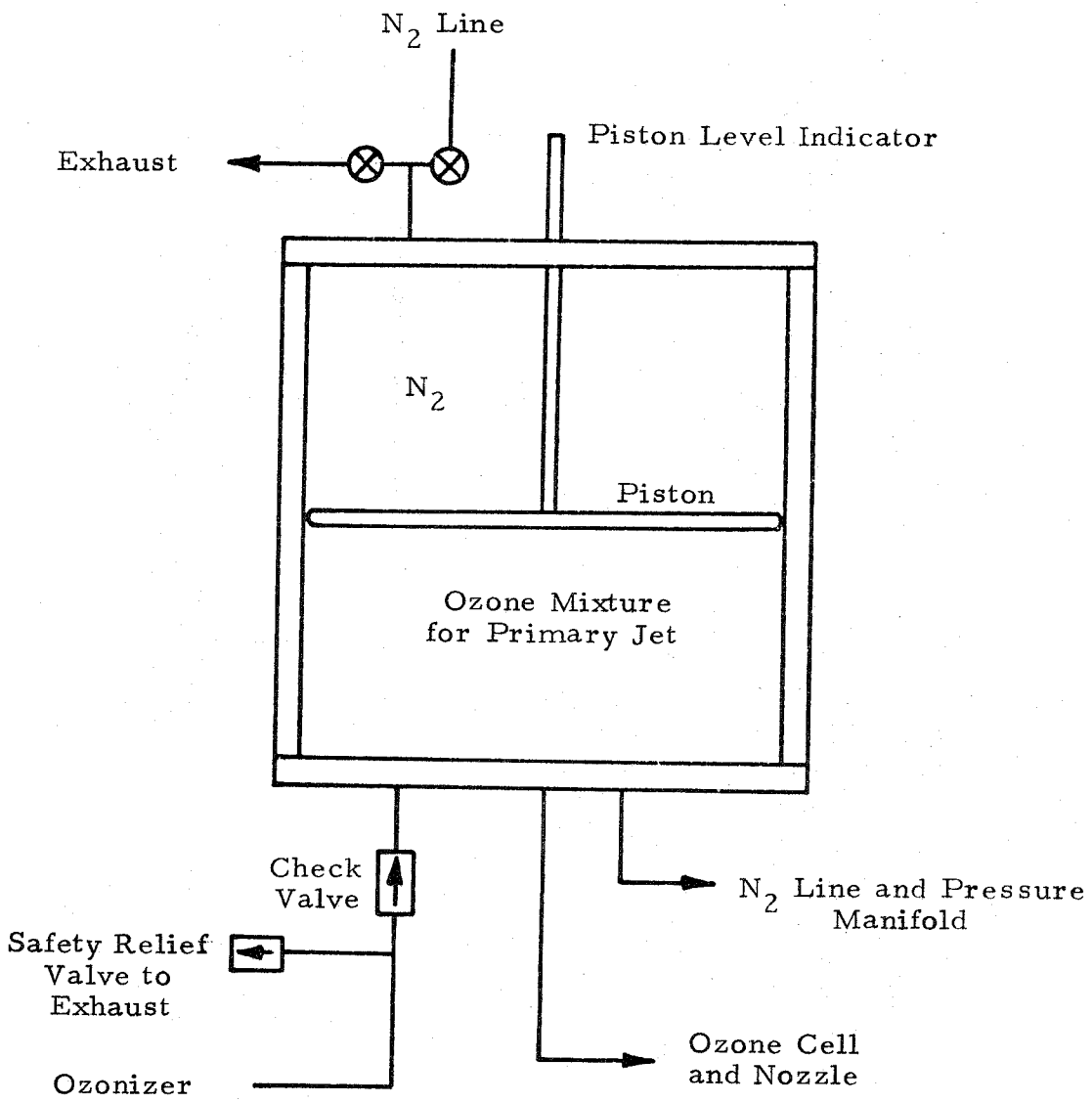

Figure 5. Ozone Storage Cylinder

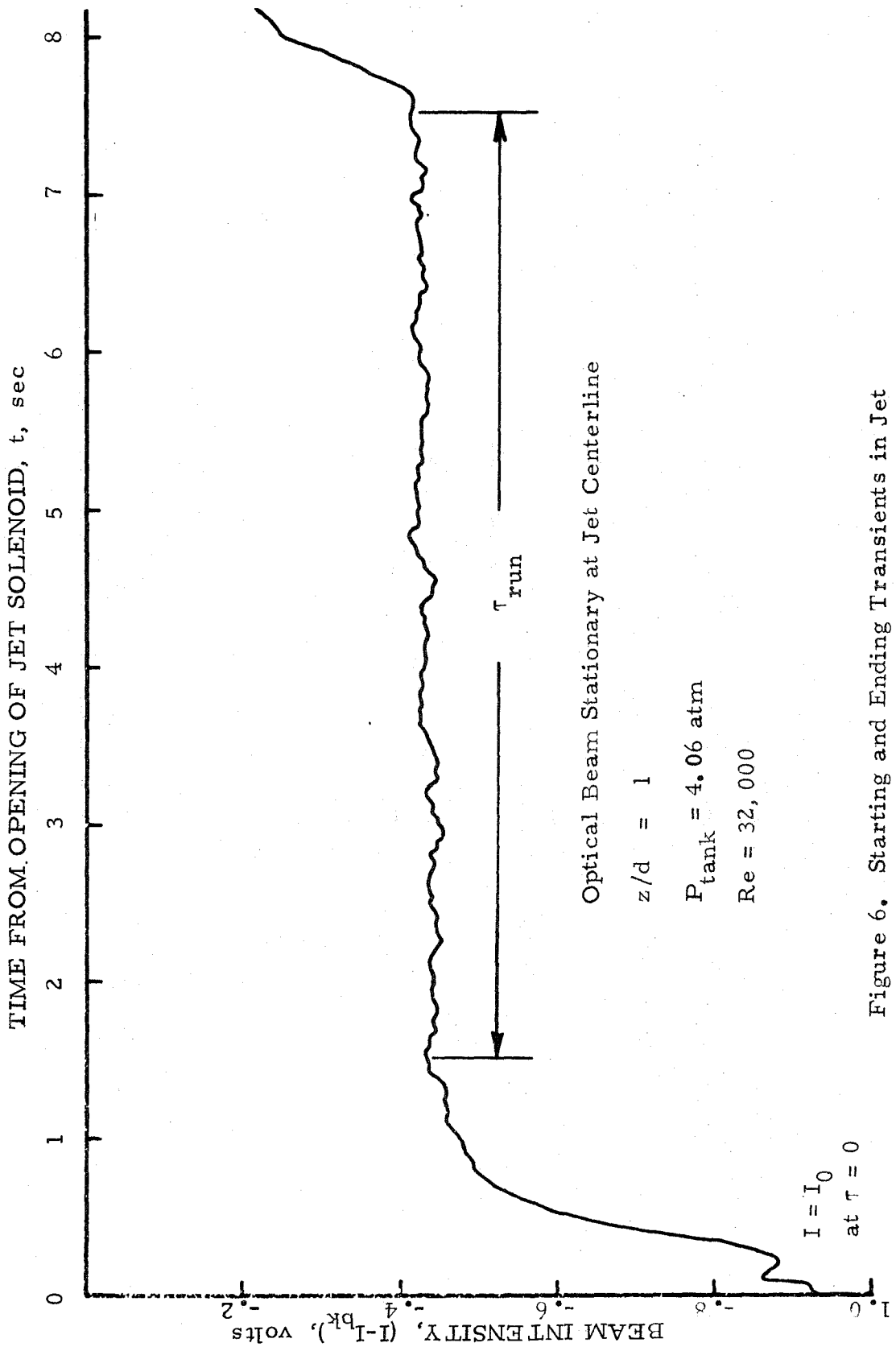

Figure 6. Starting and Ending Transients in Jet

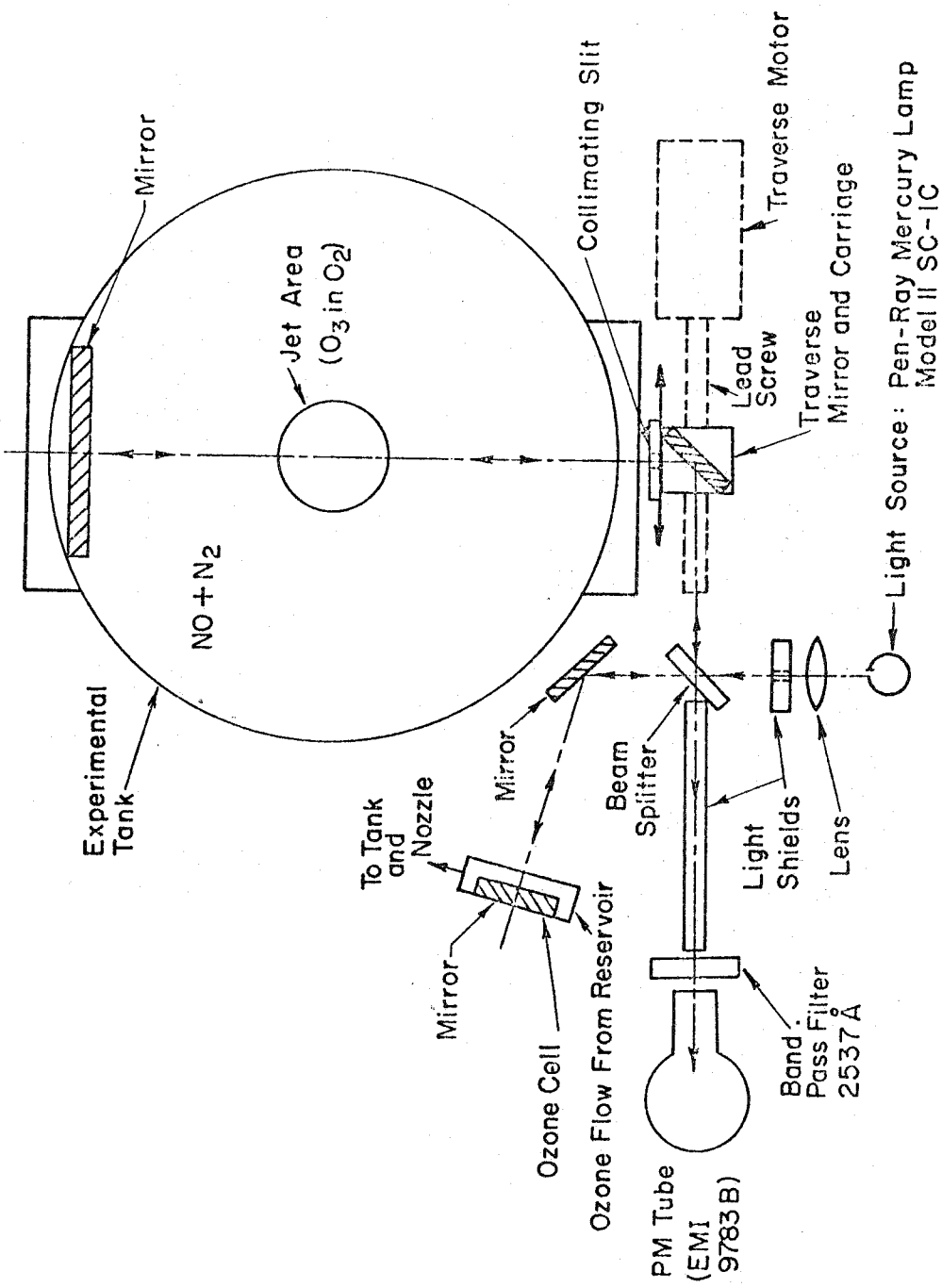

OPTICAL SYSTEM FOR CHEMICALLY REACTING JET EXPERIMENT

Figure 7.

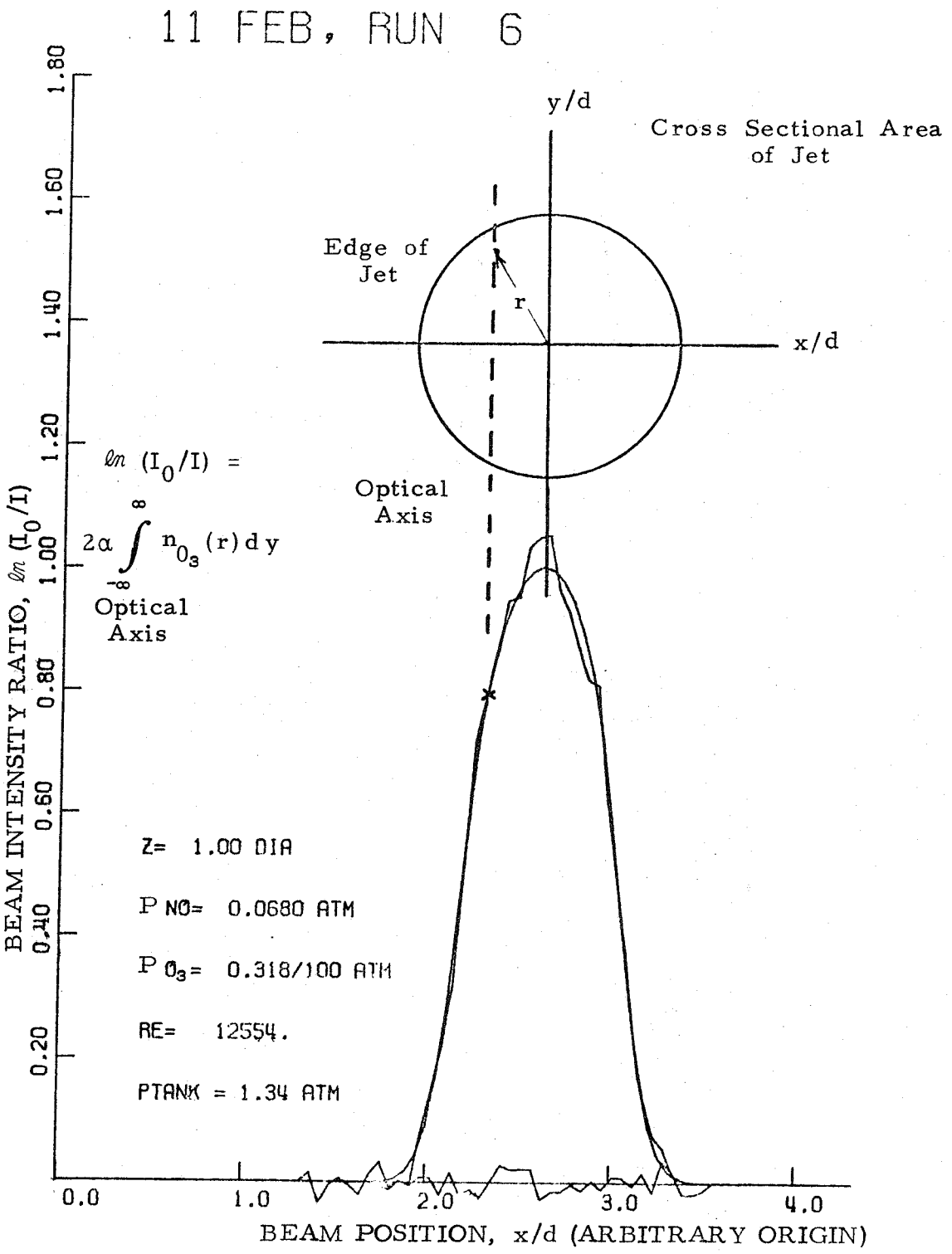

Figure 8. Absorption Profile Data for a Typical Run

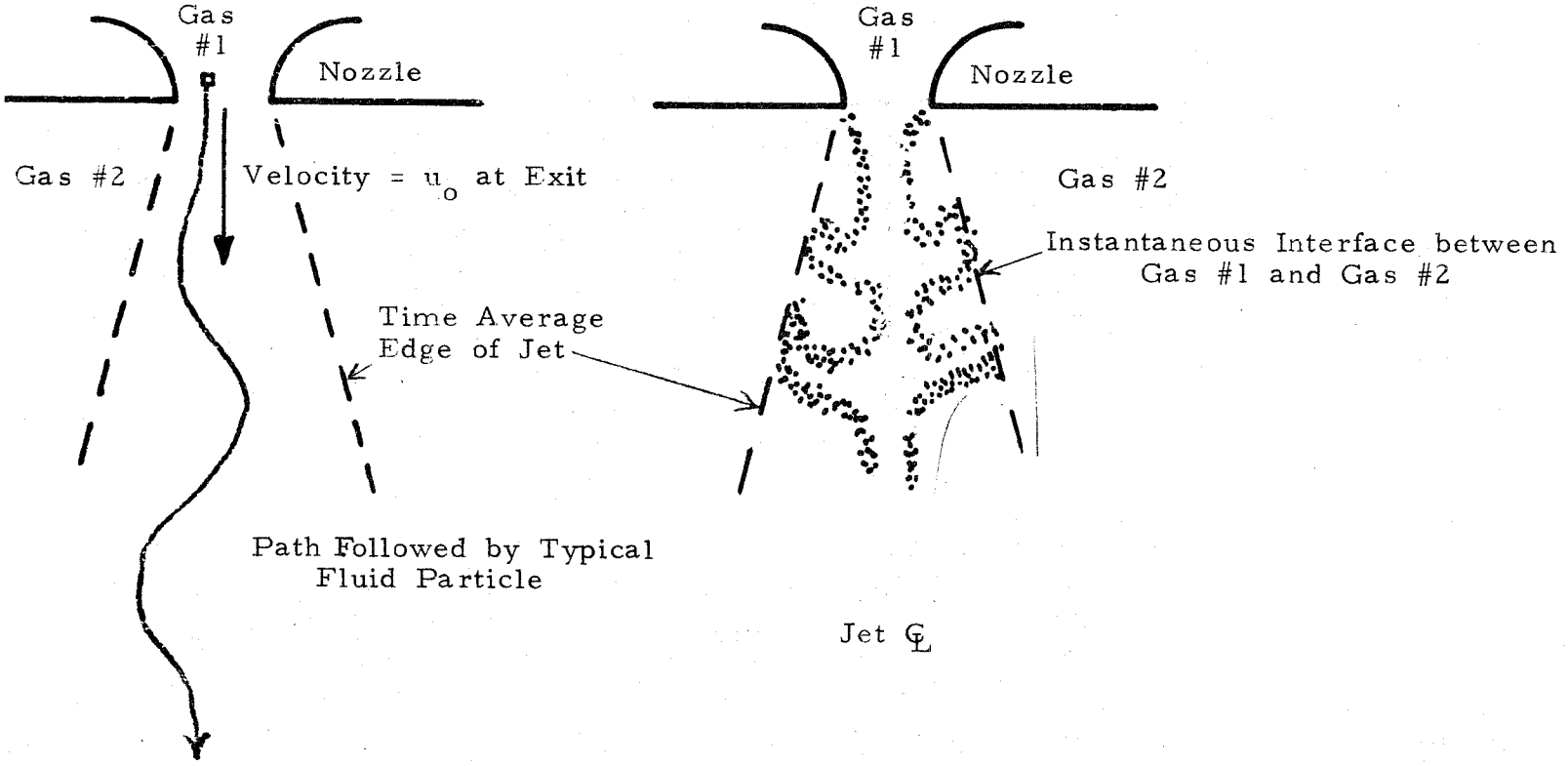

A. Streak Line (Time History of Marked Fluid Particle as it Moves Downstream)

B. Instantaneous (Schematic) Photograph of Slice through Turbulent Jet

Figure 9. Two Views of Mixing Jet

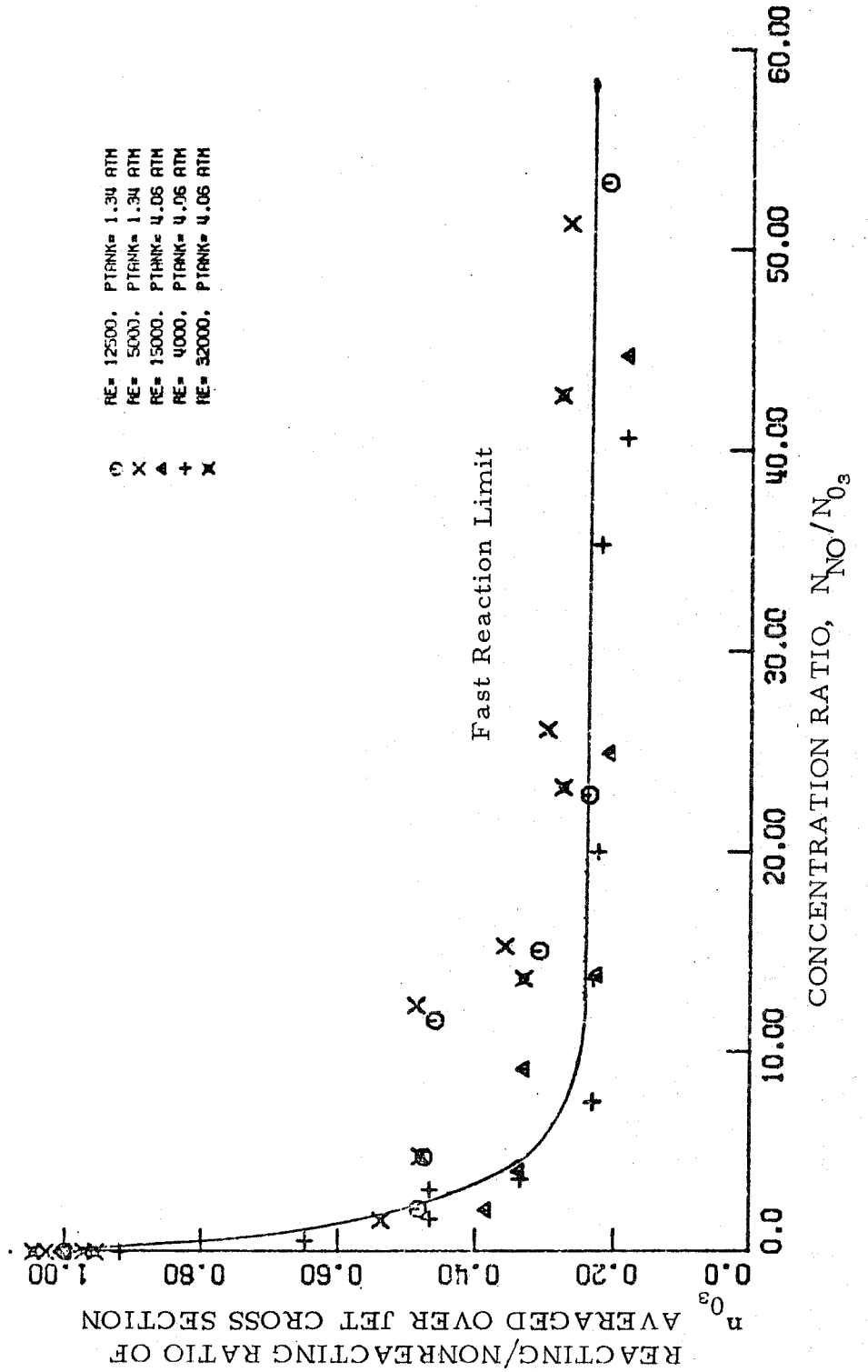

Figure 10a. Data Projection of Reacting/Nonreacting Ratio of n_{O_3} Averaged over Jet Cross Section, $z/d = 3$

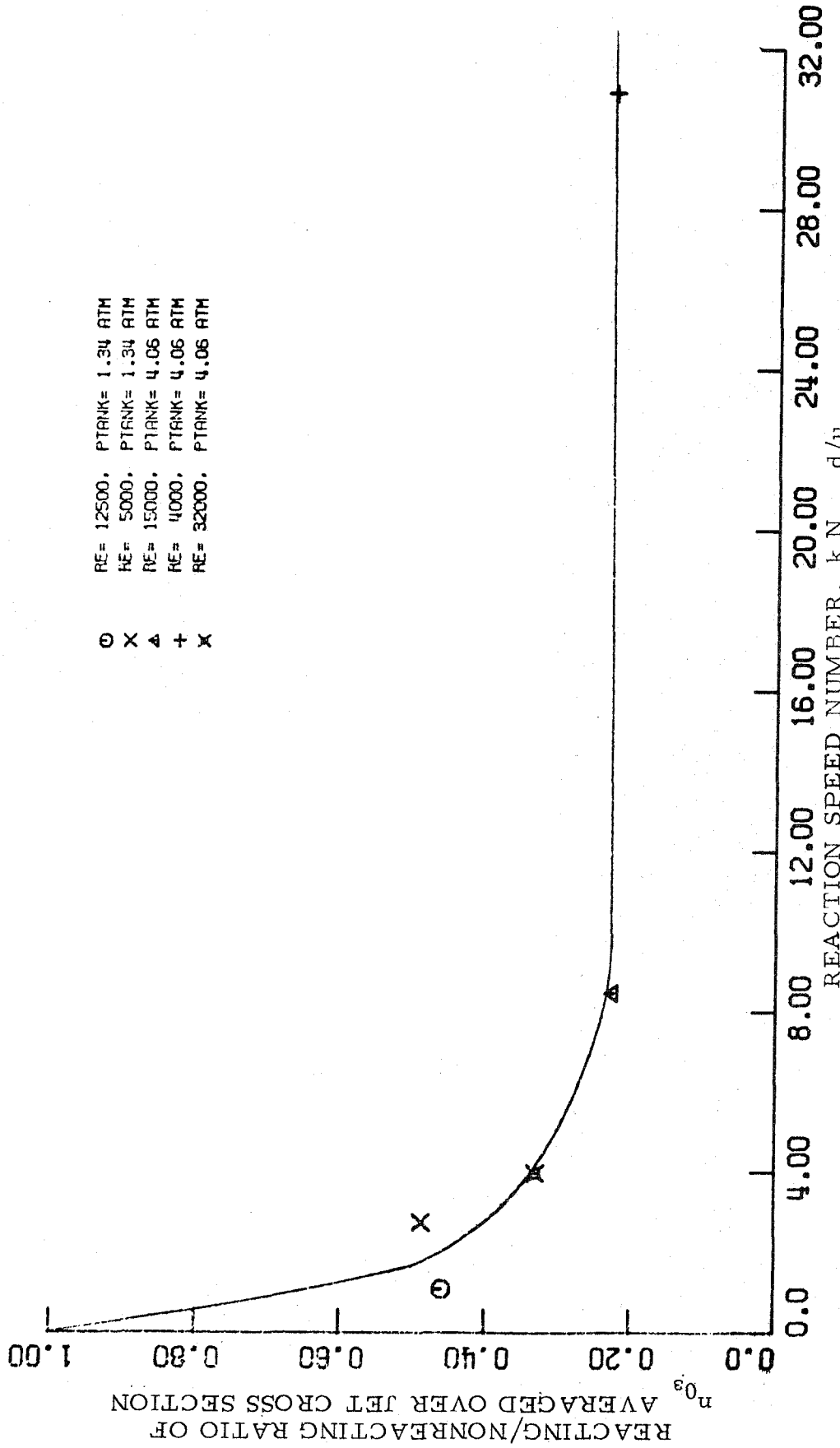

Figure 10b. Reacting/Nonreacting Ratio of n_{O_3} Averaged Across Jet Cross Section for $N_{NO}/N_{O_3} = 12.5$ and $z/d = 3$

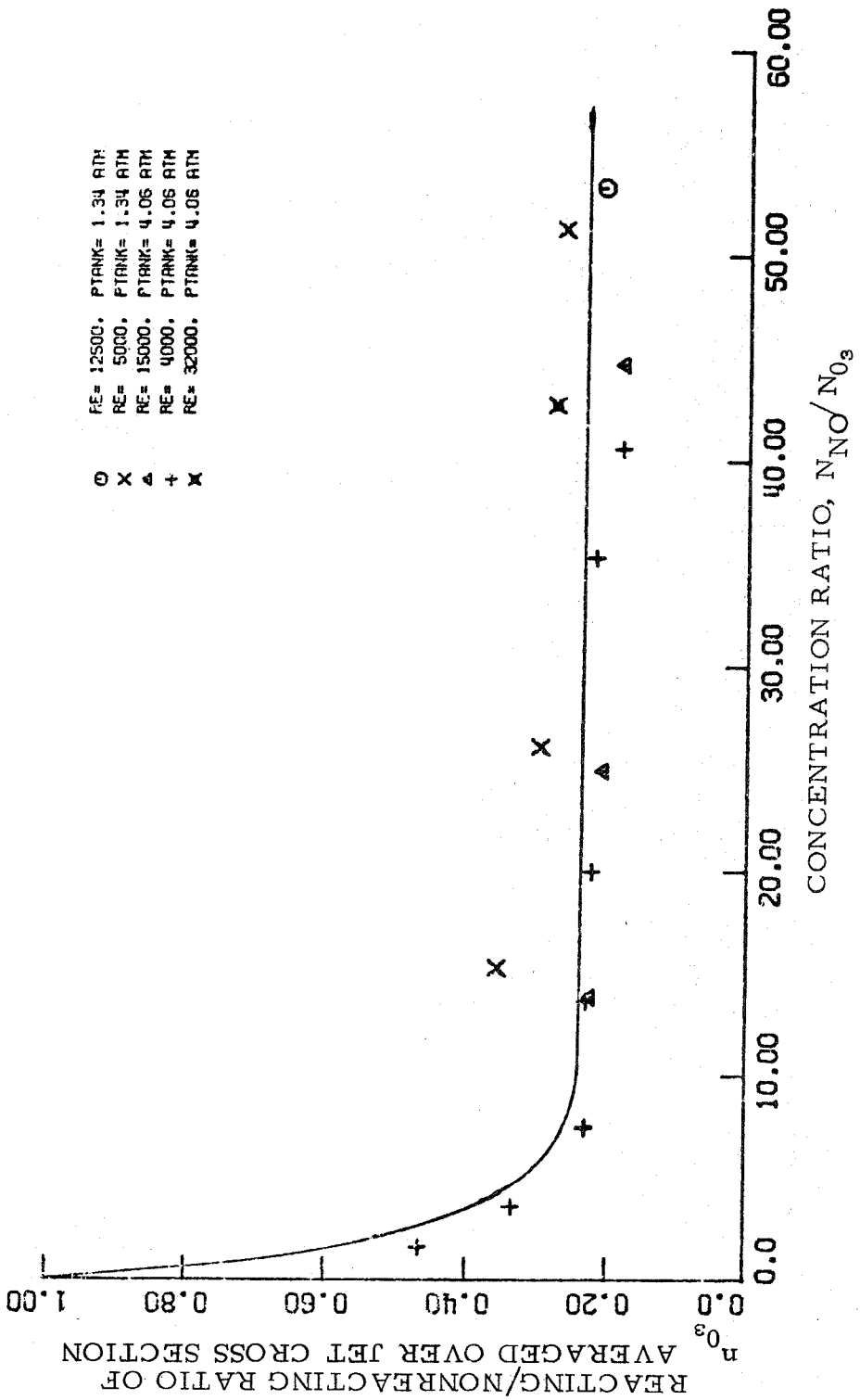

Figure 10c. Reacting/Nonreacting Ratio of n_{O_3} Averaged over Jet Cross Section for $kN_{NO}d/u \geq 8$, $z/d = 3$

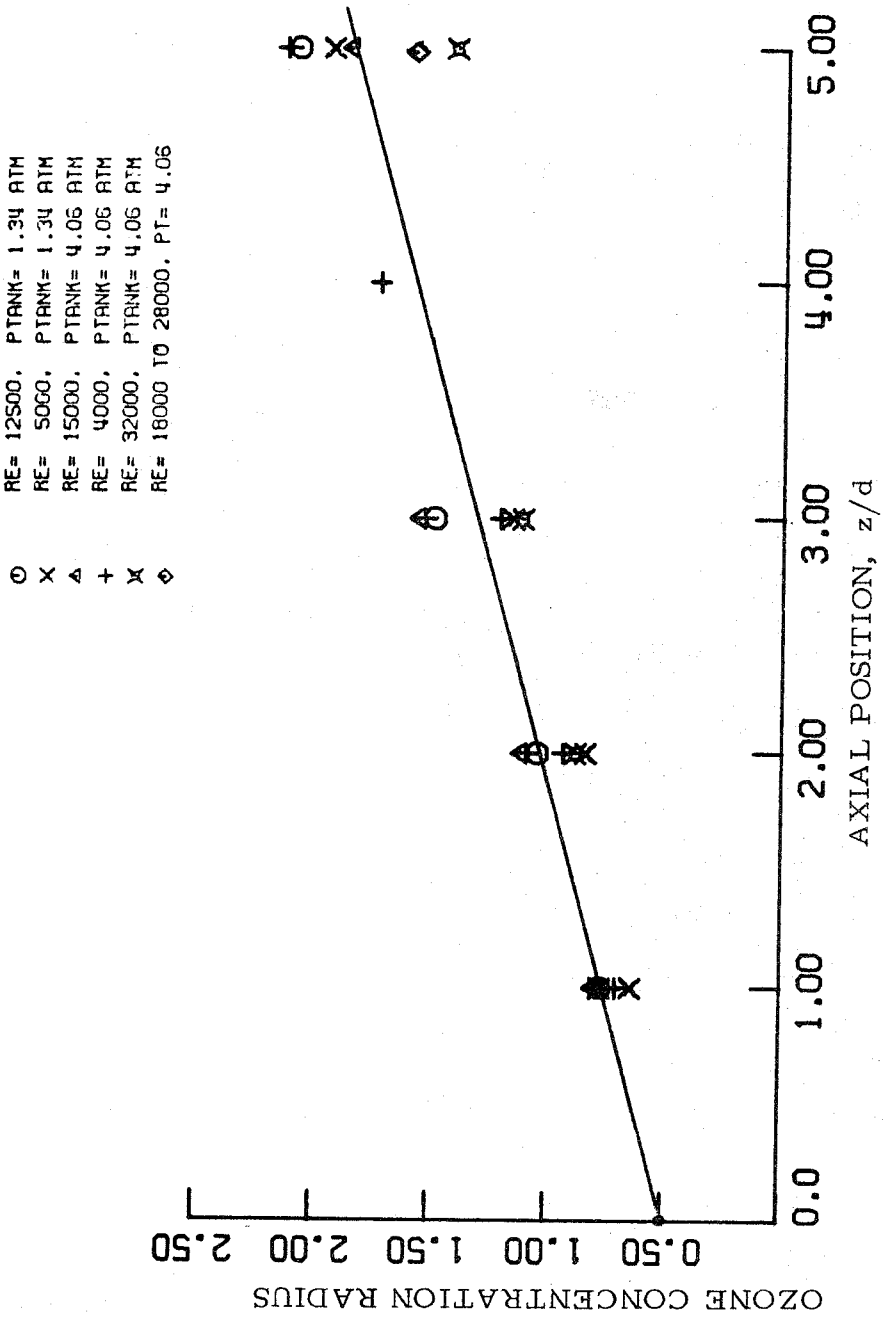

Figure 11a. The Ozone Concentration Radius for the Nonreacting Jet

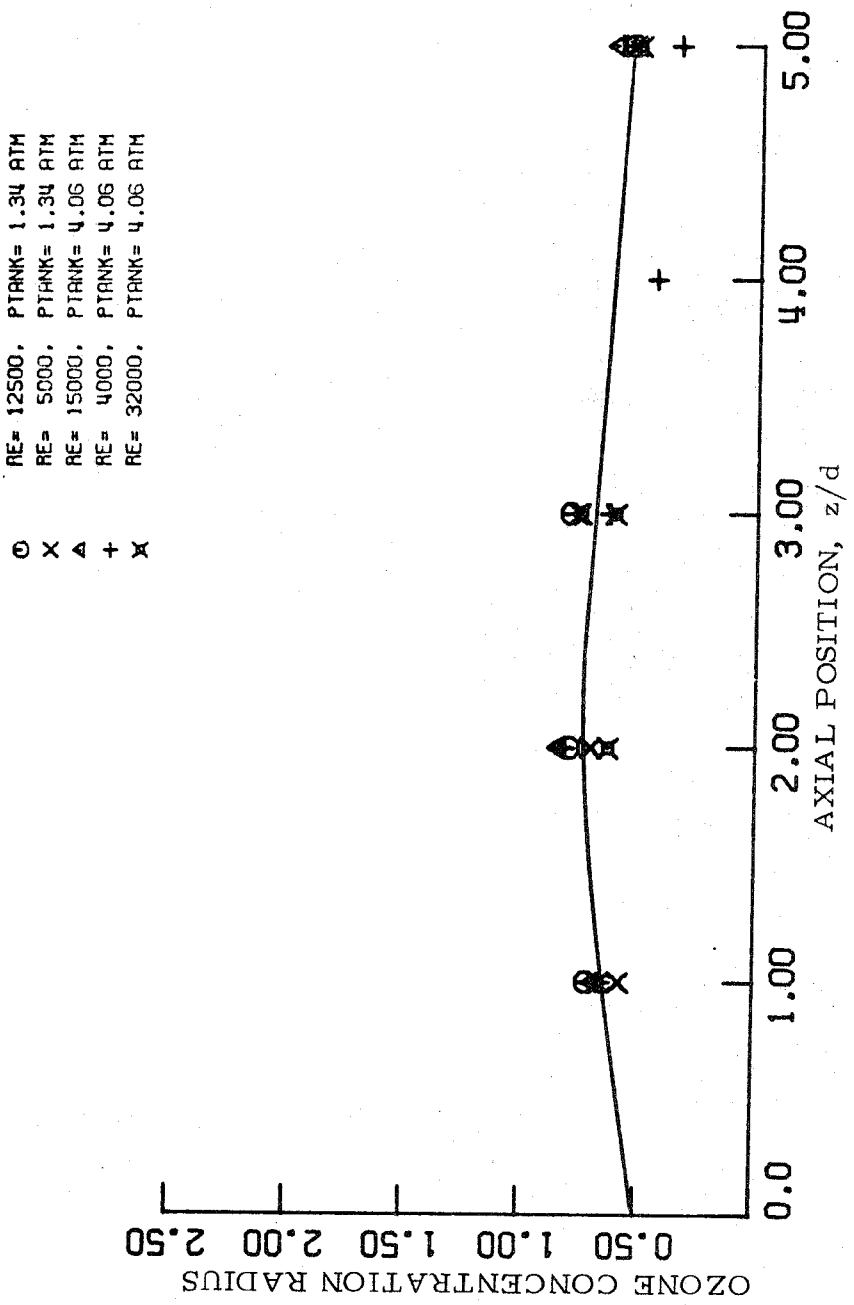

Figure 11b. Ozone Concentration Radius for Highly Reacting Jet

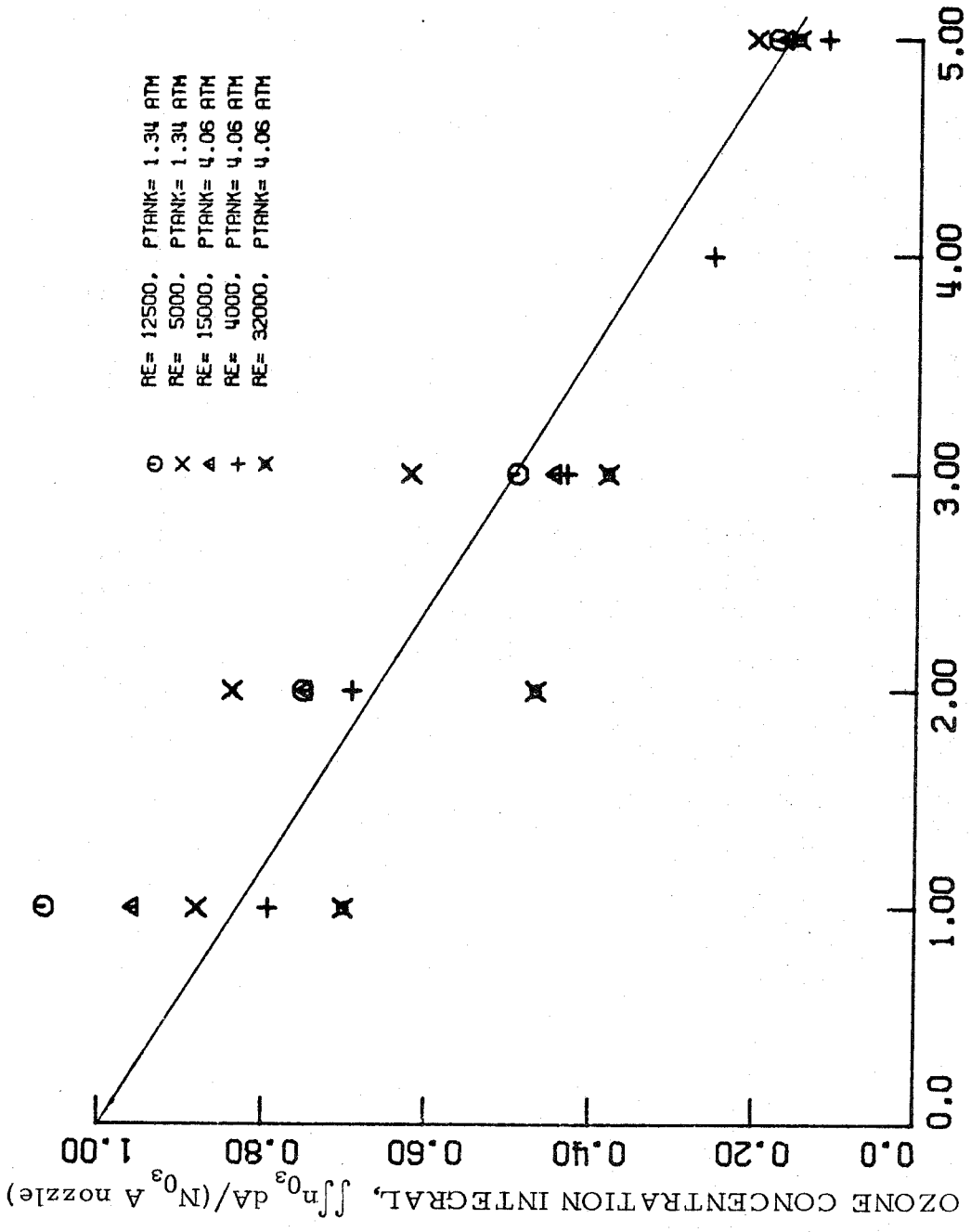

Figure 12. Ozone Concentration Integral, Highly Reacting Limit (Here Equivalent to Ozone Flux).

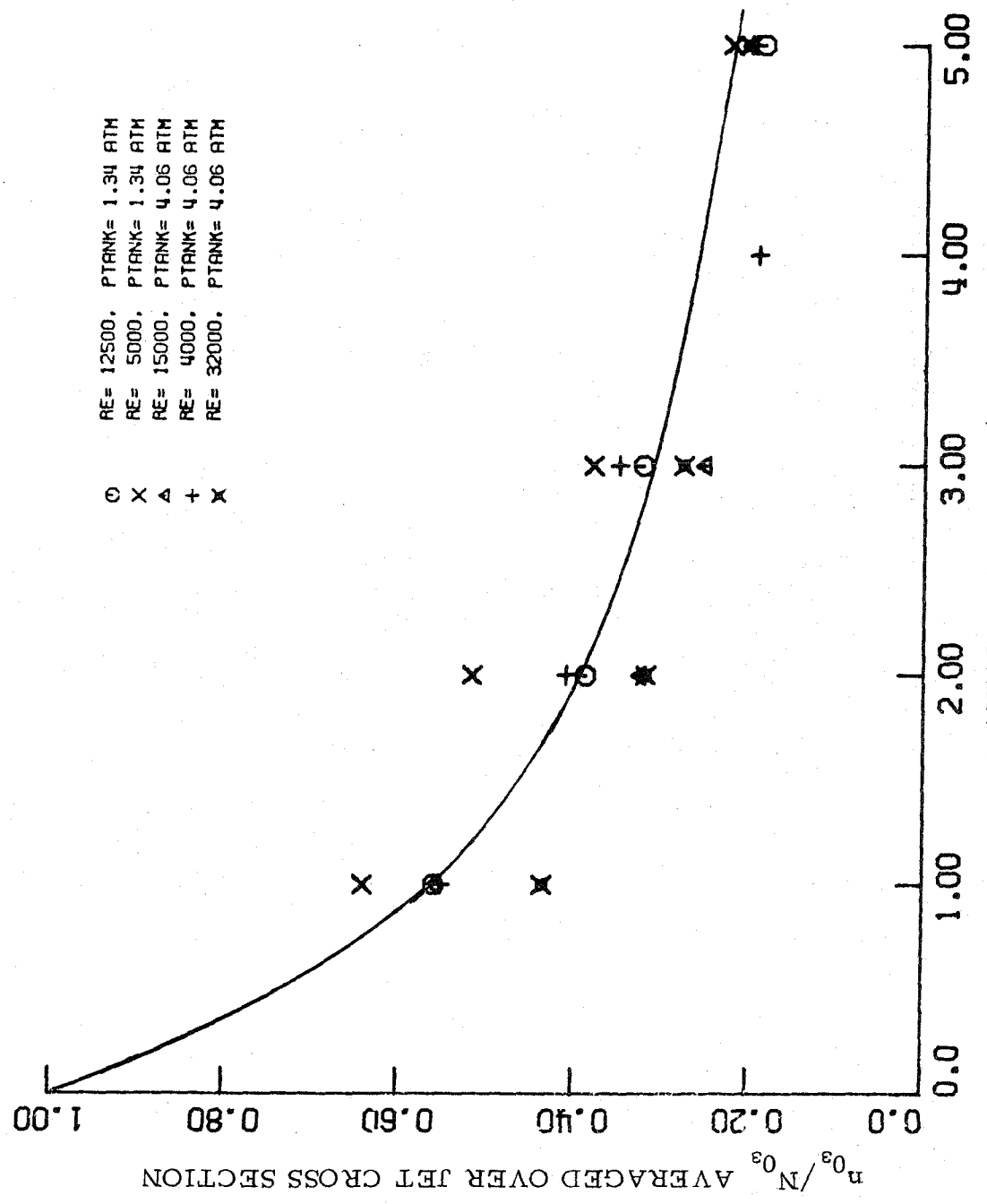

Figure 13a. n_{O_3}/N_{O_3} Averaged over Jet Cross Section for Nonreacting Jet

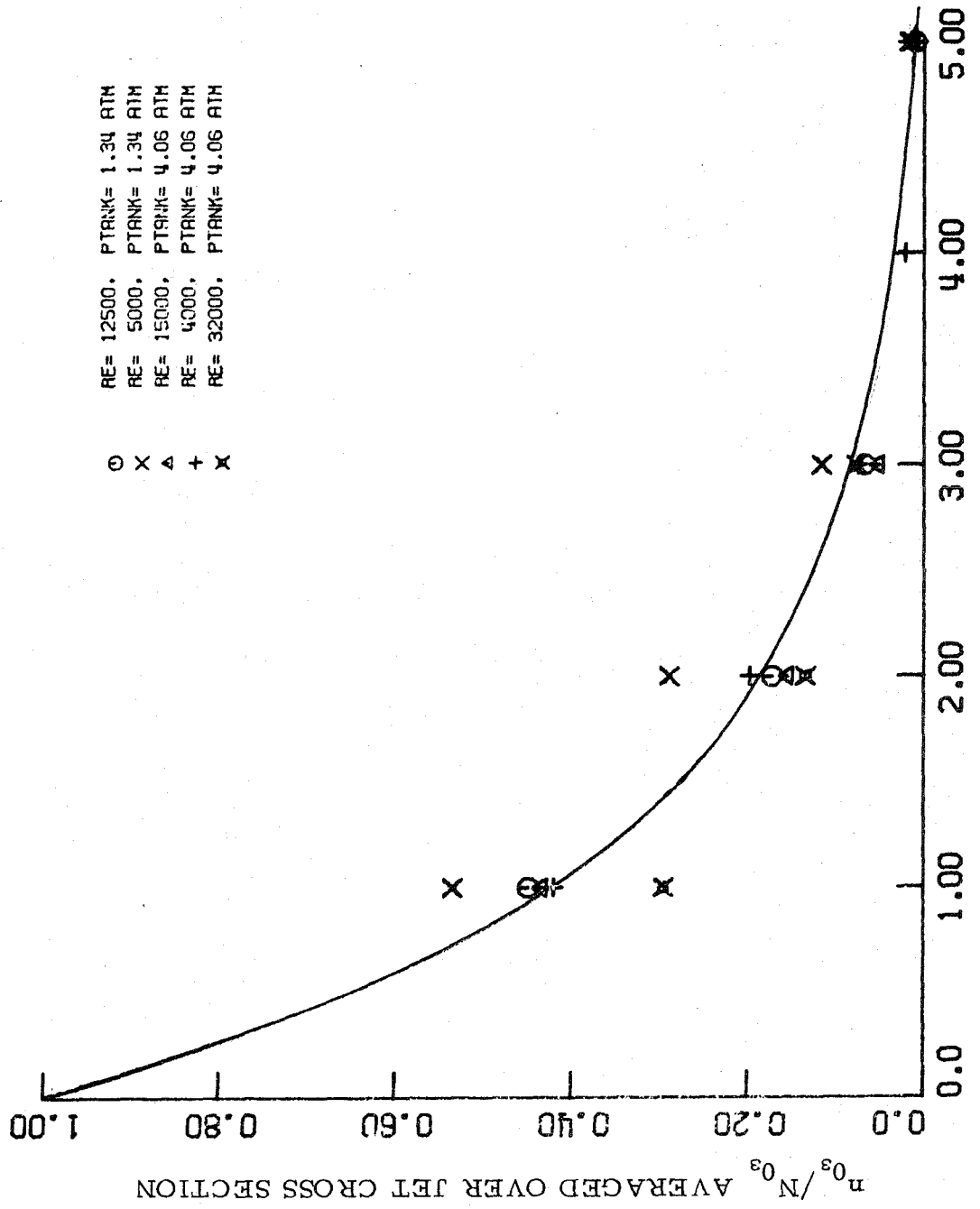

Figure 13b. n_{O_3}/N_{O_3} Averaged over Jet Cross Section for Highly Reacting Jet

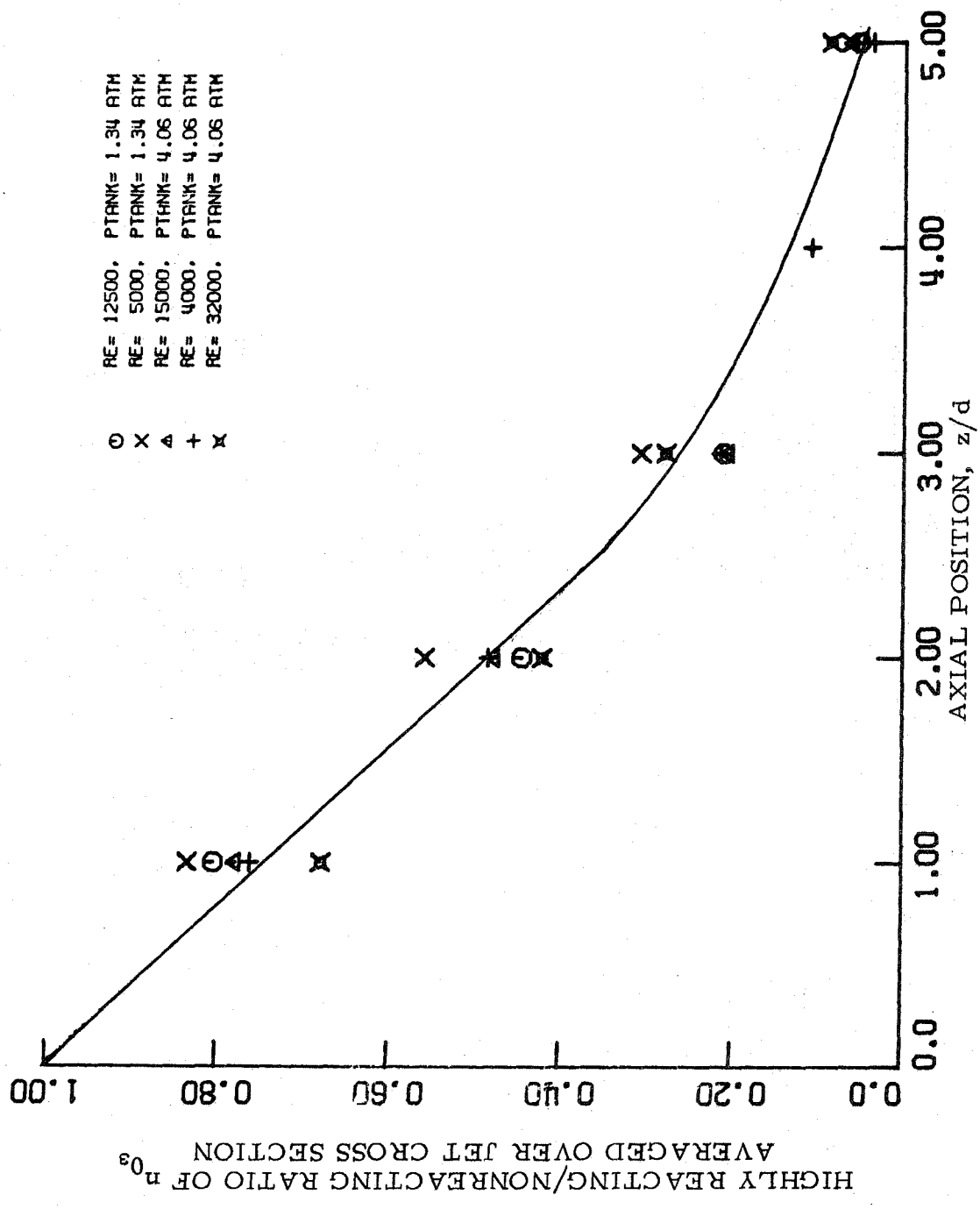

Figure 13c. Highly Reacting/Nonreacting Ratio of n_{O_3} Averaged over Jet Cross Section

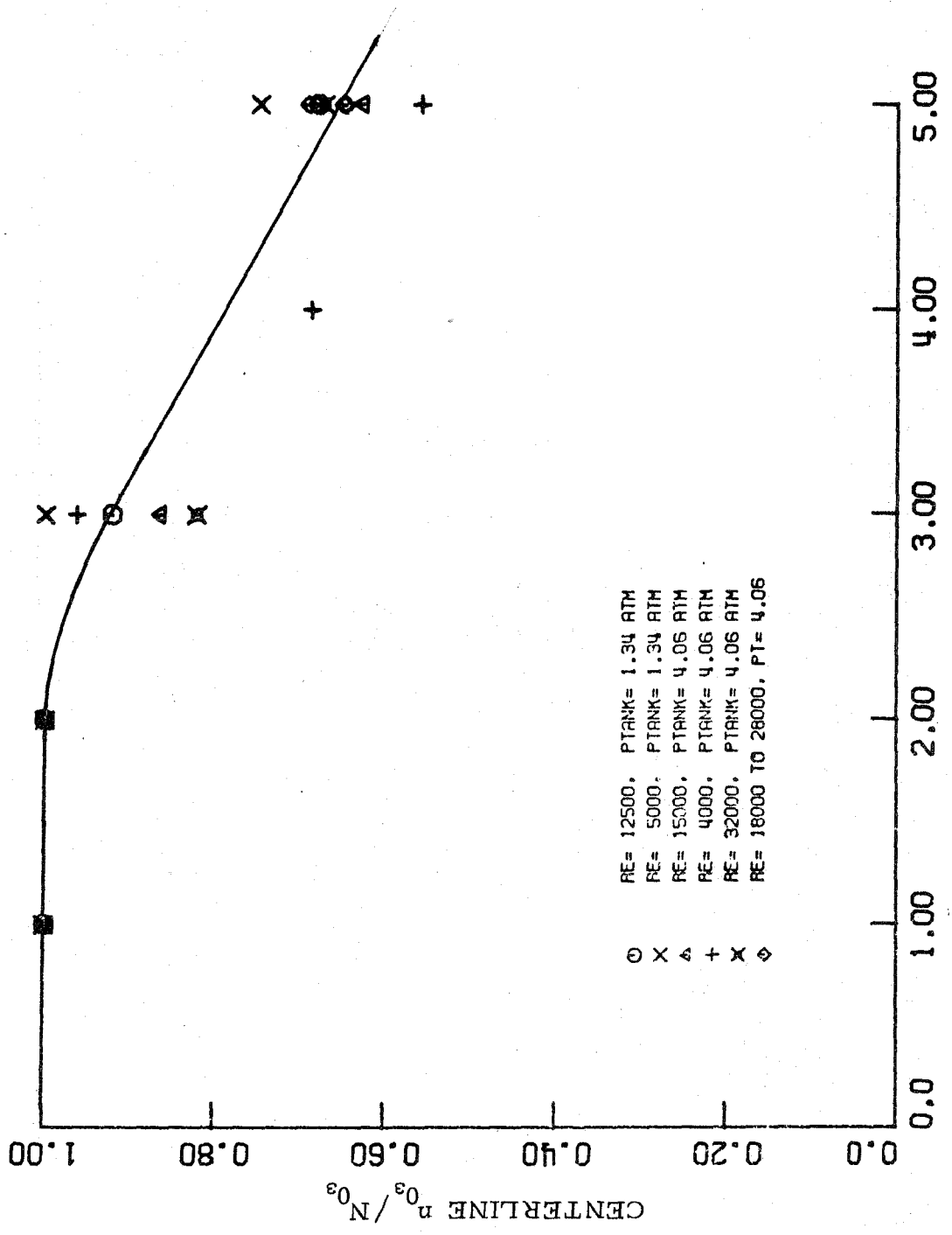

Figure 14a. Centerline n_{O_3}/N_{O_3} for Nonreacting Jet

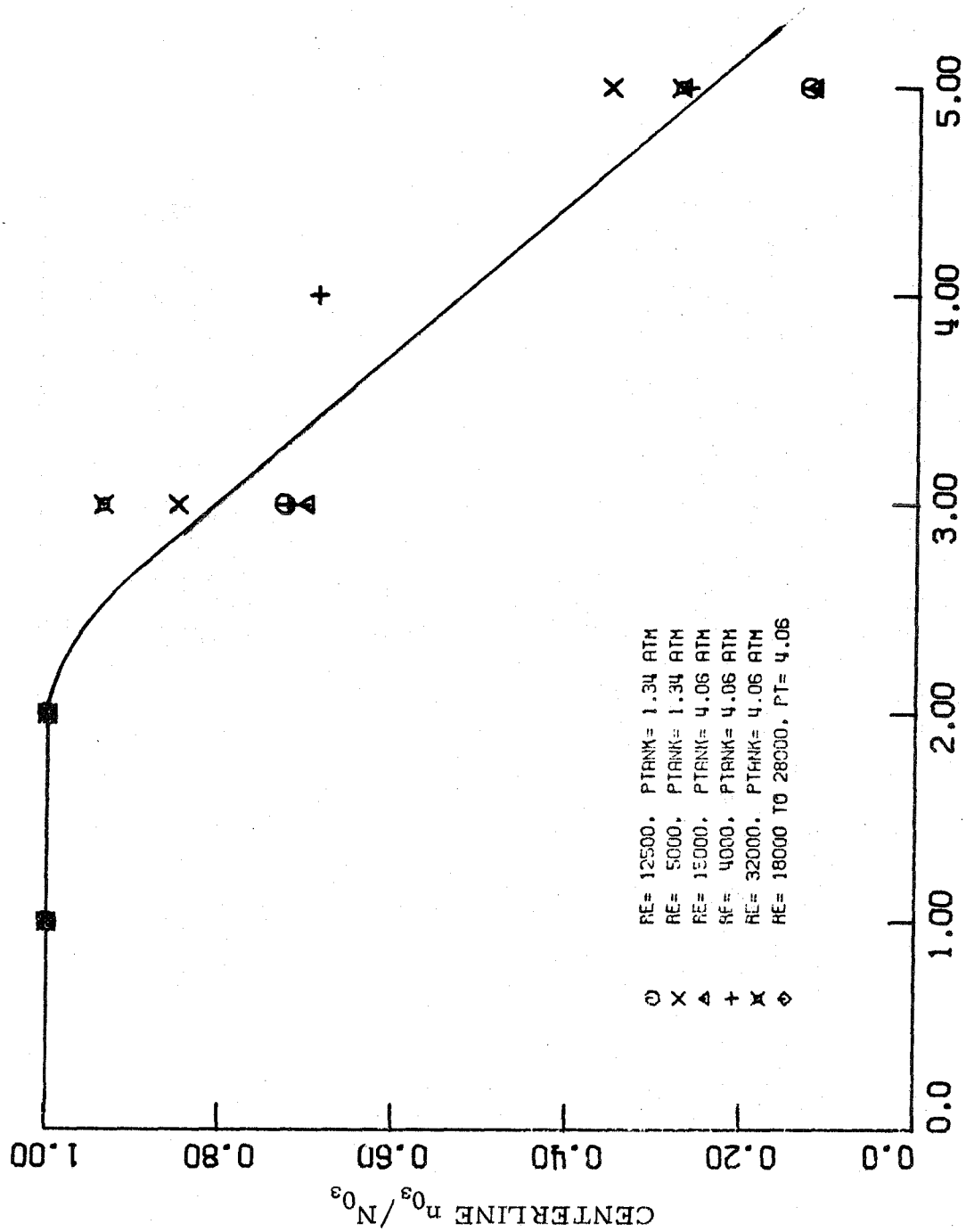

Figure 14b. Centerline n_{O_3}/N_{O_3} for Highly Reacting Jet

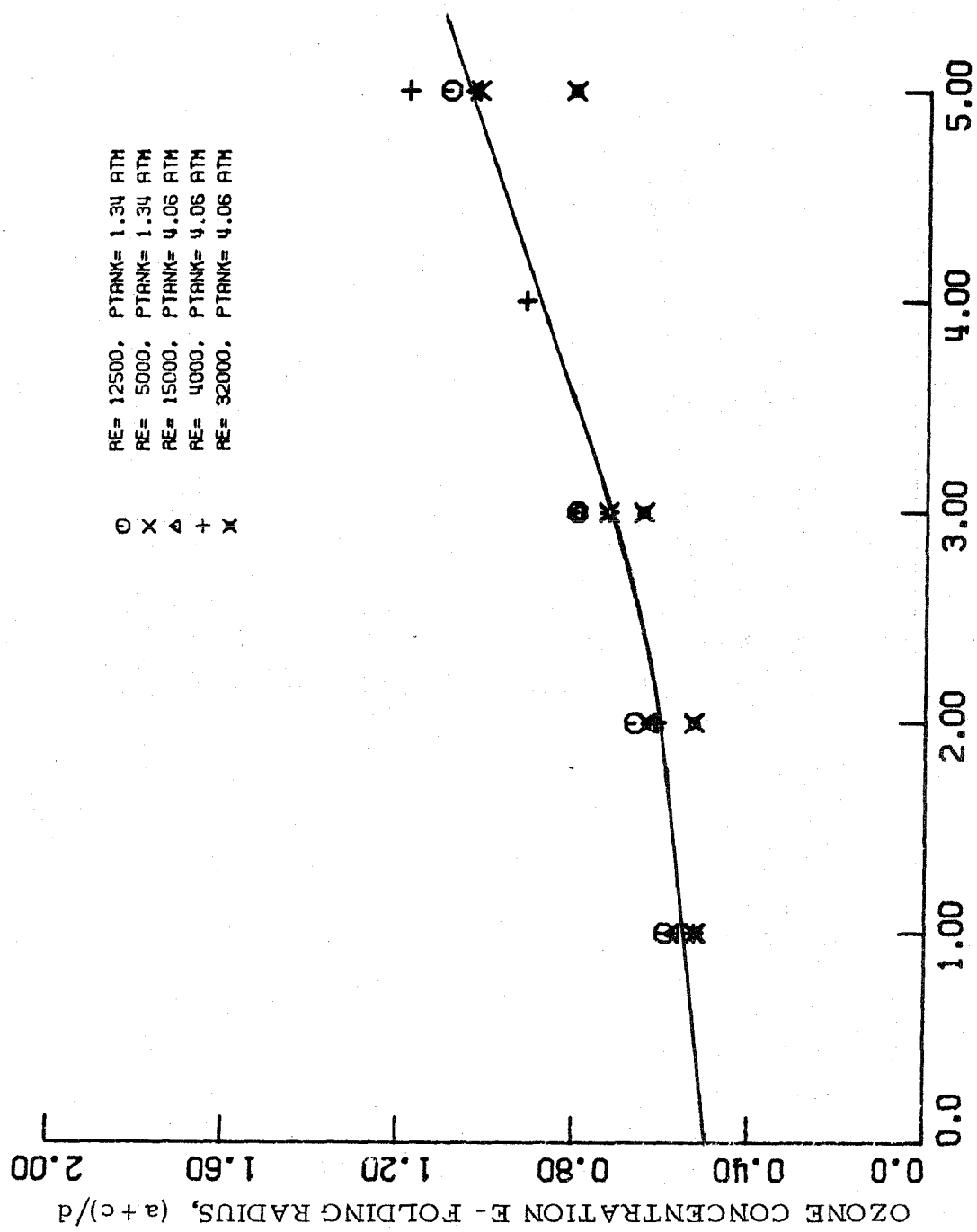

Figure 15a. Ozone Concentration E - Folding Radius for Nonreacting Jet

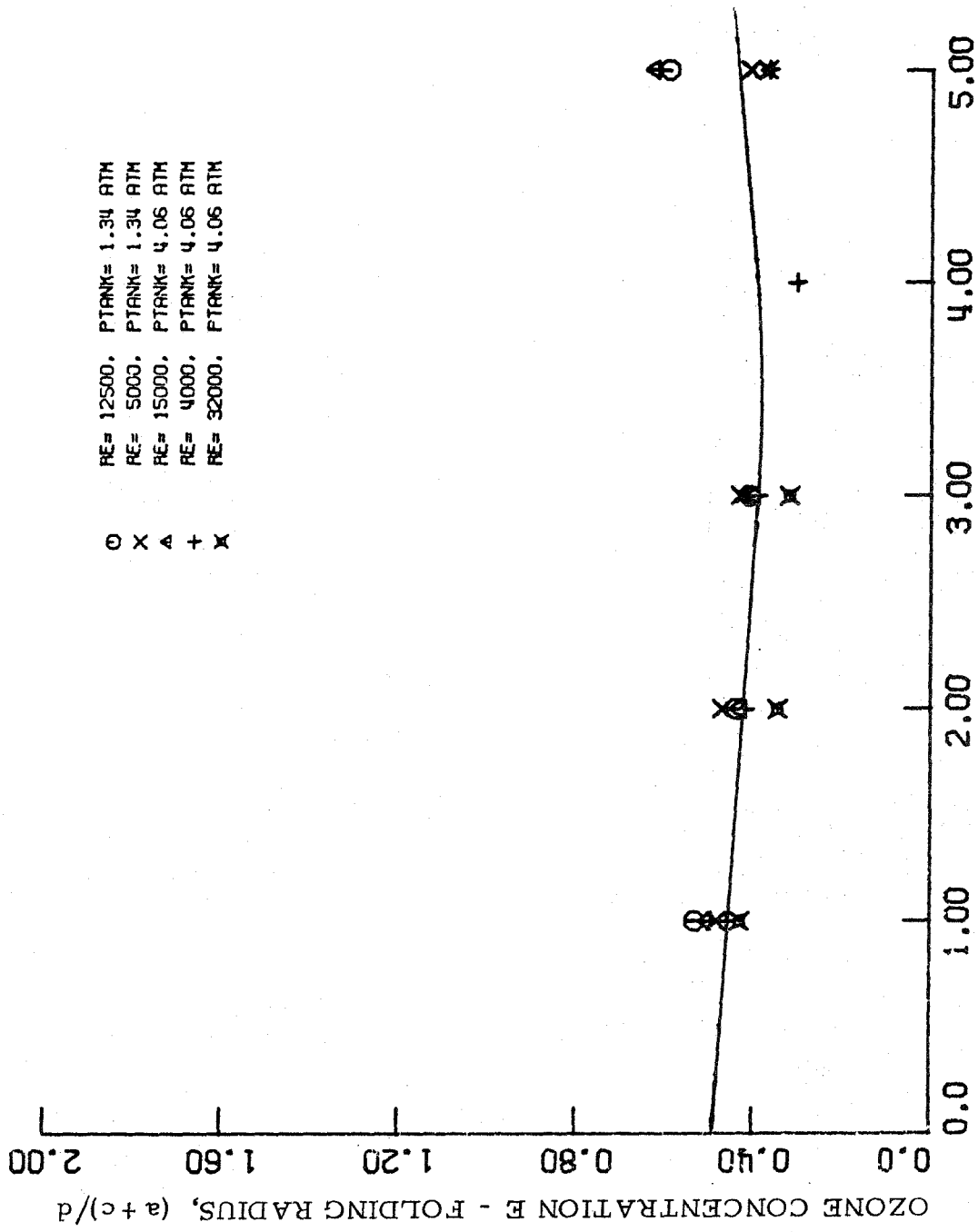

Figure 15b. Ozone Concentration E - Folding Radius for Highly Reacting Jet

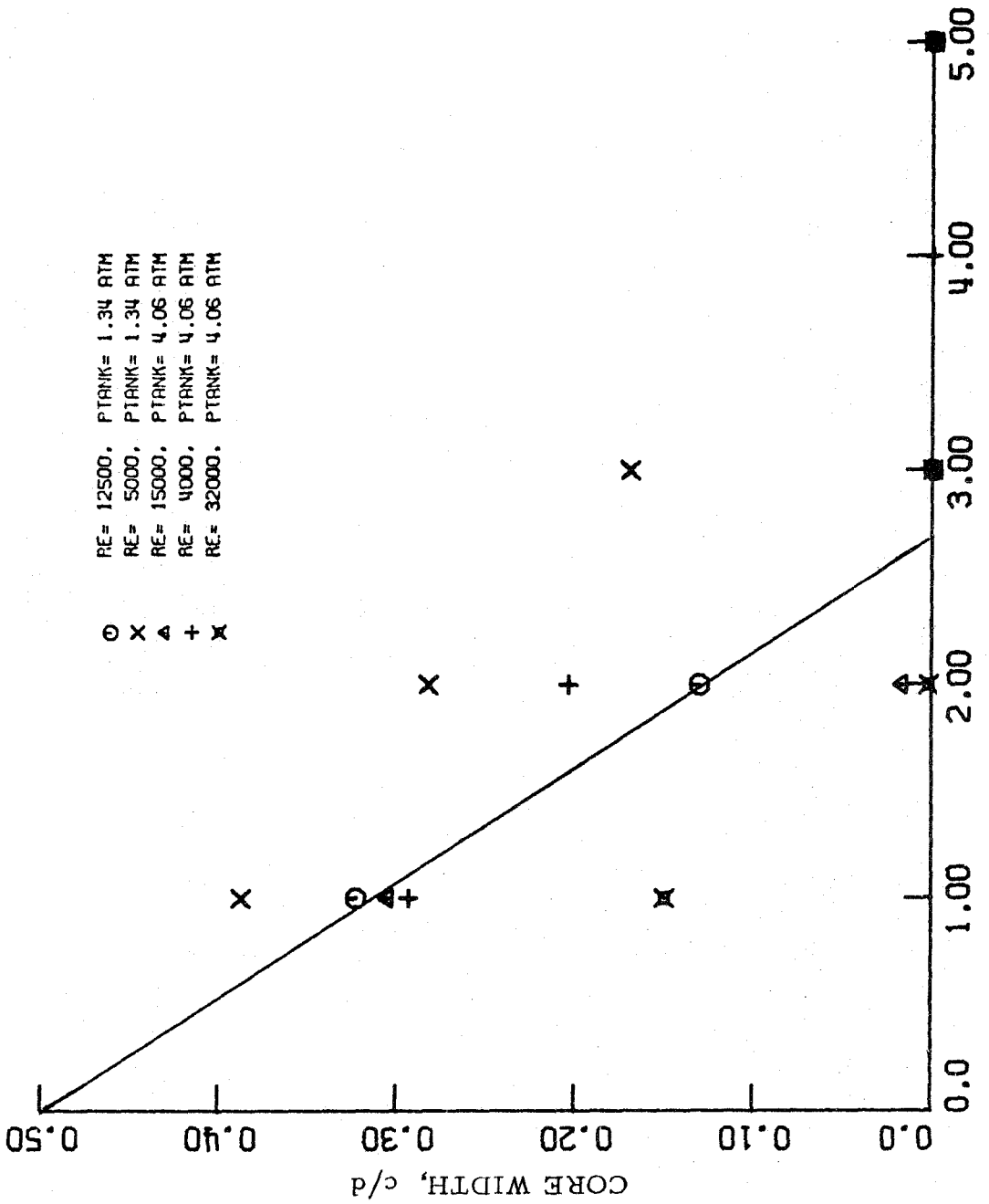

Figure 16a. Core Width of Nonreacting Jet

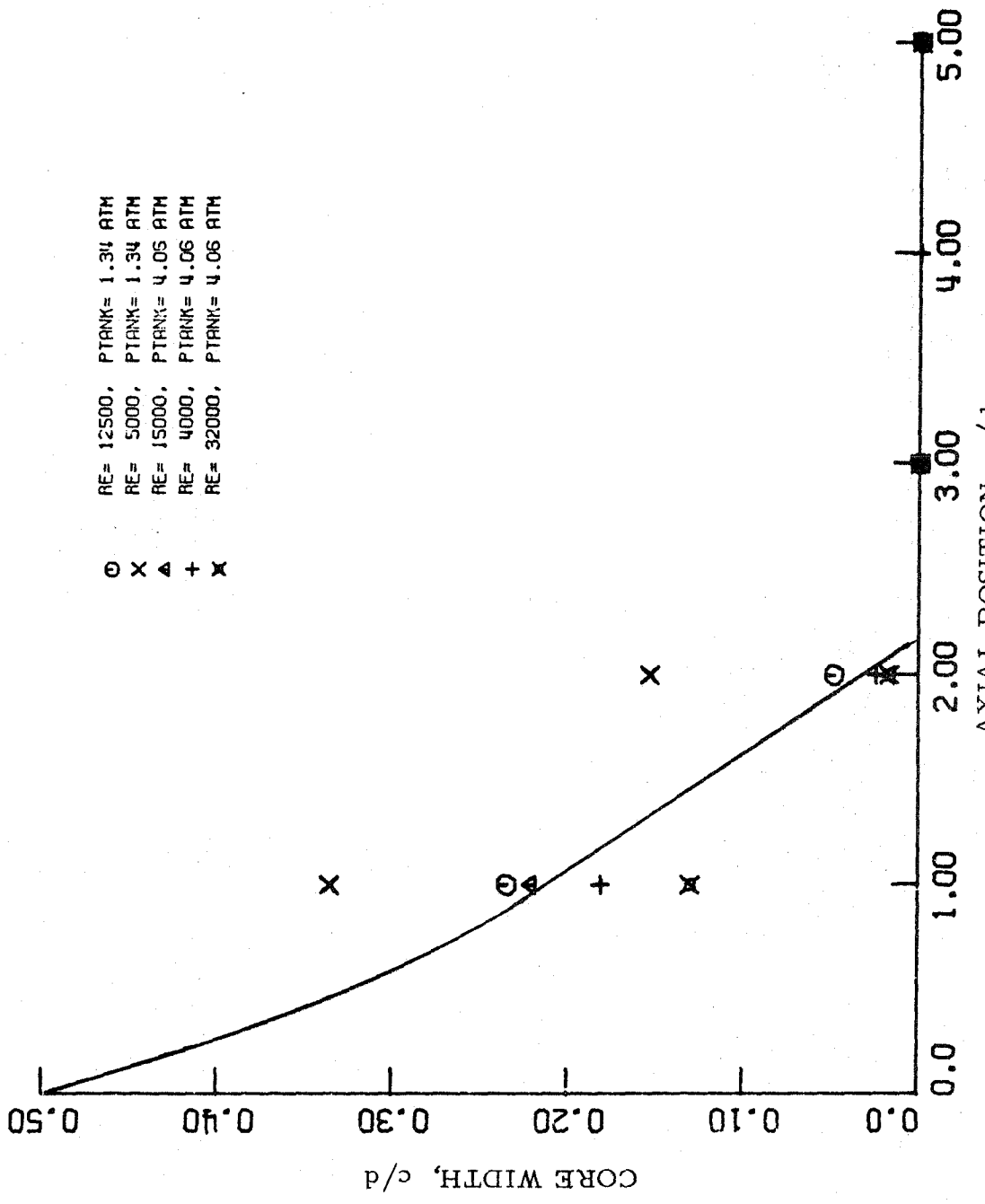

Figure 16b. Core Width of Highly Reacting Jet

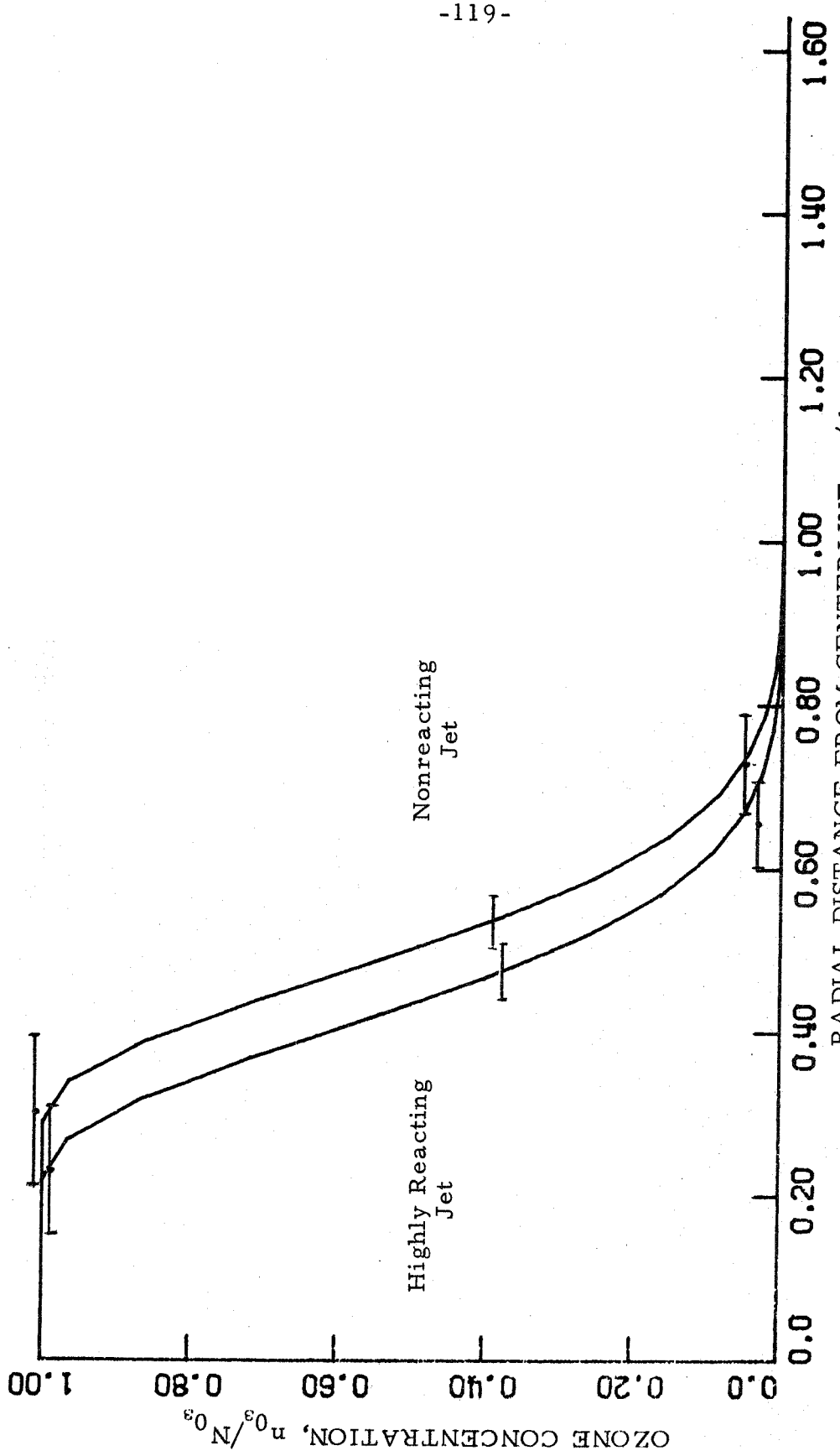

Figure 17a. Ozone Concentration Profile, Average over All Cases, z/d = 1

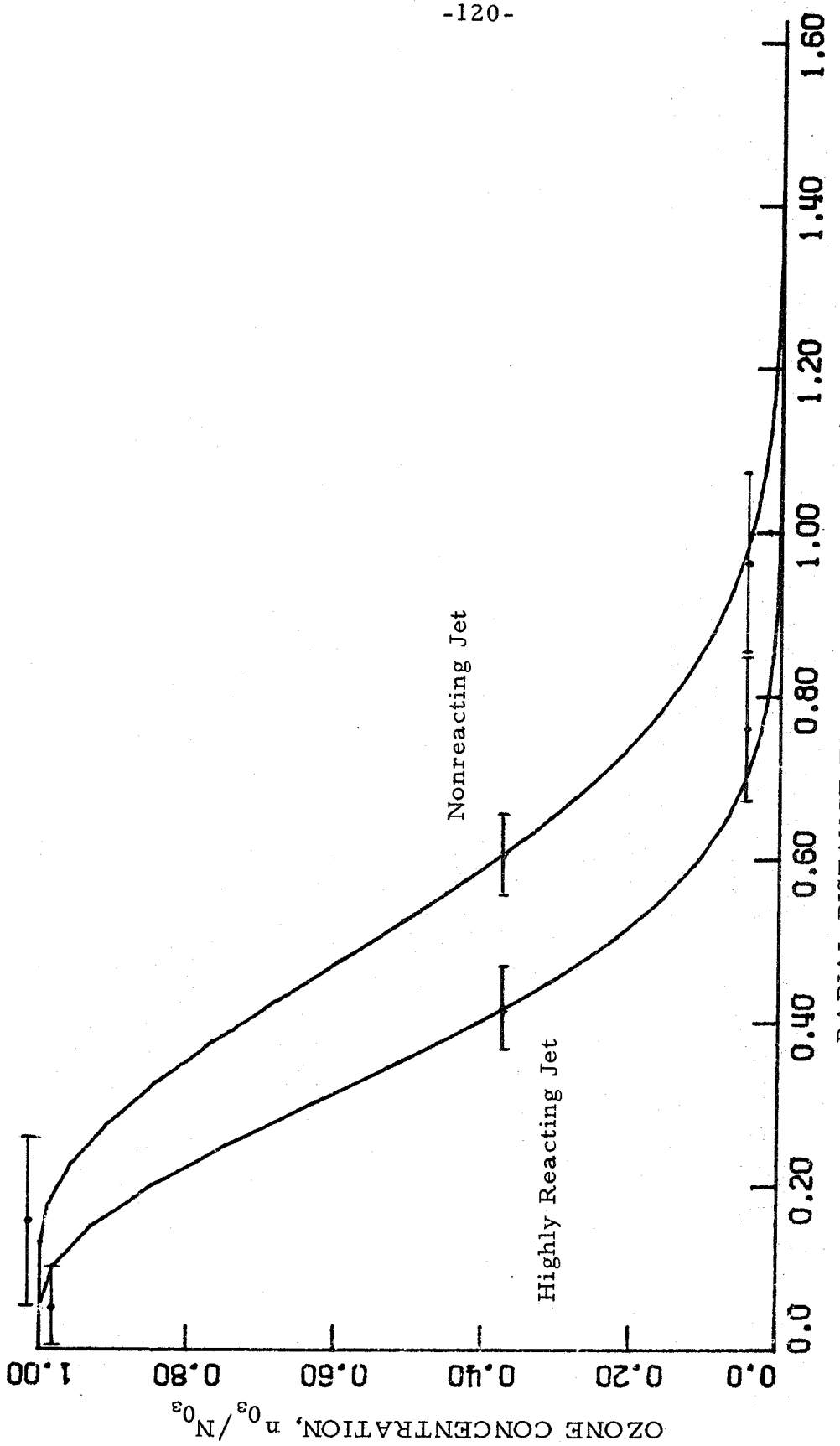

Figure 17b. Ozone Concentration Profile, Average over All Cases, z/d = 2

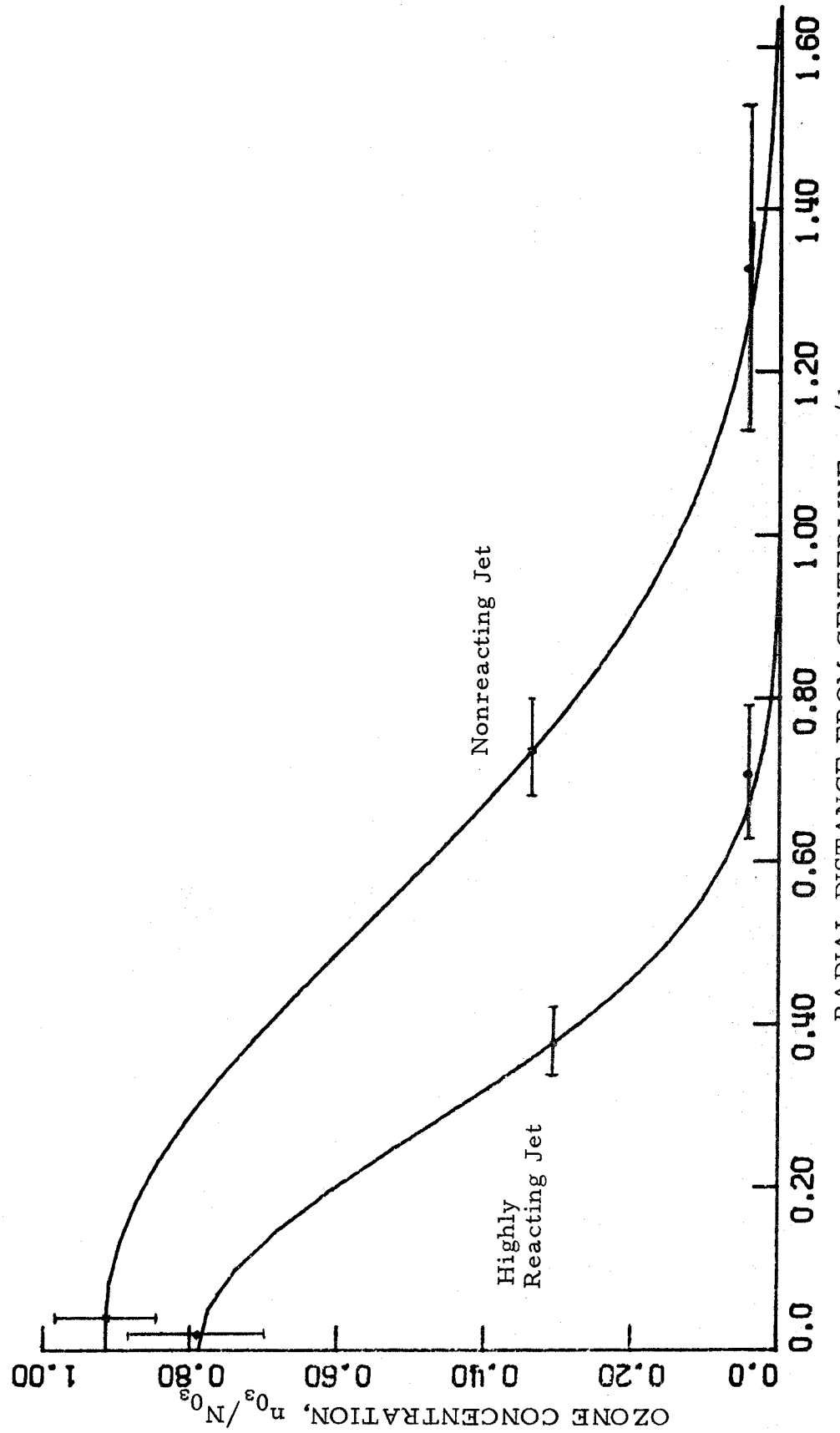

Figure 17c. Ozone Concentration Profile, Average over All Cases, z/d = 3

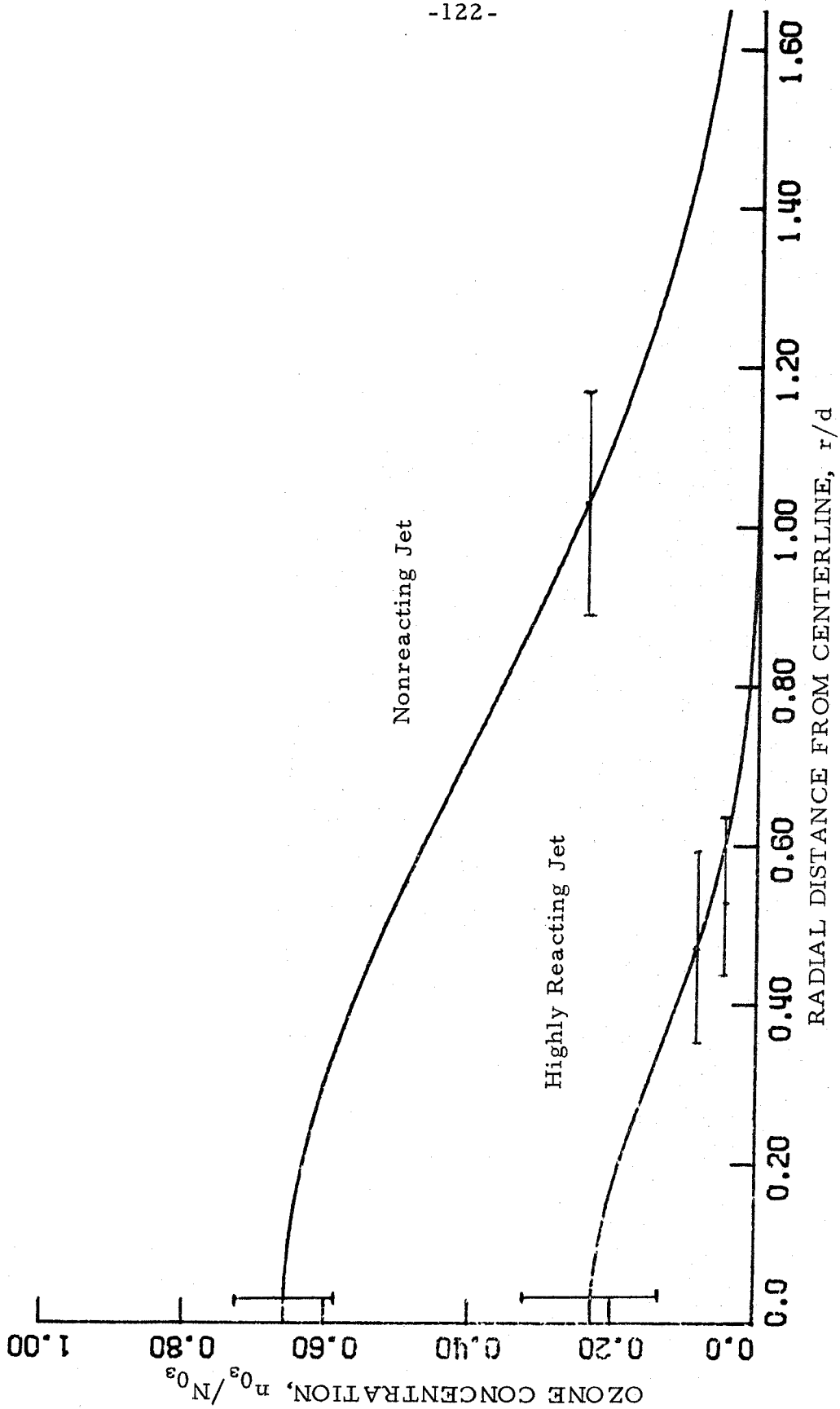

Figure 17d. Ozone Concentration Profile, Average over All Cases, z/d = 5

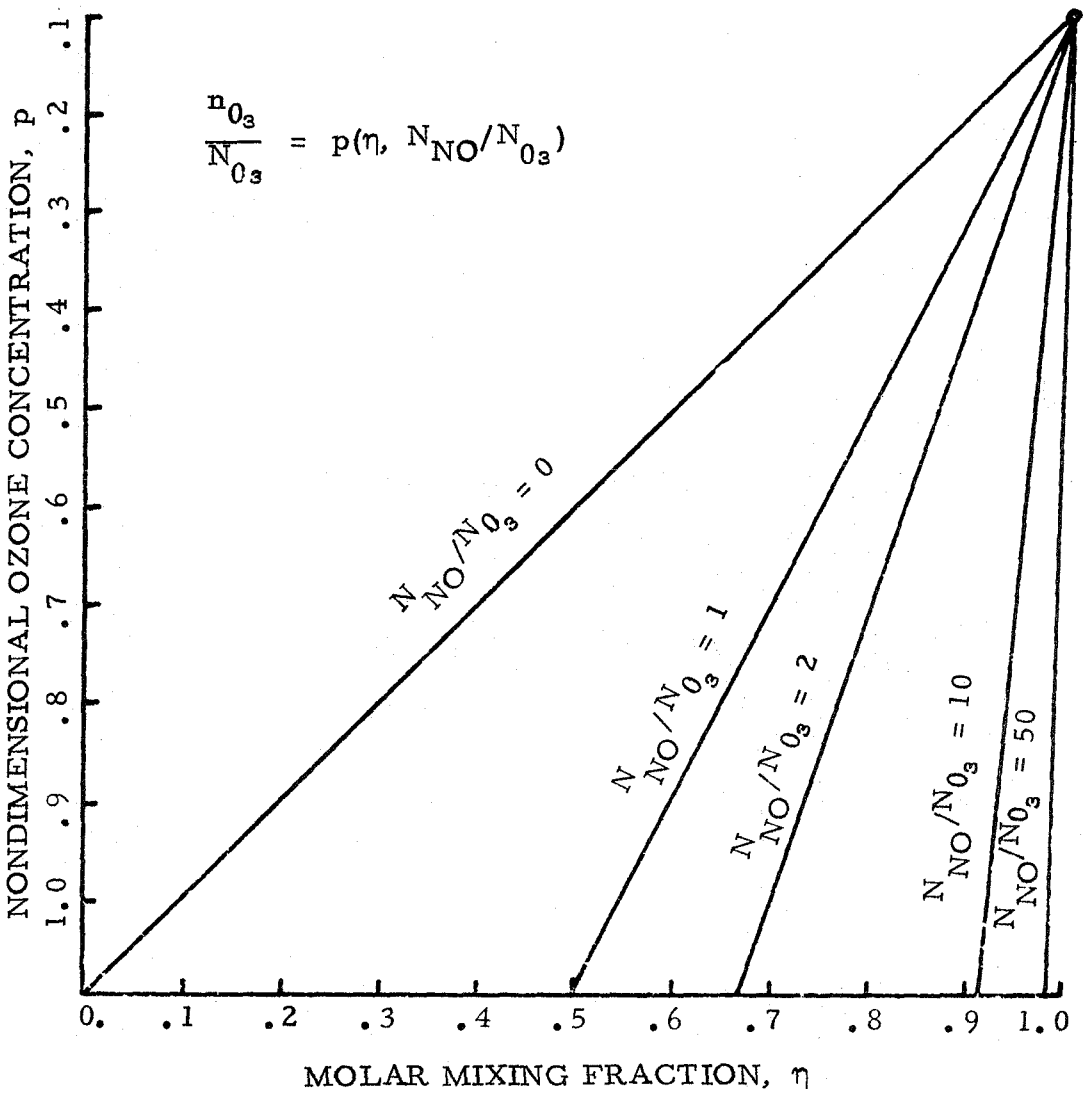

Figure 18. Nondimensional Ozone Concentration vs. Molar Mixing Fraction and Concentration Ratio

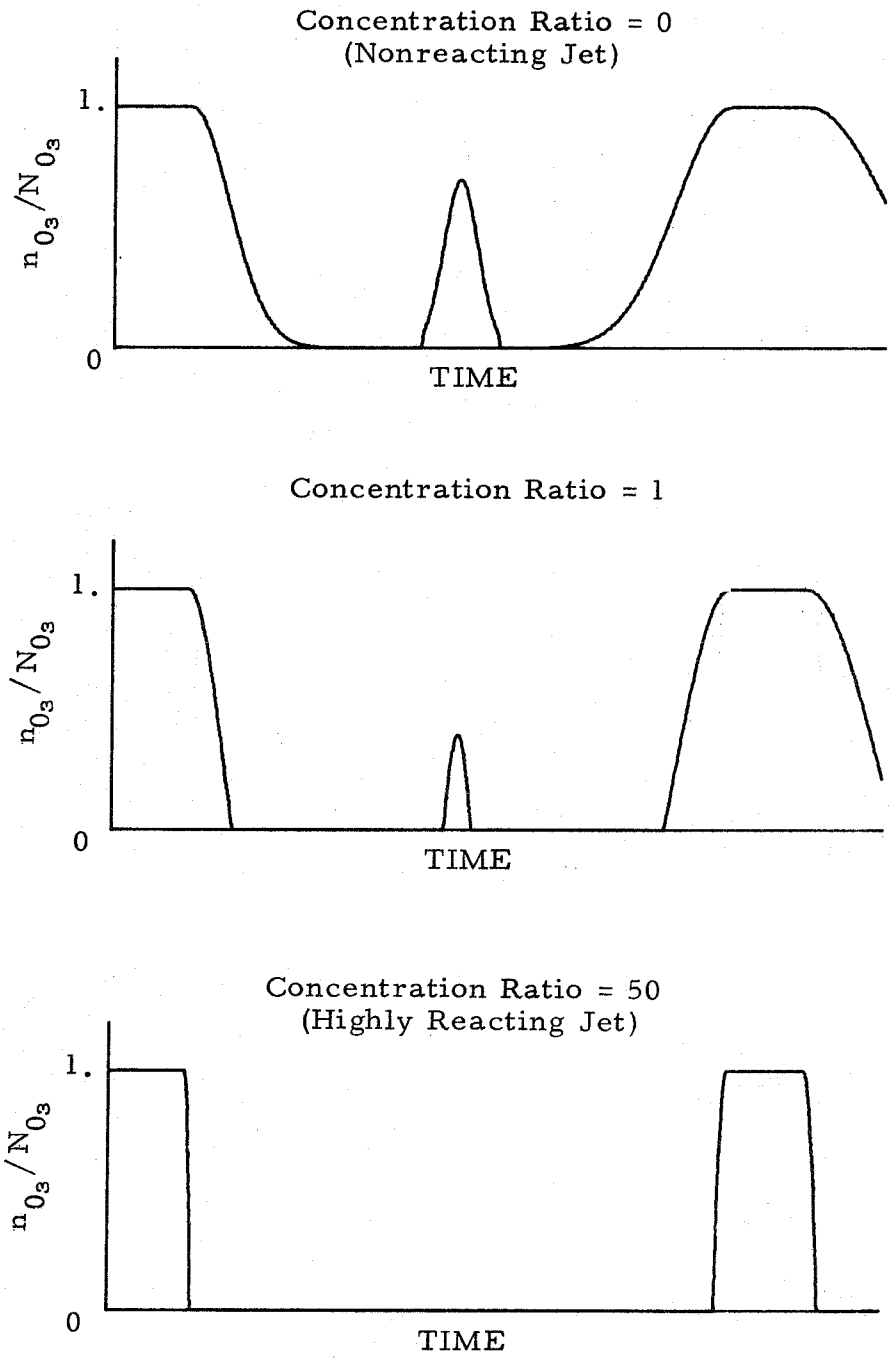

Figure 19. Example of Instantaneous Data Samples' Contribution to Time Average Measurements under Three Different Concentration Ratios

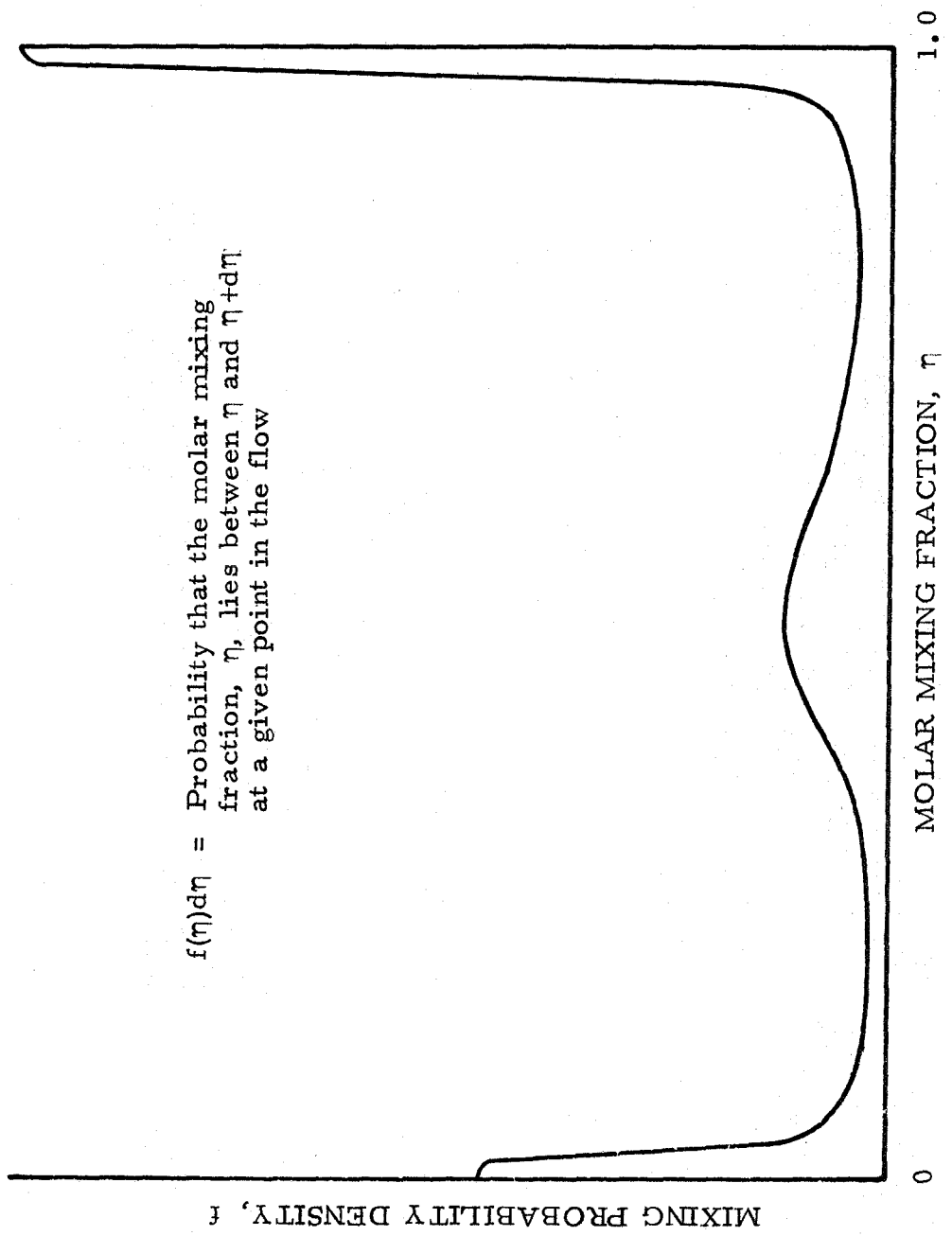

Figure 20. Schematic Mixing Probability Density Function